Exploring Growth Essential Genes in *E. Coli* using Synthetic Small RNA to Enhance Production of Phenylalanine

by

Daniel Herschel

A Thesis Presented in Partial Fulfillment
of the Requirements for the Degree
Master of Science

Approved April 2016 by the
Graduate Supervisory Committee:

David Nielsen, Chair
Xuan Wang
Cesar Torres

ARIZONA STATE UNIVERSITY

May 2016

ABSTRACT

Biomass synthesis is a competing factor in biological systems geared towards generation of commodity and specialty chemicals, ultimately limiting maximum titer and yield; in this thesis, a widely generalizable, modular approach focused on decoupling biomass synthesis from the production of the phenylalanine in a genetically modified strain of *E. coli* BW25113 was explored with the use of synthetic trans-encoded small RNA (sRNA) to achieve greater efficiency. The naturally occurring sRNA *MicC* was used as a scaffold, and combined on a plasmid with a promoter for anhydrous tetracycline (aTc) and a T1/TE terminator. The coding sequence corresponding to the target binding site for fourteen potentially growth-essential gene targets as well as non-essential *lacZ* was placed in the seed region of the of the sRNA scaffold and transformed into BW25113, effectively generating a unique strain for each gene target. The BW25113 strain corresponding to each gene target was screened in M9 minimal media; decreased optical density and elongated cell morphology changes were observed and quantified in all induced sRNA cases where growth-essential genes were targeted. Six of the strains targeting different aspects of cell division that effectively suppressed growth and resulted in increased cell size were then screened for viability and metabolic activity in a scaled-up shaker flask experiment; all six strains were shown to be viable during stationary phase, and a metabolite analysis showed increased specific glucose consumption rates in induced strains, with unaffected specific glucose consumption rates in uninduced strains. The growth suppression, morphology and metabolic activity of the induced strains in BW25113 was compared to the bacteriostatic additives chloramphenicol, tetracycline,

and streptomycin. At this same scale, the sRNA plasmid targeting the gene *murA* was transformed into BW25113 pINT-GA, a phenylalanine overproducer with the feedback resistant genes *aroG* and *pheA* overexpressed. Two induction times were explored during exponential phase, and while the optimal induction time was found to increase titer and yield amongst the BW25113 pINT-GA *murA* sRNA variant, overall this did not have as great a titer or yield as the BW25113 pINT-GA strain without the sRNA plasmid; this may be a result of the cell filamentation.

I would like to dedicate this thesis to my family; I could not have done it without the unwavering and endless support they have given to me. I would also like to dedicate this to my friends, who had to sacrifice their time and cope with the unpredictability that comes with researching biological systems. From words of encouragement to fun adventures, none of this would have been possible without the motivation from the people around me.

ACKNOWLEDGMENTS

First and foremost I would like to thank Professor Nielsen for accepting me into his lab and always pushing me to strive for greatness; I appreciate the support given to me during my time in the lab. The laboratory he created fostered a fantastic environment for discovery. I would also like to extend my appreciation to Professor Torres and Professor Wang for agreeing to serve on my graduate supervisory committee and offering such great advice along the way, and to Professor Rege for allowing me to use many resources from his laboratory.

As for my colleagues in the Nielsen lab group and beyond – to say I am forever indebted would be an understatement. To Brian Thompson and Michael Machas in particular, the help you two have given me over the past year has been invaluable; I look up to the two of you as if you were older brothers to me. I appreciate all the advice and great times we were able to share; these will truly be memories I never forget. To Matt Christensen and Sai Pavan from Professor Rege's lab, I really appreciate taking the time to help me out with the microscopy work when you both had your own dissertation defenses to focus on. To Chris Gregson and Zachary Dookeran, and Kyle Staggs, your guys' presence made the lab a lot more fun!

I would also like to acknowledge the funding from the U.S. Department of Energy, the National Science Foundation, ASU Lightworks and ASU start-up seed and grant funding which made this endeavor possible.

TABLE OF CONTENTS

Page

CHAPTER Page

CHAPTER Page

LIST OF TABLES

Table Page

LIST OF FIGURES

Figure Page

Figure Page

Figure Page

Figure Page

Figure Page

Figure Page

Figure Page

Figure Page

Figure Page

1. INTRODUCTION, MOTIVATION, AND BACKGROUND

1.1 The Current State of Chemical Processing

Petroleum, natural gas and coal have traditionally played large roles in the chemical process industries, and they all have one thing in common – they are not renewable resources which will eventually be depleted. Adding to this, these three sectors combined generated 4.77 Gt of CO_2 in the year 2004, with the entirety of the manufacturing industry generating 9.73 Gt of CO_2 in that year.[1] To put this a bit more into perspective, the entire manufacturing industry includes the sectors which are responsible for the generation of both electricity (3.59 Gt) and heat (0.29 Gt).[1] While it is hard to conceptualize a cost competitive alternative to any major manufacturing process which is entirely renewable and generates less CO_2 amongst other pollutants, certainly alternative approaches exist which may address the inevitable issues facing the manufacturing industry, and the chemical process industries in particular. Honing in in the chemical process industries, a subset of the manufacturing industries estimated to have generated 3.3 Gt of CO_2 in 2005, is perhaps one of the areas with most potential for alternative processes.[2] Not only would an alternative route of synthesis have the potential to greatly diminish associated emissions, but it could also incorporate renewable feedstock, generate high yield and titer, making it potentially more lucrative in the long run; amongst the most popular of the alternative approaches taken to generate commodity and precious chemicals has been bacterial synthesis.[3]

The potential of using bacteria as a biocatalyst is edified by considering the current means of synthesis for many commodity and specialty chemicals; not only does a route of biological synthesis offer a more sustainable means of generating a desired product that

need not be reliant on nonrenewable resources, these biological processes have also been shown to be effective on an industrial scale.[3-4] As an example to elucidate the potential of industrial scale biological processes which may use a renewable feedstock, acetone may be taken into consideration; acetone has been one of the biggest commodity chemicals throughout the past decade, amassing an industry valued at $28 million per year.[4] Although now primarily synthesized through the cumene process, which uses petroleum distillates as a precursor, acetone was at one time primarily synthesized through the Weizmann process, which relied on the anaerobic fermentation of *C. acetobutylicum*; at the height of WWI, the Weizmann process even warranted the generation of 2,000 lb of acetone per week in one single plant, located in King's Lynn, Great Britain.[4] The Weizmann process was also sustainable, with another plant located in South Africa that produced acetone from a molasses feedstock until 1982.[4] Unfortunately, as is the case with far too many biologically viable industrial scales routes of synthesis, the cumene process replaced the Weizmann process as the latter was only able to generate roughly 0.1 kg of acetone per kg of feedstock, while the former was able to generate 0.45 kg of acetone per kg of cumene, as well as generating a significant amount of phenol as a lucrative by-product.[4-5] Aside from just higher yields, the cumene process also has the inherent benefits of phenol co-generation while avoiding some of the trickiness of working with biological systems, like contamination; nonetheless, the Weizmann process shows that such large scale biological processes based on fermentation mechanisms have potential.[5] Even with the Weizmann process, not all hope is lost; much recent research and development has gone into generating thorough economic profiles for anaerobic fermentation of *C. acetobutylicum* which consider the harvest of other fermentation

products such as ethanol and butanol, modifying the feedstock composition to incorporate cheap and abundant resources like wheat straw, and genetically modifying the bacteria through different approaches to produce greater yields and final concentrations of desireables.[4,6] Appropriately engineering the factors which influence the productivity and yield of these biological processes, from operating conditions to gene expression, may once more make them competitive with the now-traditional routes of synthesis; a case study revisiting this anaerobic fermentation process with *C. beijerinckii* found production of acetone at a selling price of $1.30 per kg to be viable through rational engineering techniques, while market value throughout the past decade has hovered at the same levels.[3,6,7,8]

1.2 The Potential for Bacteria in the Chemical Process Industries

It takes much insight attained through thorough research and development to identify good candidates for industrial scale production with a biocatalyst however; as with any chemical reaction, thermodynamic and kinetic constraints must be taken into consideration.[9] In a most fundamental sense, thermodynamics is important in determining if a reaction will favor the products or reactants, while kinetics determines how fast the reaction will achieve a steady state; together, these give a good measure for the energy associated with the system.[10-11] One of the most convenient ways to measure the thermodynamics of a given reaction is through the Gibbs free energy, an intangible quantity which may be calculated through measureable physical quantities.[11] Reactions with negative Gibbs free energy values are spontaneous, generating energy, while reactions with a positive Gibbs free energy value are non-spontaneous, requiring the input of energy.[11] Therefore if a reaction has a negative Gibbs free energy, it will be

product favored; furthermore, in a biological system, if a given reaction has a positive Gibbs free energy then energy must be supplied by the cell. The more negative the Gibbs free energy is, the more spontaneous the reaction, and the more product favored it becomes; equilibrium constants are common indirect measures of the Gibbs free energy that give light to the relative ratio of the mole fraction of products relative to reactants.[11] The relationship between the total Gibbs free energy of a reaction *G*, the equilibrium constant *K*, and the mole fraction of a given species in the liquid phase x_i is expressed below for the sake of clarity,[11]

$$\ln(K) = -\frac{\Delta \mathrm{G}}{(\mathrm{R} * \mathrm{T})}$$
$$K = \Pi(x_i * \gamma_i)^{\nu_i}$$

In the relationship above, the gas constant *R*, temperature *T*, activity coefficient, γ_i, and stoichiometric coefficient, ν_i are required; furthermore, this simplified version is only valid for low to moderate pressure.[11] The Gibbs free energy is useful in genetic engineering as it may enable enhanced insight into competing reaction pathways. Assuming the reaction kinetics are equivalent, this relationship dictates the more spontaneous pathway will most likely generate more product.[11] This example also reiterates a critical point - kinetics must be taken into account. If the kinetics are favorable enough, they may act as a driving force to help mitigate some thermodynamic constraints; this is particularly useful genetic engineering because in its essence, all genetic engineering approaches modify the thermodynamics and kinetics involved with different cellular processes. In a similar fashion to the way the previous example highlighted the importance of Gibbs free energy in a set of competing reactions, the

importance of kinetics may be brought to light by considering the two reactions again seen in Figure 1,

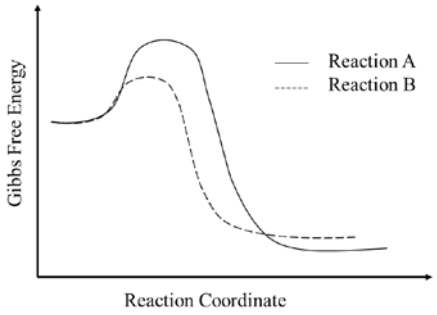

Figure 1: The Gibbs Free Energy versus Reaction Coordinate for Two Arbitrary Reactions (Solid, Dashed). Reaction A is More Thermodynamically Favorable, Indicated by the Greater Overall Change in Gibbs Free Energy, but Less Kinetically Favorable, Indicated by the Larger Activation Energy.

As seen above, there exist two reactions *A* and *B,* which may be represented by a solid line and a dashed line respectively; the two reactions both only have one intermediate formed during the overall reaction process, indicated by only one local maxima of Gibbs free energy, and this may be referred to as the activation energy for each reaction.[11] By inspection, reaction A has a larger activation energy, as it has the obviously larger increase in Gibbs free energy near the start. Under a resource limited scenario, even though reaction A is more thermodynamically favorable, kinetic constrains reflected by a higher activation energy may result in reaction B using a greater majority of the resources.[11,12] These are important considerations to take into account when considering the sophisticated reaction pathways that make up biological processes; in the context of biological systems, thermodynamics and kinetics may be finely tuned to express a desired phenotype.[12]

1.3 *E. coli* as a Candidate for Biosynthesis Applications

Although *C. acetobutylicum* was used to make a point in regards to the industrial feasibility of biological processes, amongst the most studied bacterial organisms is *E. coli*; with a rich history of pioneering breakthroughs in synthetic biology, different strains of *E. coli* have been shown capable of synthesizing diverse classes of molecules ranging from free fatty acids to phenolic compounds which may be used as fuels, specialty chemicals, and precursors.[13,14] It is worth noting that quite frequently these natural pathways are limited by the genes and enzymes native to the host strain, so synthetic components to enhance, repress and block native gene expression, or even enable foreign gene expression may be incorporated through various genetic engineering techniques.[3,12,15] Genetic engineering coupled with advances in synthetic biology enable these enhancements such as the construction of synthetic pathways, but pathways do not have to be completely synthetic – they may branch from an existing pathway as will be discussed in Figure 2.[3,12,16,17] *E. coli* is a popular candidate in genetic engineering because there is so much known about it – it has a relatively fast growth rate compared to other bacteria, it may be grown in a broad range of conditions and it is also found in humans; *E. coli* was also the organism where cloning was observed for the first time, and one of the first organisms to have its genome completely sequenced.[18,19] With this in mind, using bacteria like *E. coli* seems like a viable solution to the growing problem associated with non-renewable resources; just insert a pathway for a desired product, if necessary, and fine-tune the thermodynamics and kinetics of the process. Unfortunately, genetic engineering is not that easy; there are an unquantifiable number of different strains of *E. coli* alone, each with their own profits and conflicts, with endless numbers of approaches

and techniques taken to achieve the perfect balance of kinetics and thermodynamics. As an example to show the complexity of metabolic engineering in a real biological system, consider the synthesis of phenol from glucose via an extension of the shikimate pathway in *E. coli* as seen below in Figure 2,[17,20]

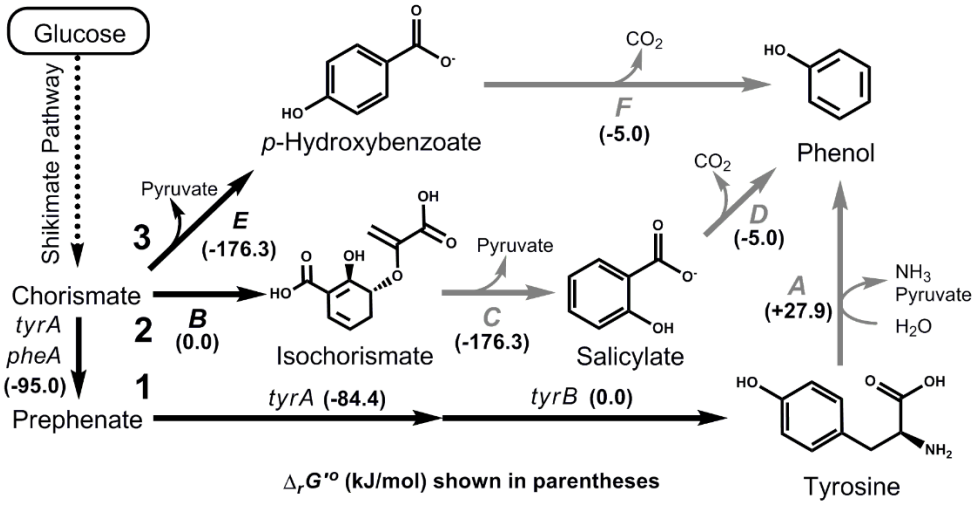

Figure 2: Three Synthetic Pathways for the Generation of Phenol from Chorismate During Fermentation in E. coli.[17]

In the figure above, there are three synthetically engineered pathways which branch from the shikimate pathway that may potentially be inserted into *E. coli*; from a thermodynamic standpoint, the first pathway might be the least favorable as it has the highest Gibbs free energy, but considering the kinetics of the enzymes involved in each step of the reaction cascade, this might not be the case.[17] Some enzymes may have higher activities, resulting in a scenario analogous to before, where kinetics have a greater influence than the thermodynamics. In any case, it is clear that genetic engineering coupled with advances in biosynthesis have unleashed a whole new world of target chemicals which may be synthesized using biocatalysts.

1.4 Metabolic Engineering: Applied Biosynthesis

In essence, while it is certain that the sustainable technology of industrial scale biological synthesis exists, it is also clear that an optimization of the associated operating costs is necessary if this is to be cost competitive; even in the revisited case of the *C. beijerinckii*, unless the process is able to bring acetone to market significantly below $1.30 per kg, there is no incentive for the main producers of this chemical to invest in such a change.[6] Nonetheless, within the realm of bioengineering, approaches oriented at bringing the price point down by addressing factors associated with the viability of the cell have garnered much attention; the rational engineering of cellular systems with the ultimate goal of expressing a desired metabolic phenotype is one prominent means of fine tuning the balance between thermodynamics and kinetics.[9,12,21] In essence, this is the underlying principle of metabolic engineering and is focused on the optimization of both intracellular and extracellular factors; it is worth noting metabolic engineering is not limited only to genetic and other intracellular approaches but rather any factor which may induce a given desired metabolic phenotype, such as environmental factors.[9,12,21,22] Often times the ultimate goal is to increase the productivity and final concentration of a target chemical when considering the use of biocatalysts in conjunction with metabolic engineering, though metabolic engineering also has other uses; for example, metabolic engineering may be used to build switchboards and circuits to act as sensors for particular environmental markers.[23,24]

1.5 Extracellular Factors in Metabolic Engineering

As mentioned, there are a lot of factors at play when considering metabolic engineering and these factors may either be extracellular or intracellular. One of the most prominent

extracellular factors in metabolic engineering is the presence of oxygen; in the case of *C. acetobutylicum*, anaerobic fermentation was used to achieve the industrial scale synthesis of acetone, but quite often biosynthesis with *E. coli* operates under aerobic conditions.[4,16] Though it is worth noting *E. coli* can still undergo respiration and fermentation under anaerobic conditions, growth conditions are much different relative to aerobic conditions; in general, less ATP is generated per mole of feedstock in anaerobic conditions, resulting in severely reduced cell densities, and reduced productivities.[25] As the lack of oxygen makes it difficult for cell growth, even though productivities are lower relative to aerobic systems, yields may approach values close to their theoretical limits because less of the ATP is used on biomass synthesis – this leaves more ATP for the production of the target chemical.[12, 26] While anaerobic growth conditions have their own profits, some cell products require a relatively large amount of energy to produce, relating back to the analogies discussed in Figure 1 and Figure 2.[12] For such target chemicals, production is often tied with growth meaning a large amount of biomass must be generated for the co-generation of a significant quantity of a desirable.[12] Other products are also synthesized in close relation to cell growth, calling for aerobic conditions in order to be viable.[27] To mitigate the conflicts of aerobic conditions which may be required for the biosynthesis of particular chemicals, diverse approaches in metabolic engineering have been explored to decouple growth from production.[24,28,29,30] A few metabolic engineering approaches aimed at decoupling growth from production will be briefly discussed before presenting the central idea of the thesis, which will examine an intracellular approach using synthetic small RNA to silence growth essential genes; this approach may be applied to a diverse class of target chemicals, enabling the continuation of biosynthesis without

biomass accumulation.[24] This is advantageous in both the case of the chemicals which need large amounts of energy for production and those tied with growth as this allows control of biomass formation, and therefore the optimization of titer and yield.

Nutrient limitation through the use of minimal media feedstock is a popular extracellular approach aimed at preventing excess biomass accumulation; in particular, controlling the levels of carbon, nitrogen and phosphorous supplied to the cell system may warrant the fine tuning of growth and productivity.[31,32] Cells need nitrogen and phosphorous for reproduction, so tuning the concentrations of these may warrant reallocation of the energy in the cell towards production of a desirable.[33] A popular way of achieving this is through the use of specialized nutrient broths which serve as media to grow the cell system in; nutrient limitation in the form of minimal media broth is also applicable for gauging efficacy in industrial scale processes as reducing the constituents of the media may result in significant savings, though a challenge presented by special growth medias used for nutrient limitation are non-traditional culturing protocols introducing more potential for mistakes.[34] For example, on top of more sophisticated formulas, minimal media may require specialized preparation if it is comprised of light or temperature sensitive components, or specialized growth if it is not pH buffered.

Another extracellular metabolic engineering approach geared at stopping biomass synthesis is the use of bacteriostatic additives which may disrupt a number of different cell mechanisms that warrant the cell to carry out regular metabolic functions but inhibit growth; suitable targets for bacteriostatic additives may be genes associated with DNA synthesis, protein synthesis, cell wall synthesis, and the cell division process.[22, 33,35]

Bacteriostatic additives may inhibit growth by acting on a particular gene to result in the buildup of a rate-limiting intermediate; the known gene targets of bacteriostatic additives also offer a convenient phenotypic comparison to gene silencing based approaches.[35] Unfortunately, scalability issues associated with the use of bacteriostatic additives such as strains developing a resistance and cost prohibition make other techniques more attractive options. Aside from nutrient limitation and bacteriostatic additives, there are other extracellular factors which may influence the metabolism of the cell and may also be optimized for biosynthesis, but do not show much potential in regards to decoupling growth and from production – factors such as temperature, pH, and aeration may be optimized, but are relatively standard depending on the viability of the bacteria.[33,22]

1.6 Intracellular Factors in Metabolic Engineering

Extracellular factors and optimization techniques play a critical role in metabolic optimization of bioprocesses and have shown potential to contribute in the separation of biomass synthesis and target chemical production, and their successes are only compounded when considering approaches taken in metabolic engineering on an intracellular, genetic level. Though as is the case with many extracellular factors, many genetic oriented metabolic engineering approaches have not been aimed at the decoupling of biomass production from synthesis of a target product because the methods of gene manipulation are not dynamic in nature, so reducing the activity of genes essential for growth would result in poor overall cell performance. Nonetheless, approaches such as over-expressing genes responsible for the production of rate-limiting intermediates or knocking out genes associated with competing pathways have seen great success in increasing overall efficiency of bioprocesses; just as with the extracellular factors

discussed above, these approaches offer the potential to be compounded with a dynamic genetic approach that turns off biomass synthesis.[36,37] As an example of how intracellular approaches are useful in metabolic engineering, consider the production of phenylalanine which is an essential amino acid. Though not dynamic in nature and does not decouple growth from production, without traditional intracellular approaches, significant concentrations of phenylalanine in *E. coli* may not be achieved; consider the pathway below which illustrates the production of phenylalanine from glucose, both in green, in *E. coli*,

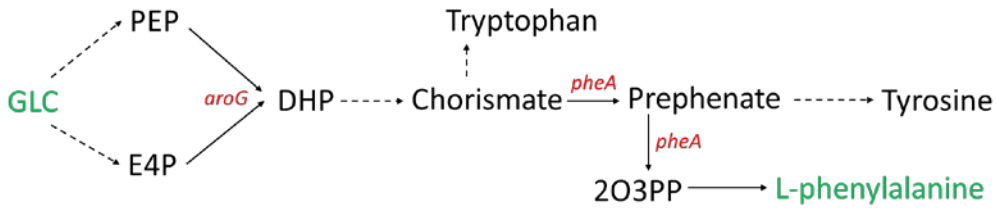

Figure 3: Pathway Showing Production of Phenylalanine from Glucose

Considering *E. coli* does not natively make high levels of phenylalanine, a strain was engineered by overexpressing the feedback resistant genes *aroG* and *pheA*, seen in red, which lead to significant increases in phenylalanine production. Overexpressing these genes reduced the flux of the intermediates to alternate pathways; for example, when overexpressing *pheA* more chorismate is used to generate prephenate than before. Just overexpressing these two genes can lead to phenylalanine concentrations of roughly 1.5 grams per liter – so while it is an effective approach, it is worth noting that further optimization would be difficult without manipulating other parameters. Finding a "global" growth-switch to decouple biomass synthesis from production could enhance already existing techniques which focus on "local" pathways like over-expressing genes.

One dynamic genetic approach aimed at turning off biosynthesis is governing RNA polymerase using an inducible promoter; it was shown that using this technique cell growth could be arrested while the cell would remain a metabolically active platform.[38] While this approach even showed success at increasing glycerol production, the lack of modularity with respect to gene targets makes this approach tricky as the promoter of each desired gene must be replaced on the chromosome if different gene targets are to be explored to better fine tune the cell system.[38] Another dynamically inducible method that can offer selection of genetic targets may not only warrant the exploration of growth essential genes on cell viability, but it would also introduce a novel metabolic engineering technique applicable to many scenarios even beyond metabolic engineering. One way of accomplishing this may be through the use of trans-encoded artificial small RNA (afsRNA), an mRNA regulator which acts through limited base pairing and may either inhibit translation of a particular gene, or degrade mRNA.[39,40]

1.7 Small RNA in Bacteria

With the discovery of riboswitches, sRNA, and CRISPR RNA, the role of RNA as regulators in cell systems has long been acknowledged; considering sRNA in particular, the emersion of trans-encoded sRNA in the past decade has unleashed much potential in synthetic biology.[40,24] Prior to the emersion of trans-encoded sRNA, only cis-encoded sRNA was understood; cis-encoded sRNA have extensive homology with a target mRNA, around 75 nucleotides, and are located on the opposite DNA strand of the target RNA, while trans-encoded sRNA may be around 20 nucleotides and are located separate from the target mRNA.[39,40] The general structure of trans-encoded sRNA may be seen below in *Figure 3*,[39]

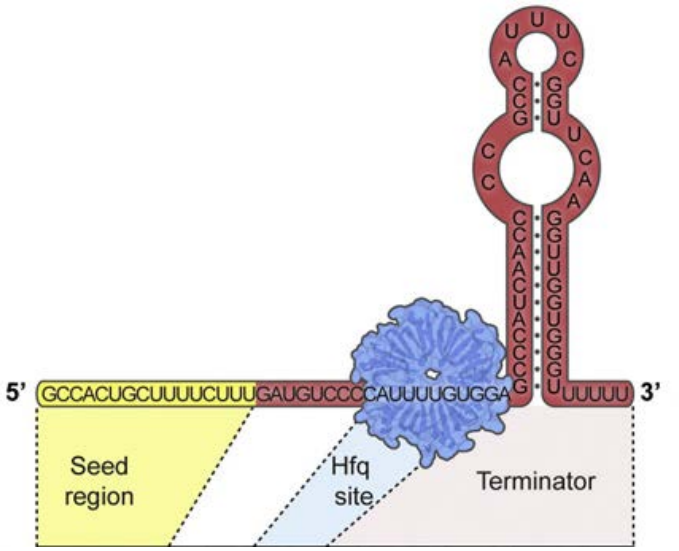

Figure 4: A General Schematic of Trans-encoded sRNA Showing the Seed Region, One Potential Hfq Binding site, and the Transcription Terminator.[39]

Trans-encoded sRNA is primarily comprised of the three regions seen above – the transcription terminator region, an Hfq binding site, and a seed region.[39] Perhaps the most interesting of the three regions is the seed region; the seed region is the region which targets the translation initiation region of a desired mRNA through a homologous sequence of nucleotides.[41,39] Studies on the seed region have shown that a seed region of around 22 nucleotides long with a binding energy of around -35 $\frac{kCal}{mol}$ generates the most stable sRNA-mRNA duplex.[24,40] Just as interesting is the Hfq protein which binds to the Hfq site; in trans-encoded sRNA, it has been shown that Hfq greatly stabilizes sRNA-mRNA duplex, while in cis-encoded sRNA the presence of Hfq was shown to decrease gene silencing effects.[30,39,42] Seen below in Figure 4 is a diagram similar to that which was presented in Figure 1, bringing to light the importance of kinetics in an environment where the total energy change is equivalent,

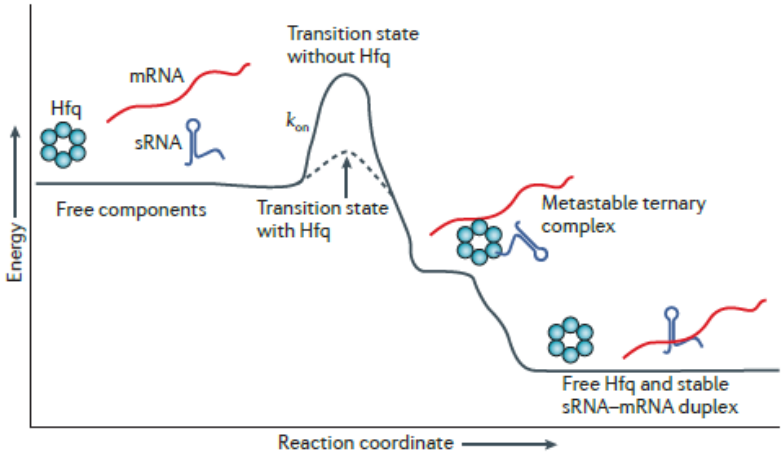

Figure 5: A Diagram of the Reaction Energy versus Reaction Coordinate for the Binding of Trans-encoded sRNA and mRNA, Mediated through Hfq.[42]

It may be seen in the figure above that the presence of Hfq as a chaperone to trans-encoded sRNA promotes formation of a sRNA-mRNA duplex. Lastly, the terminator region of the sRNA should not be overlooked either; the terminator is indirectly responsible for stabilizing the sRNA-mRNA duplex just as much as the Hfq protein, as the terminator region has been shown to control stability of the Hfq protein binding to the secondary structure of the sRNA.[43] In particular, the terminator on sRNA is a rho-independent transcription terminator which inherently contains a poly(U) tail; it is this poly-U tail which has been shown essential for Hfq binding in trans-encoded sRNA, and may even be seen in the schematic sRNA in Figure 3.[39, 43,42]

In summary, sRNA is a highly modular tool which may be exploited to target growth essential genes in order to decouple biomass accumulation and target chemical production; placing an appropriately designed afsRNA under a promoter to target a desired mRNA may be a robust way to target growth essential genes and increase productivity and yield for desirable chemicals. Furthermore, the ability to target a variety of different gene targets also makes afsRNA an attractive approach to explore in regards

to growth arrest; more than one sRNA may be placed on a plasmid, once more compounding the capabilities at hand.

1.8 Research Aims

In this thesis, synthetic trans-encoding sRNA using a scaffold based off of the naturally occurring *MicC* sRNA found in *E. coli* coupled with an additional terminator, the T1/TE terminator, and a promoter for anhydrous tetracycline are put on a plasmid with streptomycin resistance to first screen fourteen unique gene targets which may be potentially essential for growth based on mechanisms responsible for DNA synthesis, protein synthesis, cell wall synthesis, and the cell division process in the *E. coli* K-12 strain BW25113; to further characterize the growth suppression capabilities of the sRNA approach, a known non-growth-essential gene, *lacZ* is also taken into consideration.[24] Identification of the most qualified sRNA-mediated gene targets, based on an analysis of optical density, morphology, cell viability and metabolic activity, was ultimately used as criteria when selecting the best gene targets to be further screened in a strain which produces phenylalanine. The effect of decoupling growth and production through various cellular mechanisms is assessed using the sRNA to determine the best time to stop growth during the exponential growth phase for an optimal productivity and titer. The efficacy of the sRNA as a means to suppress growth while leaving the rest of the metabolism unscathed is compared to common bacteriostatic additives which are known to target particular genes. The fourteen candidate genes and *lacZ* may be seen listed below in Table 1 along with their cellular function; it is also worth noting that *fabB* and *fabH* were simultaneously targeted as well considering the fatty acid biosynthesis pathway cannot be blocked by targeting *fabH* alone, for reasons discussed in the results,

Table 1: A List of the Gene Targets Investigated with sRNA

sRNA Mediated Gene Target	Cellular Function
dnaE	DNA Polymerase
fabB	Cell Wall Biosynthesis
fabB + fabH	
fabD	
fabG	
fabH	
fabI	
folA	DNA Synthesis
folD	
folP	
lacZ	Metabolize Lactose/x-gal
murA	Cell Wall Biosynthesis
rplD	Protein Synthesis
rplP	
rpsD	
rpsE	

2. MATERIALS AND METHODS

2.1 Strains and Media

While wild-type BW25113 was the primary background strain used in the duration of the study, many variants of this strain were generated such as the pSRNA variants and the pINT-GA variants; furthermore, other strains were used for the purposes of plasmid construction. All strains used in this study are listed below in Table 2 (Next Page) *E. coli* DH5-alpha was purchased from New England Biolabs (NEB) and was used for all cloning work and plasmid maintenance. *E. coli* BW25113 was obtained from the Coli Genetic Stock Center (CGSC) and served as the host organism for all experiments in this study. *E. coli* NST74 was obtained from the American Type Culture Collection (ATCC) and served as the source of the feedback resistant gene *pheA101*. *Z. mobilis* ZM4 was also sourced from the American Type Culture Collection (ATCC), and served as the source of the promoter for the pyruvate decarboxylase (PDC) gene. *E. coli* MG1655 served as the source of the *lacZ* gene and was generated from D. R. Nielsen on behalf of A. Kato. *E. coli* strains were routinely cultured at 32ºC and 200 RPM in Luria-Bertani (LB) broth, supplemented with 100 milligram per liter streptomycin (for all pSRNA strains), 35 milligram per liter kanamycin (for all pINT-GA strains), 10 milligram per liter tetracycline (for tetracycline resistant BW25113), and/or 34 milligram per liter chloramphenicol as appropriate. To test for blue-white screening, morphology of antibiotic resistant strains, sRNA-mediated growth arrest, and phenylalanine production, relevant strains were cultured at 32ºC and 200 RPM in either LB, M9 minimal media, or M9M minimal media, each supplemented with relevant antibiotics as appropriate. A complete list of the media recipes may be found in APPENDIX D.

Table 2: List of All Strain Names and a Description; [1]DH5-alpha was Sourced from ThermoFisher, [2]BW25113 was Sourced from CGSC, [3]NST74 and ZM4 were Sourced from ATCC, and all else from This Study.

Strains	Description
E. coli DH5-alpha[1]	*dlacZ Delta M15 Delta(lacZYA-argF) U169 recA1 endA1 hsdR17(rK-mK+) supE44 thi-1 gyrA96 relA1*
E. coli BW25113[2]	*F-, DE(araD-araB)567, lacZ4787(del)::rrnB-3, LAM-, rph-1, DE(rhaD-rhaB)568, hsdR514*
E. coli NST74[3]	*aroH367, tyrR366, tna-2, lacY5, aroF394(fbr), malT384, pheA101(fbr), pheO352, aroG397(fbr)*
Z. mobilis ZM4[3]	*See References*[44]
E. coli MG1655	*K-12 F⁻ λ⁻ ilvG⁻ rfb-50 rph-1*
MG-lacZ	*E. coli* MG1655 pSRNA-lacZ
BW-cmp	*E. coli* BW25113 pACYC-DUET
BW-strep	*E. coli* BW25113 pCDF-DUET
BW-tet	*E. coli* BW25113 pRK415
BW-dnaE	*E. coli* BW25113 pSRNA-dnaE
BW-fabB	*E. coli* BW25113 pSRNA-fabB
BW-fabBH	*E. coli* BW25113 pSRNA-fabBH
BW-fabD	*E. coli* BW25113 pSRNA-fabD
BW-fabG	*E. coli* BW25113 pSRNA-fabG
BW-fabH	*E. coli* BW25113 pSRNA-fabH
BW-fabI	*E. coli* BW25113 pSRNA-fabI
BW-folA	*E. coli* BW25113 pSRNA-folA
BW-folD	*E. coli* BW25113 pSRNA-folD
BW-folP	*E. coli* BW25113 pSRNA-folP
BW-murA	*E. coli* BW25113 pSRNA-murA
BW-rplD	*E. coli* BW25113 pSRNA-rplD
BW-rplP	*E. coli* BW25113 pSRNA-rplP
BW-rpsD	*E. coli* BW25113 pSRNA-rpsD
BW-rpsE	*E. coli* BW25113 pSRNA-rpsE
pINT-GA	*E. coli* BW25113 pINT-GA
pINT-GA dnaE	*E. coli* BW25113 pINT-GA pSRNA-dnaE
pINT-GA fabD	*E. coli* BW25113 pINT-GA pSRNA-fabD
pINT-GA fabH	*E. coli* BW25113 pINT-GA pSRNA-fabH
pINT-GA folA	*E. coli* BW25113 pINT-GA pSRNA-folA
pINT-GA murA	*E. coli* BW25113 pINT-GA pSRNA-murA
pINT-GA rplD	*E. coli* BW25113 pINT-GA pSRNA-rplD

2.2 Plasmid Construction

Many plasmids were also used in the course of this study, with some plasmids used only intermediately to further construct more complex plasmids; all final plasmids below,

Table 3: A List of All Plasmids Used in This Study, Their Description and Source.

Plasmid	Description	Source
pKSV45	p15A ori, Amp^r, *tetR*, P_{tet}	Prather Lab (MIT)
pACYC-DUET	RK2 ori, Cmp^r, *lacI*, P_{T7}	Novagen
pCDF-DUET	cloDF13 ori, $Strep^r$, *lacI*, P_{T7}	Novagen
pRK415	oriV, Tet^r, P_{lac}	Novagen
pSRNA	cloDF13 ori, $Strep^r$, *tetR*, P_{tet}	This study
pSRNA-dnaE	dnaE target binding sequence inserted into pSRNA	This study
pSRNA-fabB	fabB target binding sequence inserted into pSRNA	This study
pSRNA-fabBH	fabB and fabH target binding sequence inserted into pSRNA	This study
pSRNA-fabD	fabD target binding sequence inserted into pSRNA	This study
pSRNA-fabG	fabG target binding sequence inserted into pSRNA	This study
pSRNA-fabH	fabH target binding sequence inserted into pSRNA	This study
pSRNA-fabI	fabI target binding sequence inserted into pSRNA	This study
pSRNA-folA	folA target binding sequence inserted into pSRNA	This study
pSRNA-folD	folD target binding sequence inserted into pSRNA	This study
pSRNA-folP	folP target binding sequence inserted into pSRNA	This study
pSRNA-lacZ	lacZ target binding sequence inserted into pSRNA	This study
pSRNA-murA	murA target binding sequence inserted into pSRNA	This study
pSRNA-rplD	rplD target binding sequence inserted into pSRNA	This study
pSRNA-rplP	rplP target binding sequence inserted into pSRNA	This study
pSRNA-rpsD	rpsD target binding sequence inserted into pSRNA	This study
pSRNA-rpsE	rpsE target binding sequence inserted into pSRNA	This study
pgRNA-bacteria	ApaLI ori, Amp^r, P_{AmpR}	Qi, et al. (2013)[45]
pS3	pBR322 ori, Amp^r, P_{lac}	Moore (1995)
pINT-GA(fbr)	ColE1 ori, Kan^r P_{PDC} (PDC Gene Promoter from *Z. mobilis) aroG*[15] and *pheA*[101] inserted into BglII and XhoI sites.	This study

Genomic DNA (gDNA) was prepared using the ZR Fungal/Bacterial DNA MiniPrep™ (Zymo Research) according to manufacturer protocols. DNA sequences were PCR amplified using a BioRad iCycler system with Q5® High-Fidelity DNA Polymerase (NEB) according to manufacturer protocols with custom designed DNA oligonucleotide primers (see Table A 1, Appendix B) synthesized by Integrated DNA Technologies (Coralville, IA). Amplified linear DNA was purified using the Zymo Research DNA Clean & Concentrator™ kit (Zymo Research). Purified DNA fragments and plasmids were digested using select restriction endonucleases (NEB) according to manufacturer protocols. Digested DNA fragments were separated using gel electrophoresis and purified using the Zymoclean™ Gel DNA Recovery kit (Zymo Research) and ligated with T4 DNA Ligase (NEB) according to manufacturer protocols. Ligation reactions were transformed into chemically competent *E. coli* DH5-alpha and selected for by plating on LB solid agar containing antibiotics, as appropriate. Transformant pools were screened with the use of colony PCR and confirmed by DNA sequencing.

Plasmid pKSV45 was a kind gift from Kristala Prather (MIT). [46] Plasmids pCDF-DUET, pACYC-DUET, and pRK415 were sourced from Novagen. To construct the pSRNA backbone vector, the Strep^{r}-cloDF13 and tetR-Ptet cassettes were PCR amplified from pCDF-DUET and pKSV45, respectively, and combined with a custom synthesized sRNA scaffold component (GenScript) using circular polymerase extension cloning (CPEC) (see Appendix A for complete sequence).[41,47] To construct each individual pSRNA vector for targeted growth arrest, custom DNA oligonucleotides were synthesized to include the target binding sequence unique to each respective gene target. Individual sRNA scaffold components were PCR amplified using said primers, and combined using CPEC resulting

in the construction of pSRNA-dnaE, pSRN-fabB, pSRNA-fabBH, pSRNA-fabD, pSRNA-fabG, pSRNA-fabH, pSRNA-fabI, pSRNA-folA, pSRNA-folD, pSRNA-folP, pSRNA-murA, pSRNA-rplD, pSRNA-rplP, pSRNA-rpsD, and pSRNA-rpsE (see Appendix B for target binding sequences).

To ultimately construct pINT-GA, first the intermediate plasmid pINT-Ppdc was constructed (not listed in Table 3). To construct pINT-Ppdc, pgRNA-bacteria was digested with *EcoRI* and *XhoI* to obtain the origin of replication (ColE1) and antibiotic resistance (*Kan*^{r}).[45] Then, the promoter for the pyruvate decarboxylase gene (*PDC*) in *Z. mobilis* ZM4 was PCR amplified and ligated with the digested pgRNA. The plasmid pINT-Ppdc contained *BglII* and *XhoI* sites after the promoter to allow for BioBrick-like insertions. Next, *aroG*^{15} was amplified via PCR from pS3 and inserted into the *BglII* and *XhoI* sites to create pPDC-aroG(fbr). Finally, *pheA*^{101} was PCR amplified from the genome of NST74 and inserted into the *BglII* and *XhoI* sites of pPDC-aroG(fbr) to create pPDC-aroGpheA(fbr), otherwise known as pINT-GA(fbr) in this paper.

2.3 Strain Construction

E. coli BW25113 was individually transformed with all growth-related sRNA plasmids: pSRNA-dnaE, pSRNA-fabB, pSRNA-fabBH, pSRNA-fabD, pSRNA-fabG, pSRNA-fabH, pSRNA-fabI, pSRNA-folA, pSRNA-folD, pSRNA-folP, pSRNA-murA, pSRNA-rplD, pSRNA-rplP, pSRNA-rpsD, and pSRNA-rpsE. This resulted in the construction of the corresponding fifteen BW25113 strains: BW-dnaE, BW-fabB, BW-fabBH, BW-fabD, BW-fabG, BW-fabH, BW-fabI, BW-folA, BW-folD, BW-folP, BW-murA, BW-rplD, BW-rplP, BW-rpsD, and BW-rpsE.

MG1655 was also individually transformed with the plasmid pSRNA-lacZ to target the *lacZ* gene, resulting in MG-lacZ.

Additionally, to construct the chloramphenicol, streptomycin, and tetracycline resistant background BW25113 strains, BW25113 was individually transformed with the plasmids pCDF-DUET, pACYC-DUET and pRK415 respectively.

Finally, to construct the BW25113 strains pINT-GA dnaE, pINT-GA fabD, pINT-GA fabH, pINT-GA folA, pINT-pINT murA, and pINT-GA rplD, *E. coli* BW25113 was co-transformed with the plasmids pINT-GA(fbr) and pSRNA-dnaE, pSRNA-fabD, pSRNA-fabH, pSRNA-folA, pSRNA-murA, and pSRNA-rplD, respectively.

2.4 Protocol for Seed Preparation

All seeds were inoculated in LB broth, and appropriate antibiotics were added using a working concentration of 1 microliter of antibiotics per milliliter of culture and any other relevant additives such as x-gal in the case of *lacZ* gene expression; a final concentration of 10 milligrams per liter, 100 milligrams per liter, 34 milligrams per liter, and 35 milligrams per liter were achieved for tetracycline, streptomycin, chloramphenicol, and kanamycin respectively, for relevant antibiotic resistant strains. Seeds for background strain BW25113 were prepared from a frozen stock by using a sterile pipette tip to introduce a visible amount of bacteria into LB. Seeds for the everything else, which contained plasmids, were generated from freshly transformed plates by selecting one bacterial colony and introducing it into LB, with appropriate antibiotics added to screen for colonies expressing antibiotic resistance. Seeds were incubated in a an automatic shaking incubator (Innova 44, New Brunswick Scientific) at 200 RPM and 32 °C for approximately twelve hours before use.

2.5 Screening Candidate Gene Targets for sRNA-Mediated Growth Arrest

To investigate potential gene targets for sRNA-mediated growth arrest, relevant strains were cultured in LB using 24 or 48 well plates (CytoOne, USA Scientific) with a working volume of one milliliter and one half milliliter, respectively. Overnight seed cultures, prepared as above, were used to inoculate well plates (1% v/v inoculum) supplemented with antibiotics, as appropriate. Well plates incubated in a microplate reader (Multiskan Spectrum, Thermo Scientific) for 36 hours at 480 rpm and 32 °C. During the 36 hour incubation period, well plate cultures were induced when reaching an optical density at 600 nm (OD_{600}) of ~0.4, by the addition of 1 mg/mL anhydrous tetracycline (aTc) to achieve a concentration of 0.5 μg of aTc per mL of culture. Well plate incubation then resumed. In the specific case of MG1655-lacZ and in addition to the relevant antibiotics to screen for transformants, 2 microliters per milliliter of 20 milligram per milliliter x-gal was added to achieve a concentration of 0.04 milligrams per milliliter for gene expression; it is also worth noting that these variants were induced at the start of the experiment.

2.6 Assaying Cell Morphology and Viability

To investigate the effects of sRNA-mediated growth arrest on cell morphology, relevant strains were cultured in M9 minimal media in 24 or 48 well plates (CytoOne, USA Scientific) for ~36 hours and imaged using a Zeiss AxioObserver D1 inverted microscope (Carl Zeiss MicroImaging Inc.). To investigate the effects of sRNA-mediated growth arrest on cell viability, relevant strains were cultured once more in M9 media, but in a shake flask environment. Then before imaging, staining using the LIVE/DEAD BacLight Bacteria Viability Kit (Molecular Probes) according to manufacturer protocol was

performed at the 42 hour mark. As before, cells were observed using a Zeiss AxioObserver D1 inverted microscope (Carl Zeiss MicroImaging Inc.). Sample preparation for microscopy analyses consisted of transferring cells (5 microliters) to 25 x 75 mm glass microscope slides (Santa Cruz Biotechnology), and cover slipping with 18 x 18 mm glass cover slips (Santa Cruz Biotechnology); the shaker flask experiments reached much higher cell densities, so in this case cells were diluted for imaging purposes. Microscope images were post-processed and analyzed using ImageJ software, where a cell size distribution was generated using the built-in particle analysis tool (see Appendix E for protocol).[48,49]

2.7 Metabolic Analysis of Contents in Shake Flask Cultures

Overnight seed cultures were used to inoculate (1% v/v inoculum) 50 mL M9 minimal media, containing 20 grams per liter of glucose and appropriate antibiotics. Strains were cultured in 250 mL baffled shake flasks at 32ºC and shook at 200 RPM; at an OD_{600} ~3.0, 25 microliters of 1 milligram per milliliter aTc was added. Culturing then resumed under the same conditions for a total of 72 hours, with periodic sampling for OD_{600} measurements and metabolite and catabolite analysis via HPLC, as described below. The pH was determined using Hydrion test strips with a range of detection from 4.5 to 7.5 (Micro Essential Lab) and manually maintained at 6.8 by periodic addition of 0.4 gram per milliliter K_2HPO_4 (Sigma-Aldrich).

2.8 HPLC Settings for Metabolic Analysis

Culture samples were first centrifuged at 11,000*g* for 3 minutes followed by subsequent supernatant transfer to glass HPLC vials; all samples were diluted 1:2 with 1 N HCl prior

to analysis. Metabolite analysis was performed using a Hewlett Packard 1100 series HPLC system. Separation of phenylalanine was achieved using a reverse-phase Hypersil Gold aQ C18 column (4.6 x 150 mm; Thermo Fisher) operated at 45ºC with a constant flow rate of 0.8 milliliters per minute consisting of 85% 5 *mM* H_2SO_4 and 15% acetonitrile. The eluent was monitored using a diode array detector (DAD) set at 215 nm. Glucose analysis was performed using the same HPLC system equipped with a RID detector and an Aminex HPX-87H column (BioRAD, Hercules, CA) operated at 35ºC, eluted with a constant flow rate of 0.55 milliliters per minute consisting of 5 *mM* H_2SO_4. External calibrations were developed and used to quantify each metabolite of interest.

3. RESULTS

3.1 Optical Density Screening Results in BW25113 Strain

After constructing the BW25113 strain and its variants, initial screening was performed in LB broth using a plate reader assay. A list of the names for all the strains used for this screening process may be seen in Appendix C, while Appendix F shows the OD_{600} versus time data for the screening process in LB. After gauging the response of the dynamic optical density data in LB, the candidates were analyzed in M9 minimal media; the initial LB screening served as indication that should the strains not grow in M9 media, it is the result of a missing essential nutrient which may be found in LB.

The proceeding figures detail the results of the plate reader assay in M9 media for all BW25113 pSRNA variants. In the screening process, anhydrous tetracycline was added to achieve a final concentration of 0.5 micrograms per milliliter, at an OD_{600} of approximately 0.4 to induce the sRNA plasmid early on in the exponential growth phase to activate expression; this concentration of anhydrous tetracycline used was shown effective to activate gene expression while not influencing the OD_{600} behavior of background strain BW25113 without the sRNA plasmid, as seen in Panel A of Figure 5 below.

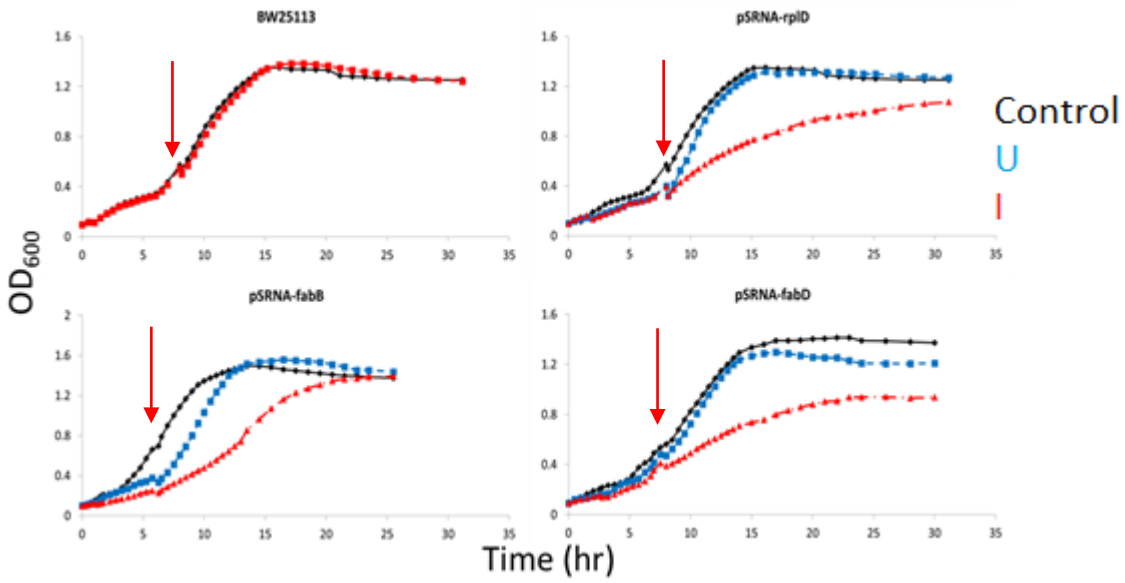

Figure 6: The Relationship between OD_{600} and Time after the Addition of Anhydrous Tetracycline (Induced, Red) at an OD_{600} of 0.4 for BW25113 (Control, Black) and pSRNA Variants (Uninduced, Blue) Grown in M9. BW25113, top left; BW-rplD, top right; BW-fabB, bottom left; BW-fabD, bottom right.

As seen in the figure above, *fabB* was not an effective gene target relative to *fabD* and *rplD*; while the addition of aTc apparently slowed the exponential growth phase in all cases seen above, growth seems to pick back up in the case of *fabB* and reach the OD_{600} of the uninduced and background strain. The growth does not appear to ever reach the final value of the control strains in the case of *rplD* or *fabD*, though it is interesting to note the increased OD_{600} of the uninduced wild type strain in the case of the *fabD* gene target. In all cases seen in Figure 5 above, the uninduced strain has a similar growth profile to the background strain, except in the case of *fabB*, where the uninduced pSRNA variant appears to experience a slight lag in reaching exponential growth phase, but otherwise remains the same. It is also worth noting in Figure 5 above that all the strains above appeared to grow at the same rate during exponential growth phase and have a

similar lag phase. The figure below shows other interesting data, the results of the plate reader assay for the *fabI*, *fabG*, *folA*, and *folD* gene targets,

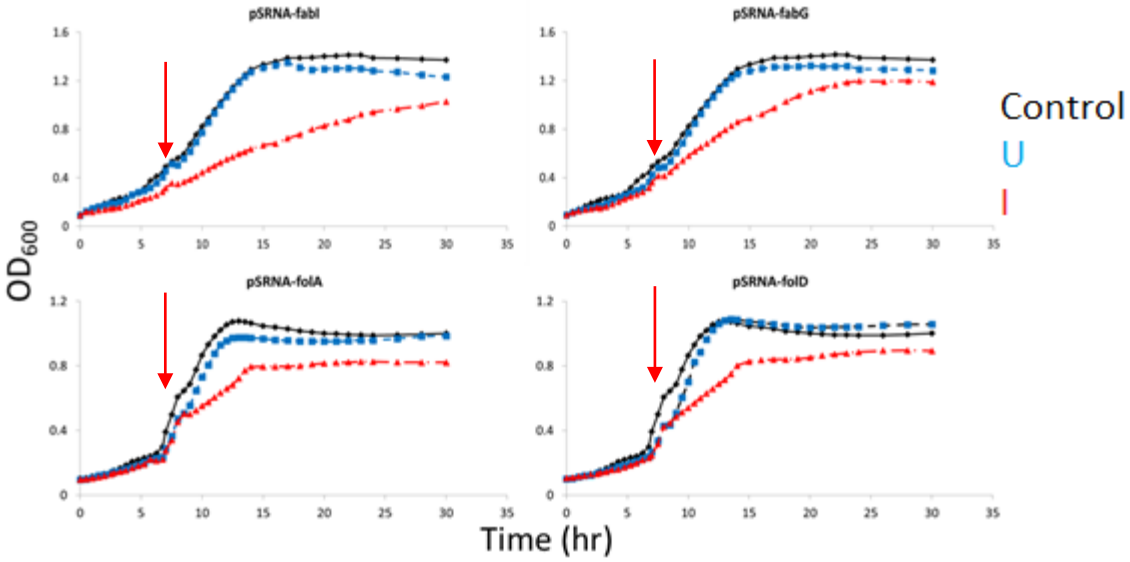

Figure 7: The Relationship between OD_{600} and Time after the Addition of Anhydrous Tetracycline (I; Induced, Red) at an OD_{600} of 0.4 for BW25113 (C; Control, Black) and pSRNA Variants (U; Uninduced, Blue) Grown in M9. BW-fabI, top left; BW-fabG, top right; BW-folA, bottom left; BW-folD, bottom right.

In the figure seen above, the induced *fabI* and *fabG* pSRNA variants never seem to experience an immediate cease in growth like the *folA* and *folD* variants; furthermore, the induced *fabG* strain in particular does not appear to have significantly diminished the OD_{600}. While all four variants above had relatively similar lag phases, the *folA* and *folD* strains had a fast exponential growth phase indicating they might be good to consider for a scale-up application as they may be cultured with greater predictability. Seen below in Figure 7 is the relationship for the gene targets *folP*, *murA*, *rpsD*, and *rplP*,

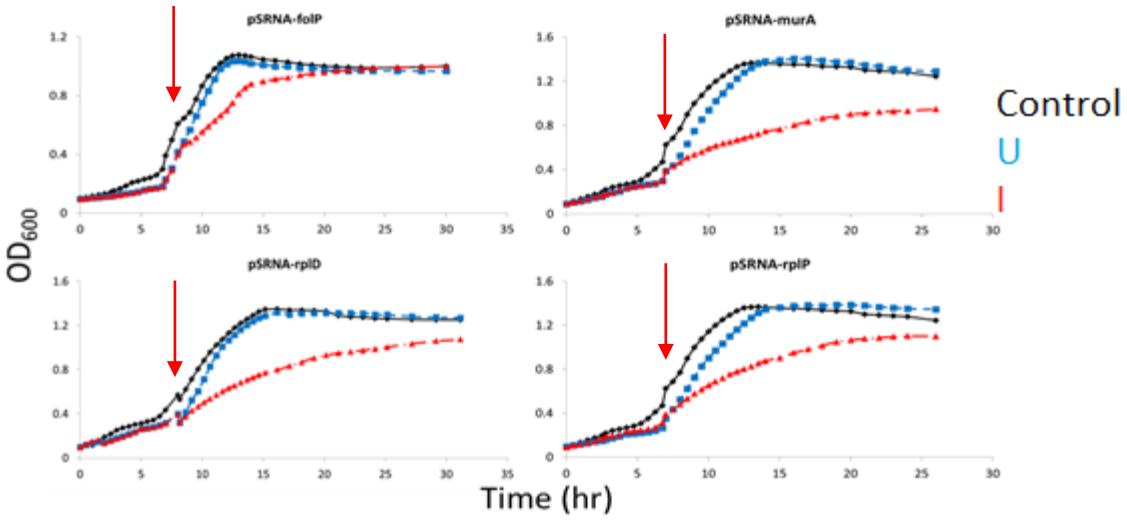

Figure 8: The Relationship between OD_{600} and Time after the Addition of Anhydrous Tetracycline (Induced, Red) at an OD_{600} of 0.4 for BW25113 (Control, Black) and pSRNA Variants (Uninduced, Blue) Grown in M9. BW-folP, top left; BW-murA, top right; BW-rpsD, bottom left; BW-rplP, bottom right.

In the figure seen above, it appears that both *folP* and *rpsD* did not have a significant reduction on the OD_{600} relative to the background strain; the *murA* strain resulted in a lower OD_{600} relative to the background strain, but it is interesting to note that neither *murA* nor *rplP* had the same immediate cease in growth that *folA*, *folD* and even, to a degree, *folP* appeared to show above. All four strains had similar lag phases and growth rates during the exponential growth phase; once more it is worth noting the slight overall lag associated with the uninduced pSRNA variants, though it does not result in a diminished optical density it is consistent across many cases. This could be due to the streptomycin resistance putting a burden on the cells, which is further investigated. In Figure 8 seen below, the final four gene targets, *rpsE*, *fabBH*, *dnaE*, and *fabH* are explored,

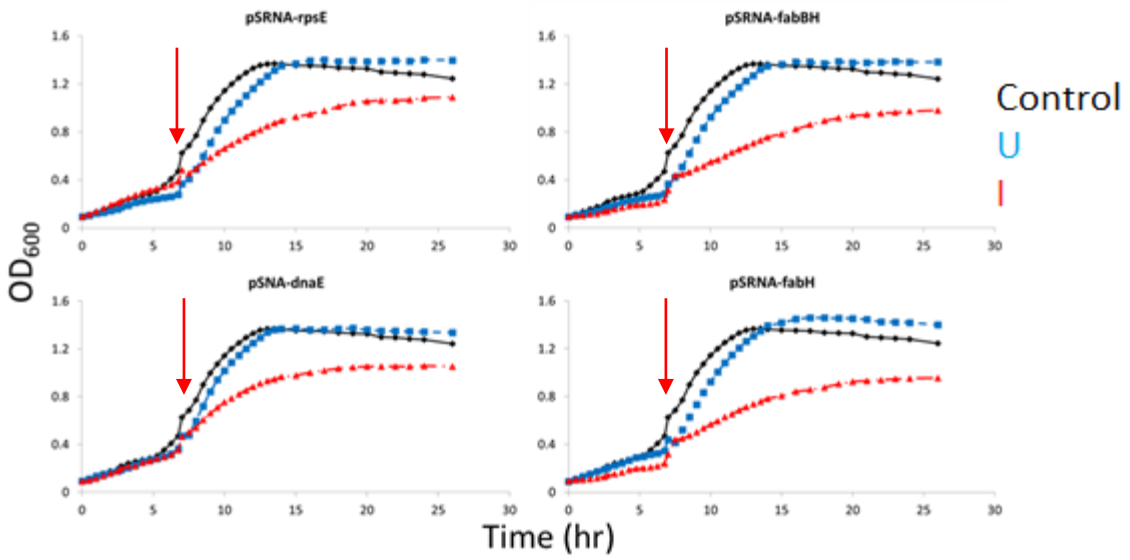

Figure 9: The Relationship between OD_{600} and Time after the Addition of Anhydrous Tetracycline (Induced, Red) at an OD_{600} of 0.4 for BW25113 (Control, Black) and pSRNA Variants (Uninduced, Blue) Grown in M9. BW-rpsE, top left; BW-fabBH, top right; BW-dnaE, bottom left; BW-fabH, bottom right.

In the figure above, the first thing to note is once more the shift in growth associated with the uninduced pSRNA variant, as was the trend in many cases before. Another thing to consider is the similar lag phases and productivity during exponential growth phase, as was also a trend seen in earlier pictures. However, the targets *fabBH*, *dnaE*, and *fabH* appeared to do a considerable job at stopping growth. The gene target *rpsE* performed relatively well compared to other gene targets such as *rpsD* and *folP* as seen in Figure 7. Finally, in Figure 9 below, a summary of the OD_{600} relative to the uninduced background strain at the final time point for the induced and uninduced pSRNA variants may be taken into consideration,

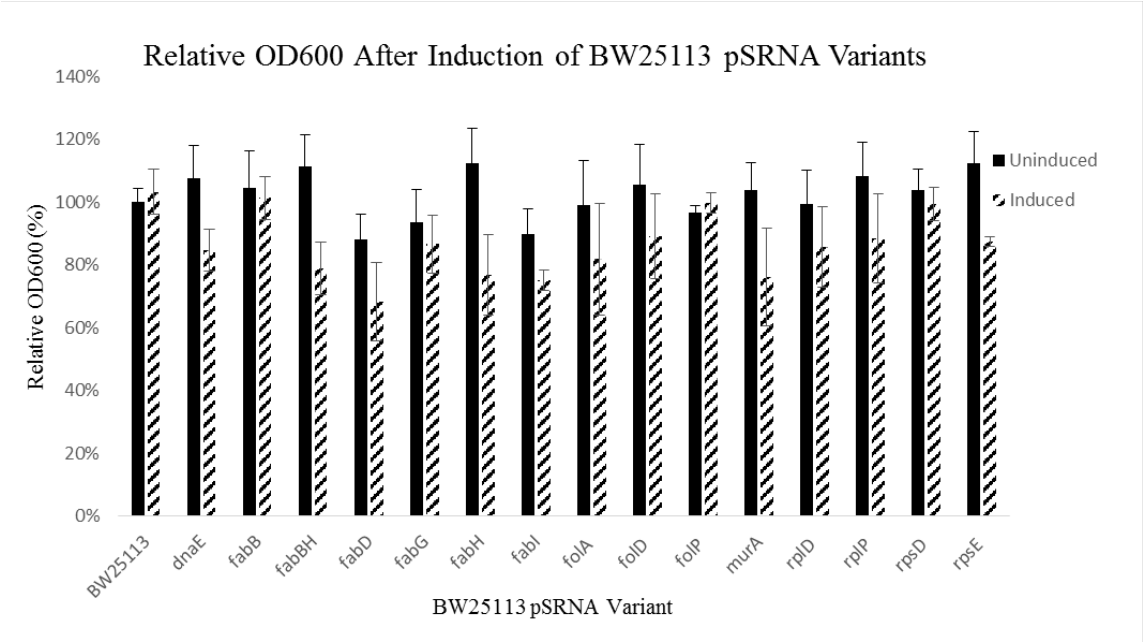

Figure 10: A Comparison of the OD_{600} Relative to the Uninduced Background Strain BW25113 for the Induced and Uninduced pSRNA Variants.

The bar graph seen above warrants comparison of the large number of candidates in a fashion where general trends may be easier to visualize. The black bars seen in the graph above represent the uninduced wild-type BW25113 and the respective uninduced pSRNA variants, which more or less are within 20% of the uninduced background strain; the striped bars represent the induced pSRNA variants, and in the case of these candidates there is a diverse response though in general it is clear that growth is suppressed. Some candidates such as *fabB*, *fabG*, *folP*, and *rpsD* did not appear to significantly diminish growth, while others such as *fabI*, *folD*, and *rpsE* were more effective, but had interesting morphology as will be seen below. The six candidates chosen for phase two of this study had effective growth inhibition and interesting morphology changes; these candidates are *dnaE*, *fabD*, *fabH*, *folA*, *murA*, and *rplD*. It is interesting to note that all of the genes targeted were shown to be essential for viability with the exception of *fabH*; thoughts on potential reasons for the performance observed is summarized in the discussion section.

3.2 Morphology Screening Results in BW25113 Strain

Following each plate reader experiment that occurred in the M9 minimal media using the BW25113 pSRNA variants, each well plate was imaged on slides using a microscope; a relative size distribution of the cell sizes using the ImageJ automatic particle analysis tool was performed to quantify the changes in morphology for each strain (protocol found in Appendix E). The images below represent small sections of a larger image which was captured at this same resolution; a cut-out essentially, for the purposes of visualization. A scaled down version of the larger image would render the cells undistinguishable from the background. Seen below in Figure 10 are the morphology results for the background strain, in Panel A, and the first three pSNA variants targeting the genes *dnaE*, *fabB*, and *fabBH*, as seen in Panels B, C, and D respectively.

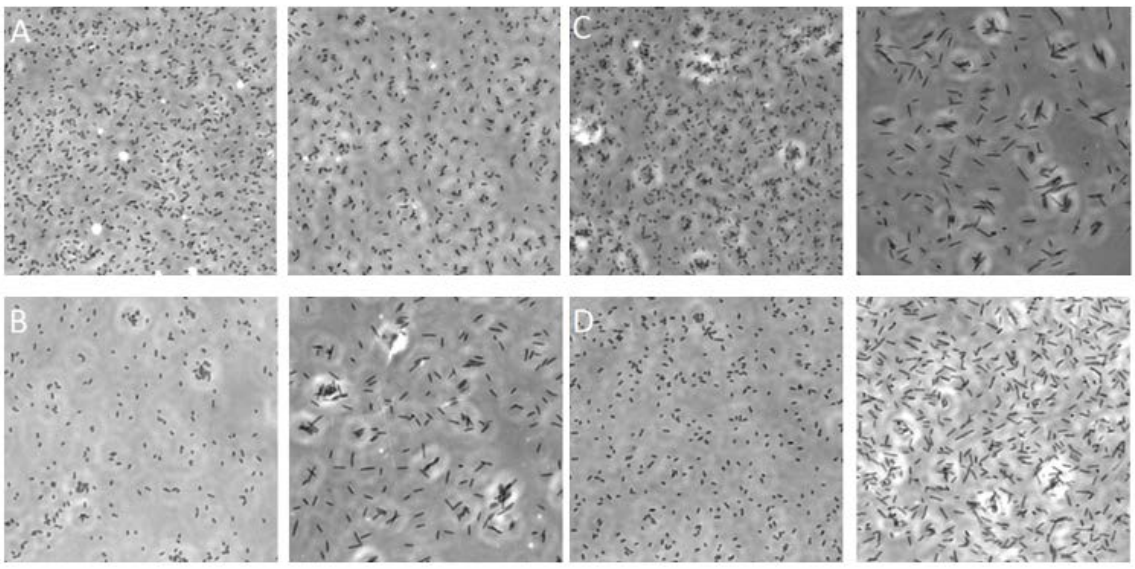

Figure 11: Microscopy Images Showing morphology of Uninduced (Left) and Induced (Right) Cells for BW25113 pSRNA Variants Grown in M9 at the Final Time Point from the Plate Reader Assay; Panel A: BW25113, Panel B: BW-dnaE, Panel C: BW-fabB, Panel D: BW-fabBH.

It is clear in the case of Panel A from inspection by the naked eye that the morphology of the induced cells is not significantly different from that of the uninduced background strain when comparing to the changes in morphology observed in panels B, C, and D. In the latter panels, the morphology changes are a more evident after induction; the cells have a more rod-like, longer profile resulting in a larger size which is visible to the naked eye, indicating filamentation occurred to some degree. A similar trend follows suit for the rest of the induced strains that have the pSRNA plasmid, indicating the increase in size may be a result of anhydrous tetracycline activating the promoter for the afsRNA, or possibly the streptomycin resistance; quantifying the relative size change and looking at this in combination with the optical density results may elucidate a correlation between growth inhibition and increased cell size.

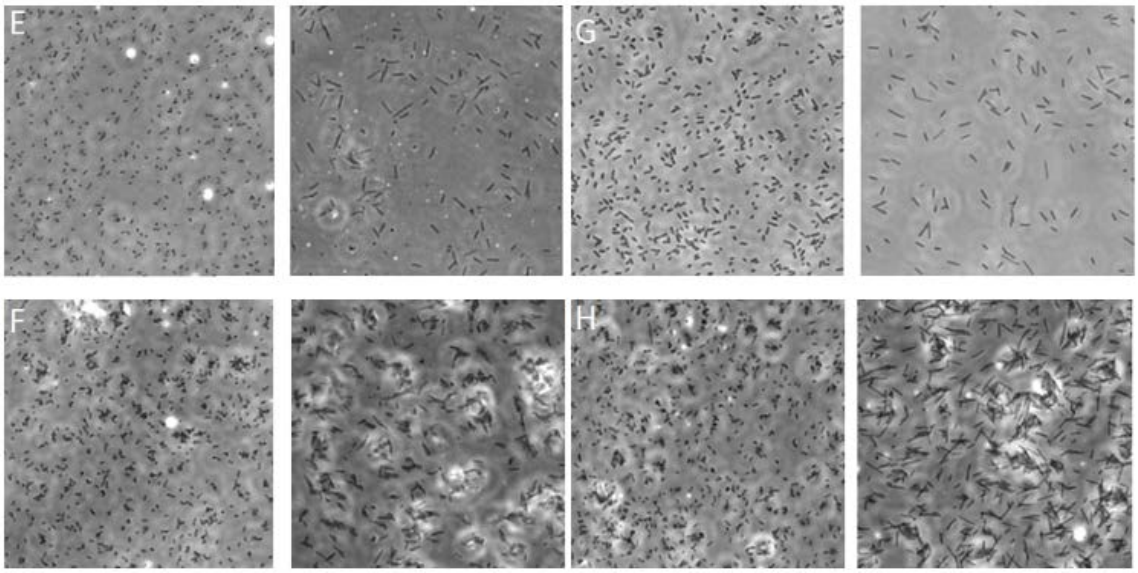

Figure 12: Microscopy Images Showing morphology of Uninduced (Left) and Induced (Right) Cells for BW25113 pSRNA Variants Grown in M9 at the Final Time Point from the Plate Reader Assay; Panel E: BW-fabD, Panel F: BW-fabG, Panel G: BW-fabH, Panel H: BW-fabI.

Seen above in Figure 11 are the microscopy pictures for the candidates *fabD*, *fabG*, *fabH*, and *fabI*; it appears in all four cases that the uninduced variants appear to have the same smaller morphology as the background strain, indicating the presence of the plasmid may not affect the size of the cell when uninduced. The induced variants however show the same longer, rod-like morphology seen before. The same may be true for the cases of *folA*, *folD*, *folP*, and *murA* seen below in Figure 12,

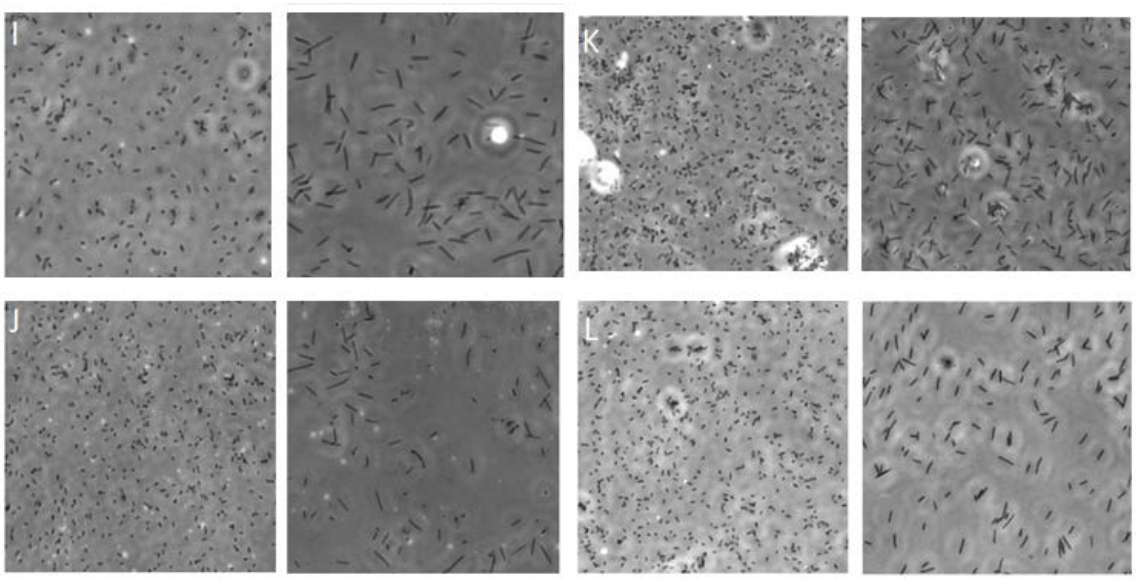

Figure 13: Microscopy Images Showing morphology of Uninduced (Left) and Induced (Right) Cells for BW25113 pSRNA Variants Grown in M9 at the Final Time Point from the Plate Reader Assay; Panel I: BW-folA, Panel J: BW-folD, Panel K: BW-folP, Panel L: BW-murA.

As noted, there is a trend in the morphology between the induced and uninduced variants, but this trend is hard to quantify with the naked eye and requires quantification to investigate the relationship between the degree of growth suppression and the degree of size. While the suppression of growth using the afsRNA seems to go along with an increase in cell size, and uninduced afsRNA results in cell sizes equivalent to the background strain, the images show that strains in which growth was not significantly

suppressed, relative to the uninduced background strain and the uninduced corresponding pSRNA variant, still experienced some degree of size increase. While this indicates another potential application for the afsRNA – to control cell size without affecting optical density and see how the resulting filamentation affects nutrient flux to the cell – the degree to which this is possible is outside the scope of this investigation and was not further pursued. Nonetheless, as was the case in the figures above, the same morphology differences in the induced and uninduced pSRNA variants may be seen below in Figure 13,

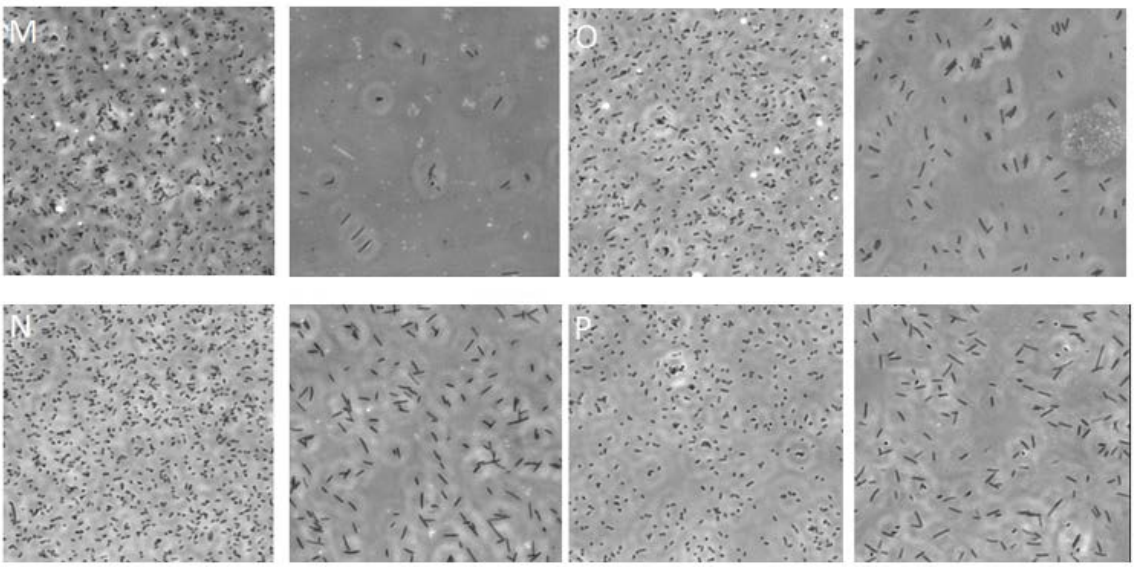

Figure 14: Microscopy Images Showing Morphology of Uninduced (Left) and Induced (Right) Cells for BW25113 pSRNA Variants Grown in M9 at the Final Time Point from the Plate Reader Assay; Panel M: BW-rplD, Panel N: BW-rplP, Panel O: BW-rpsD, Panel P: BW-rpsE.

In summary, the microscopy pictures show clear changes in morphology after the aTc-inducible promoter was activated; these morphology changes were quantified using ImageJ to determine if activation of the plasmid containing the afsRNA resulted in changes to cell morphology. Quantifying these changes in cell morphology enables them

to be compared to the changes in optical density to discern important trends in the data. It is worth reiterating the protocol used to quantify morphology changes may be found in appendix E. The bar graph shown below in Figure 14 represents a similar metric to that shown in Figure 9, wherein the relative size change compared to the uninduced background strain BW25113 is taken into consideration. This once more allows a nice way to summarize the general results for the large number of candidates,

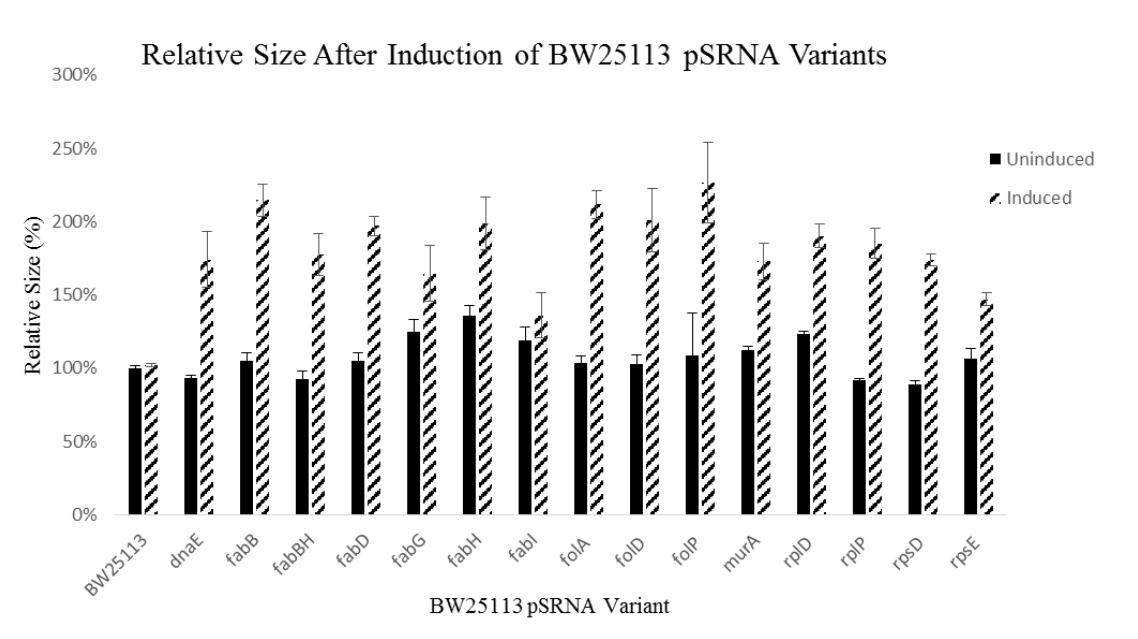

Figure 15: Relative Cell Size for the BW25113 pSRNA Variants With and Without Anhydrous Tetracycline Induction; Cells Cultured in M9 Media.

The morphology changes for most of the pSRNA variants are very robust, indicating for cases like *folP* and *fabB* that even when optical density was relatively unaffected, morphology was still changed. Nonetheless, the uninduced variants for the most part have similar cell size relative to the uninduced background strain, while the induced background strain shares a nearly identical size with this strain. This filamentation seen in the induced variants indicates there might be stress on the cells, and could be a result of

the cells trying to increase nutrient flux to mitigate for the suppressed vital gene function; the slight filamentation seen in some of the uninduced variants may also suggest that the plasmid based approach is stressful to the cell as well. In order to establish a candidate selection process for the second phase of this study while also further analyzing the relationship between the optical density and cell size, a scatter plot was generated for the induced variants which may be seen in Figure 15 below,

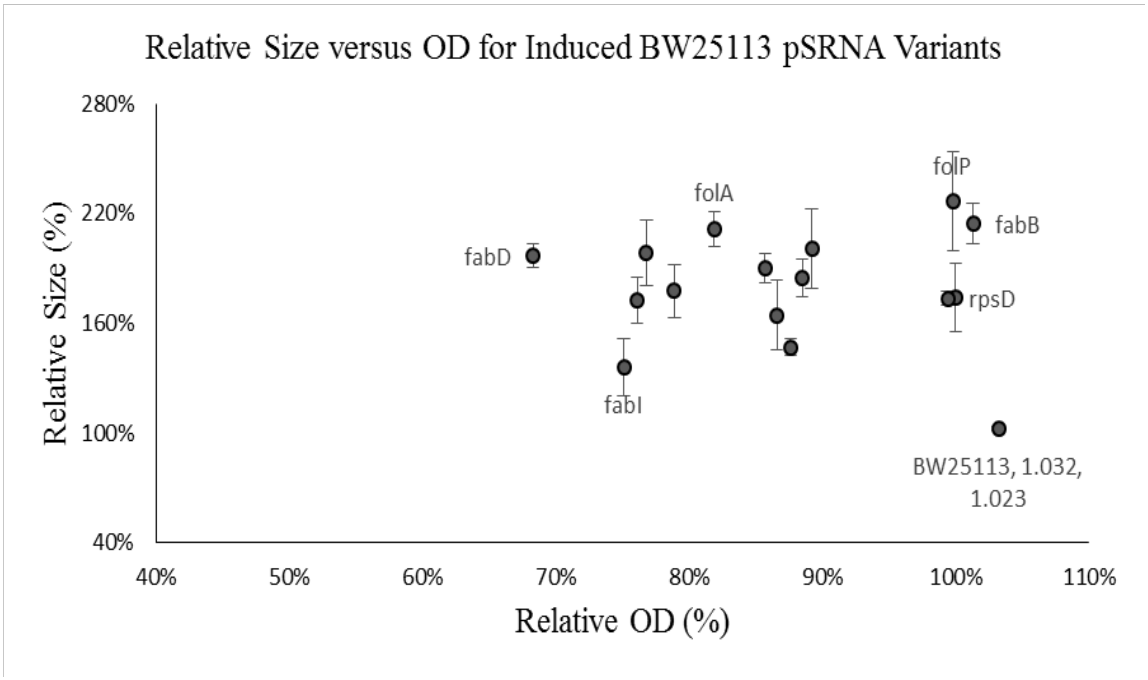

Figure 16: A Scatter Plot Illustrating the Relative Size versus the Relative OD for Induced pSRNA Variants at the Final Time Point of the Plate Reader Assay

The figure above shows interesting results as it is now easier to visualize the robust morphology changes associated with the induced pSRNA variants, but it also shows the large distribution in relative OD_{600} change. This could imply that even when growth is not suppressed, the afsRNA or streptomycin resistance on the plasmid still results in an increased cell size; the lack of growth suppression could indicate the gene being targeted is not growth essential. This could also mean that when transcription of the targeted gene

is inhibited using the afsRNA, it puts a burden on the cell that may be overcome by increasing nutrient flux by increasing cell size. As a final possibility, activation of the anhydrous tetracycline promoter or streptomycin resistance on the plasmid may contribute to the increased cell size independent of the functionality of the sRNA scaffold on the plasmid, but this is unlikely because different changes in cell size were seen depending on each of the genes being targeted, and targeting different genes requires changing the seed region of the sRNA scaffold implying that the gene being targeted by the sRNA, at least to some degree, has an effect on the cell size. While any background changes in cell size associated with simply activating the aTc promoter would be unavoidable using the plasmid-based system at hand, detecting if this is a contributing factor may be possible by constructing a strain without the sRNA scaffold but still containing the promoter and terminator and gauging the effect on cell size after induction. Integrating the plasmid onto the chromosome where it would not need any promoter or antibiotic resistance may eliminate any background increases in the cell size. Nonetheless, there is a large cluster of candidates encompassing OD_{600} that ranges from 75% to 90% of the uninduced background strain, but there are also targets like *fabD* which appear to have a significantly diminished OD_{600} with a larger cell size, and targets like *fabB* where the cell size is still significantly increased, but the OD_{600} is nearly the same as the uninduced background strain. Based on the optical density results seen in Figure 5 through Figure 8, coupled with the microscopy results summarized in Figure 14 while taking into consideration the mechanism of action associated with each target gene, six candidates from this initial pool of sixteen were selected for progression. The six

candidates that are further explored in the following sections of the results are BW-dnaE, BW-fabD, BW-fabH, BW-folA, BW-murA, and BW-rplD.

3.3 *lacZ* and Bacteriostatic Screening Results in BW25113 Strain

To supplement the results above and gain more insight in regards to the underlying mechanism of the sRNA, the strain MG1655 was used to screen the ability of the pSRNA plasmid to suppress gene function without inhibiting growth as this strain contains the *lacZ* gene, which enables the cells to metabolize lactose; metabolizing an analogue compound of lactose, x-gal, results in the cells expressing a visibly blue phenotype. This sheds light on the efficiency of the inducible-sRNA system to block translation of a desired gene while also elucidating inherent side effects which may be growth-associated as only the metabolism of lactose should be inhibited when the sRNA system is induced and growth should otherwise not be affected. These inherent, growth-associated side effects that would be obvious in the case of targeting a gene like *lacZ* would otherwise be masked by targeting the growth-essential genes, as their primary purpose is to suppress growth anyways. Seen below are the results from the *lacZ* experiment in MG1655 in M9 media,

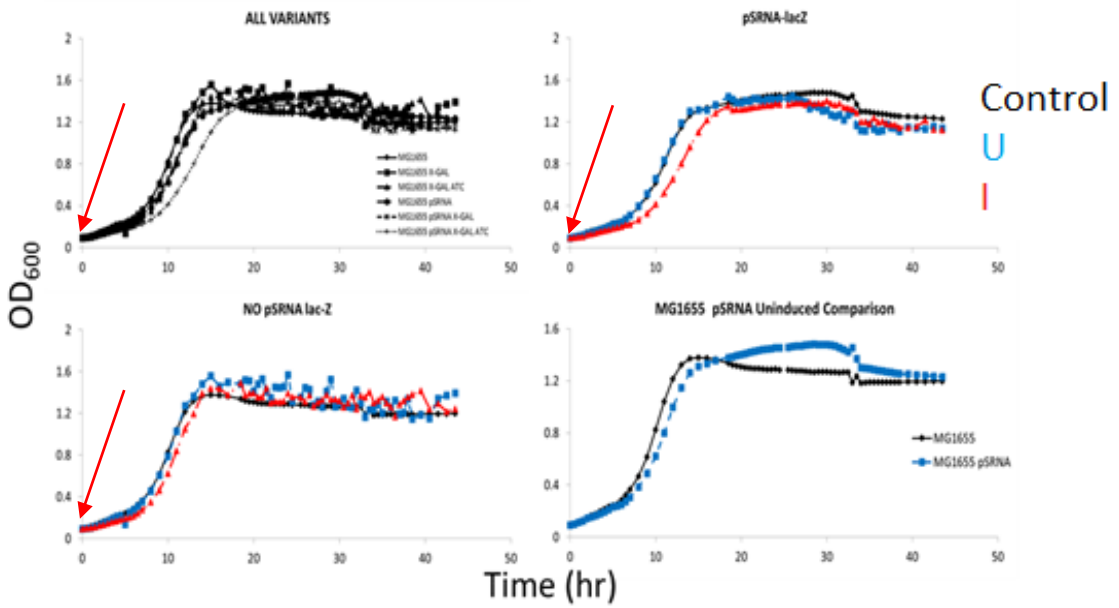

Figure 17: The Relationship between OD_{600} and Time after the Addition of Anhydrous Tetracycline (Induced, Red) at an OD_{600} of 0 for MG1655 (Control, Black) and MG-lacZ Variants (Uninduced, Blue) Grown in M9. All Variants, Top Left; Only MG-lacZ Results, Top Right; Only MG1655 Results, Bottom Left; Uninduced Comparison, Bottom Right.

It is interesting to note in the figure above the strong variation seen particularly in the MG1655 and MG1655-lacZ strain where x-gal was added – the variation in OD_{600} is likely due to the precipitation of the blue product associated with the metabolism of x-gal. Nonetheless this experiment shows the sRNA does not appear to have much of a burden on genes which are not growth essential as there is a relatively unscathed growth profile for the induced pSRNA-lacZ variant, though it did keep the cells from turning blue.

In the figure above it may also be seen in the MG1655 and MG-lacZ strain wherein no x-gal or aTc was added that the strains have a relatively similar growth profile, and overall it appears the aTc did not have an effect on the background MG1655 strain at all.

Seen below are the resulting microscopy images; it is clear from inspection that the cells are all relatively the same size,

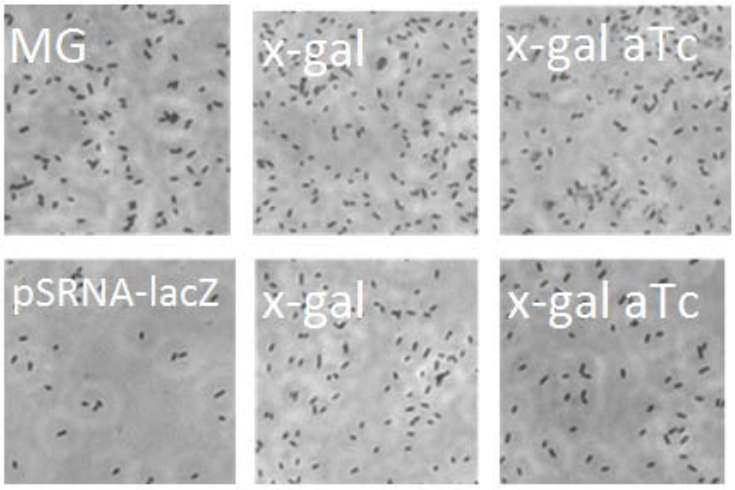

Figure 18: Microscopy Images Showing Morphology of MG1655 (Top Row) and MG-lacZ (Bottom Row) Grown Grown in M9 (Left), with the Addition of x-gal (Middle) and with the Addition of x-gal and aTc (Right), at the Final Time Point from the Plate Reader Assay.

The images above show there is not much filamentation present in the induced cells, nor in the cells where x-gal was added. It also shows the presence of the pSRNA-lacZ plasmid did not result in filamentation as MG-lacZ without x-gal and aTc seemed to have a similar morphology as well. The cell sizes were quantified as seen below,

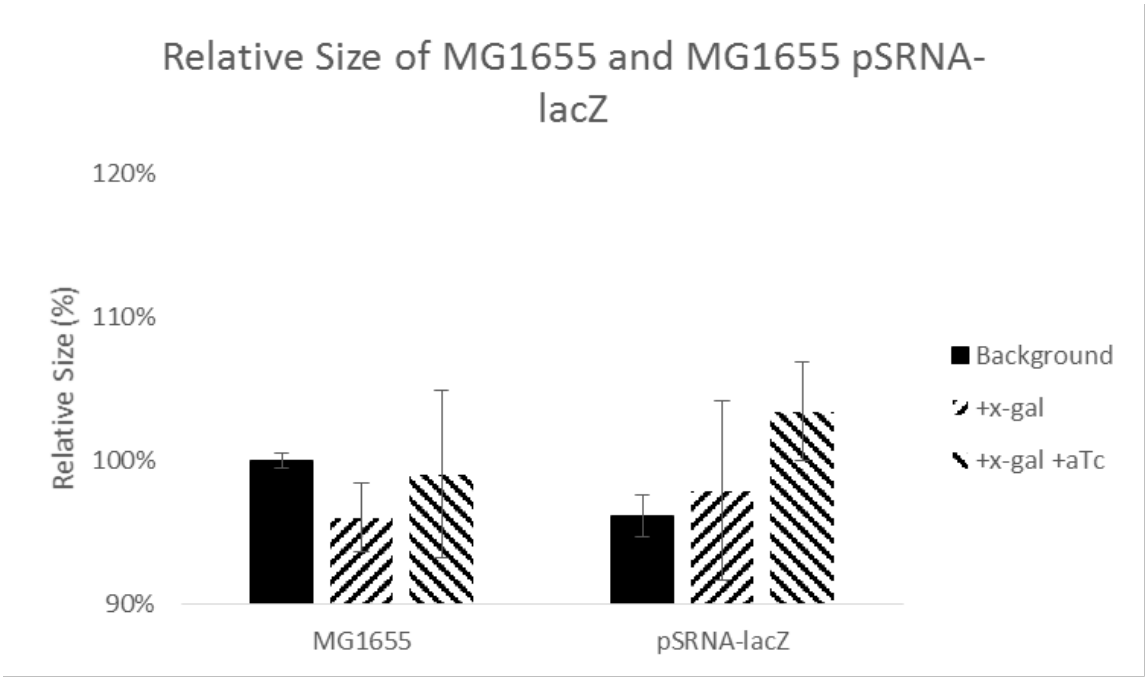

Figure 19: Relative Cell Size for the MG1655 pSRNA Variants With and Without x-gal and Anhydrous Tetracycline Induction; Cells Cultured in M9 Media.

It is worth noting that the size difference is very small relative to the uninduced background strain for all variants; while the pSRNA-lacZ variant that was induced with x-gal and aTc seemed to have the largest change in size, it was not significant and the microscopy images show that it did not result in filamentation. This suggests the size differences seen were a result of the sRNA targeting growth essential genes. In a similar fashion as before, a scatterplot may be seen below in which the relative size and optical density are shown in the same graph,

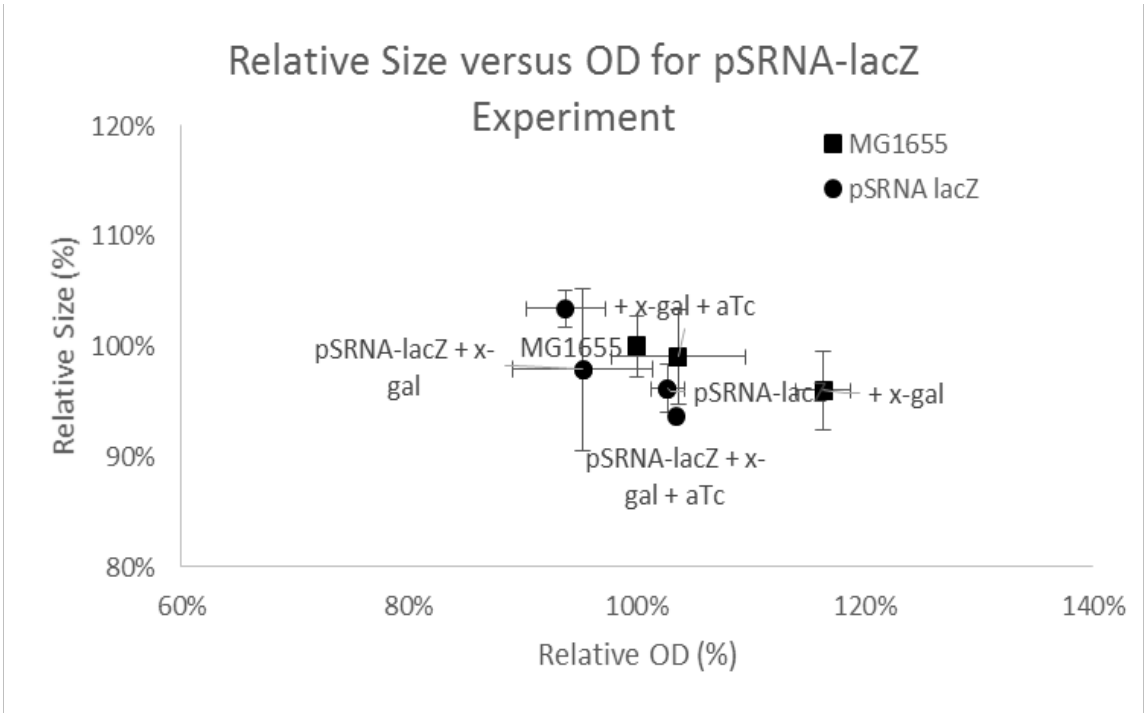

Figure 20: A Scatter Plot Illustrating the Relative Size versus the Relative OD for the *lacZ* variants at the Final Time Point of the Plate Reader Assay.

While this graph reinforces the tight data in which there does not seem to be much of an effect of the optical density as a result of targeting the non-growth essential gene *lacZ* it also supports the results from the first phase of the study wherein it was found that the filamentation does not have a significant effect on the optical density. It is worth considering in this case in particular that the filamentation was not significant in any of the cells and the growth was also not suppressed; this suggests the sRNA is responsible for growth suppression and that this is a result of targeting growth essential genes.

To also gauge the inherent effect of the common bacteriostatic additives chloramphenicol, tetracycline, and streptomycin in regards to growth suppression and morphology, an experiment was conducted wherein these additives were used to suppress growth in wild-type BW25113 and the resulting morphology was quantified; in this

experiment, a BW25113 strain resistant to each of these bacteriostatic additives was also generated to gauge the inherent morphology changes associated with these additives even in a scenario where growth should not inhibited. This is insightful as the BW25113 pSRNA variants all have streptomycin resistance and the pINT-GA pSRNA variants additionally have chloramphenicol resistance so it once again may show growth related side-effects associated with this plasmid based system; while it appears that the morphology of the BW25113 pSRNA variants is unaffected based on the results from the uninduced pSRNA variants relative to the uninduced background strain, it is insightful to see if this is also the case for chloramphenicol and tetracycline. Seen below is the resulting optical density response for the wild-type *E. coli* BW25113 strain with the bacteriostatic additives, and the relevant resistant variants,

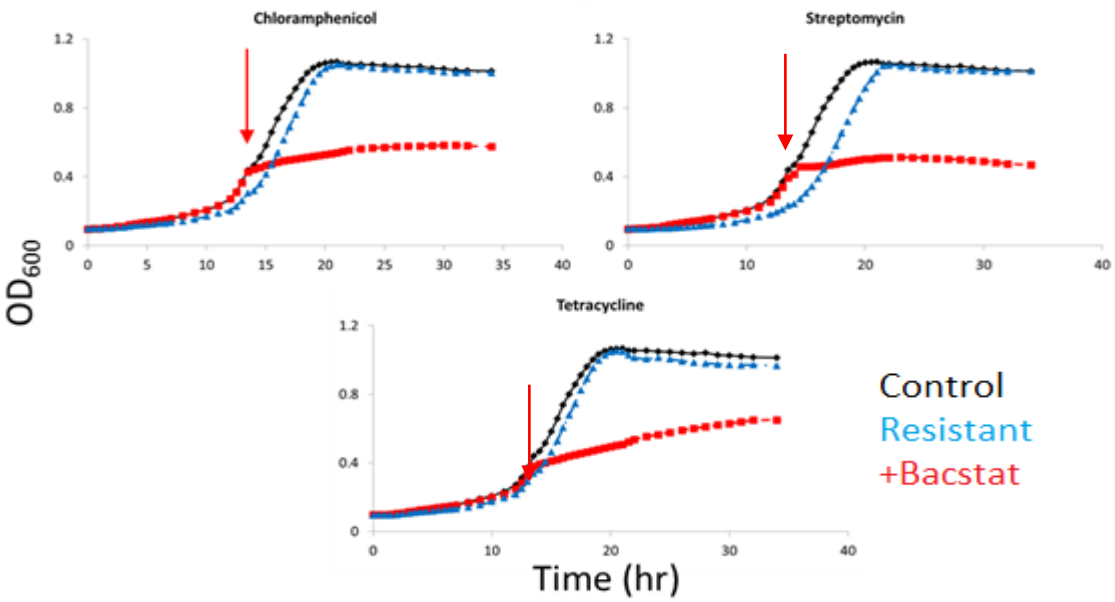

Figure 21: The Relationship between OD_{600} and Time after the Addition of Chloramphenicol (Top Left), Streptomycin (Top Right), and Tetracycline (Bottom Left) at an OD_{600} of 0.4 (Bacstat, Red) for BW25113 (Black, Control) and Resistant Strains (Blue) Grown in M9.

Though it may come as no surprise, the bacteriostatics effectively suppressed growth in the wild-type strain while not suppressing growth in the resistant strains. The growth suppression associated with the bacteriostatic additives takes effect much more rapidly than what was observed with the pSRNA approach, especially in the cases of streptomycin and chloramphenicol. In these cases, there is nearly no change in optical density once the cells are induced. The dynamic optical density data associated with the bacteriostatic resistant strains is also insightful; while there seems to be a delay associated with each resistant strain relative to the wild-type BW25113 strain, tetracycline has the smallest delay in growth while streptomycin has the largest delay in growth. The plasmid-based system used in the pSRNA approach relies on a streptomycin resistance, which may have further implications in scale-up approaches as there was a consistent lag seen in the growth of this strain relative to the background strain for many of the variants. This lag may be a result of the high concentration of streptomycin used in the plasmid selection process, 100 mg/L, but it may also be the result of the plasmid placing a burden on the cells. Nonetheless, also interesting is the resulting morphology from the aforementioned strains; in the microscopy pictures shown below, inspection with the naked eye reveals that all the cells appear to be of the same order of magnitude in terms of length scale, indicating that minimal filamentation occurs as a result of neither the bacteriostatic additives nor the plasmids providing resistance. Filamentation occurs as a result of stress on the cell amongst many reasons. Further inspection also reveals that chloramphenicol added to the wild-type BW25113 strain seemed to result in no morphology changes, with a consistent cell size. The streptomycin had a bit of

filamentation occurring, with a mix of cells that were small and large, but it is clear in the case of the tetracycline that consistent filamentation occurred.

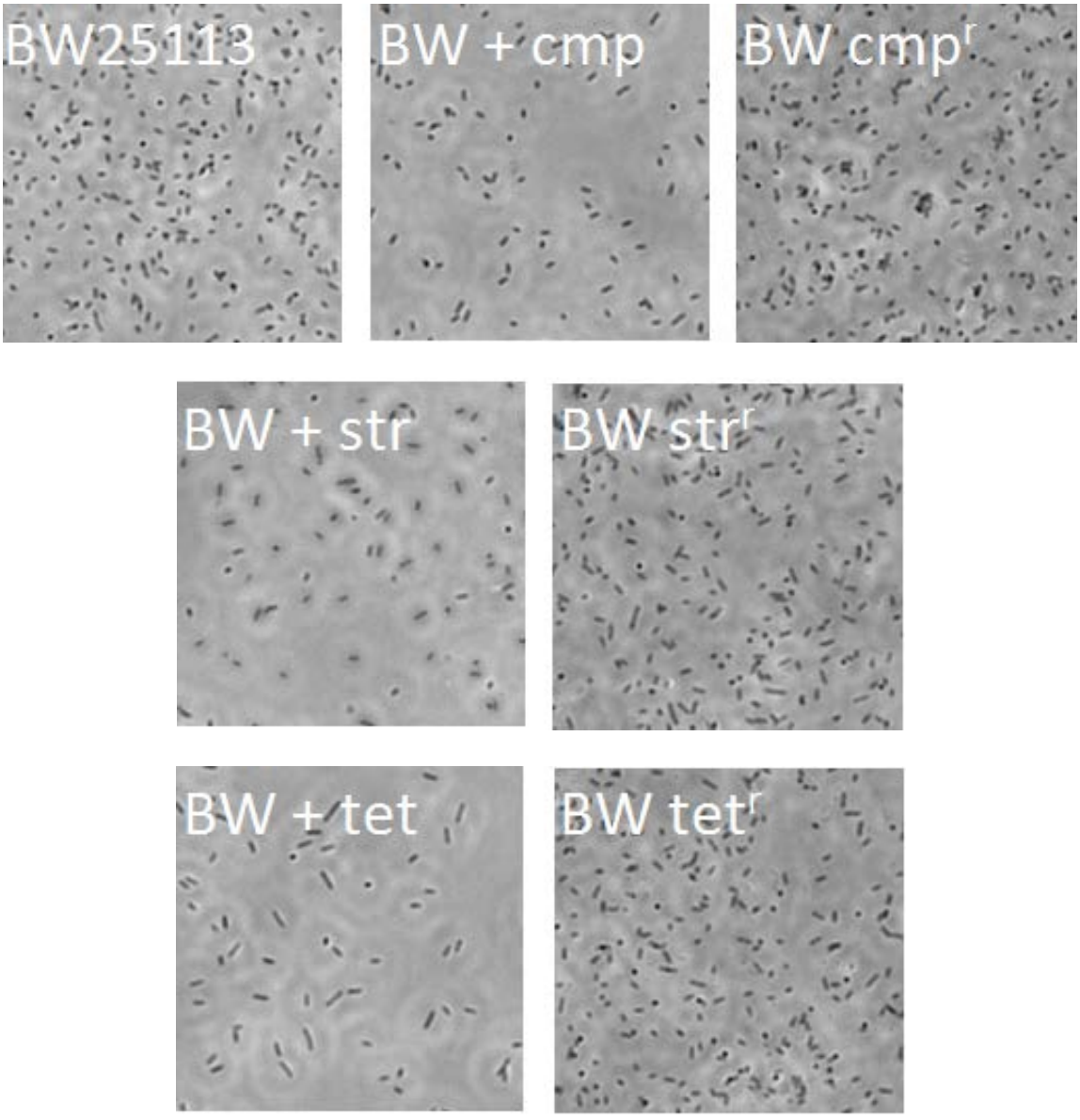

Figure 22: Microscopy Images Showing Morphology BW25113 and Relevant Resistant Strains with the Addition of Relevant Antibiotics, Grown in M9. Images Taken at the Final Time Point from the Plate Reader Assay.

Inspecting the BW25113-cmp, BW25113-str, and BW25113-tet strains which contain plasmids for resistance to chloramphenicol, streptomycin and tetracycline respectively, it

is fairly hard to distinguish any differences in the average cell size relative to the wild-type BW25113 strain. Seen below is an average cell size of all the cells, normalized to the cell size of the wild-type BW25113 strain,

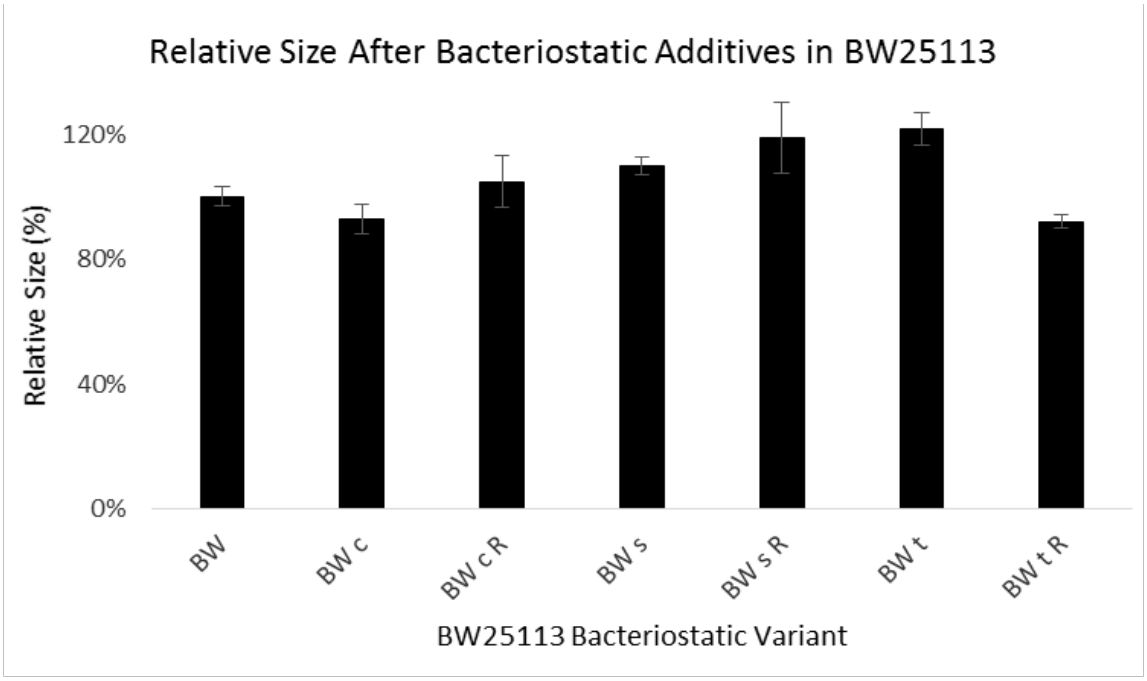

Figure 23: Relative Cell Size for BW25113 with Antibiotics and Antibiotic Resistant Strains; Cells Cultured in M9 Media.

This relative cell size distribution, when coupled with the dynamic optical density data, elucidates interesting trends. The BW25113 wild-type strain with tetracycline added took the longest to stop growth, and it resulted in the most filamentation amongst the bacteriostatic additive based approach; furthermore, the streptomycin-resistant BW25113-strep strain also took the longest to reach stationary phase, and it had the most filamentation amongst the plasmid-based strains. The filamentation associated with the streptomycin resistance may be a contributing background factor in the filamentation seen in the BW25113 pSRNA variants. To further gauge the relationship between the

optical density and the degree of filamentation, as was explored in the screening of the pSRNA system, an analogous scatterplot is presented in the figure below,

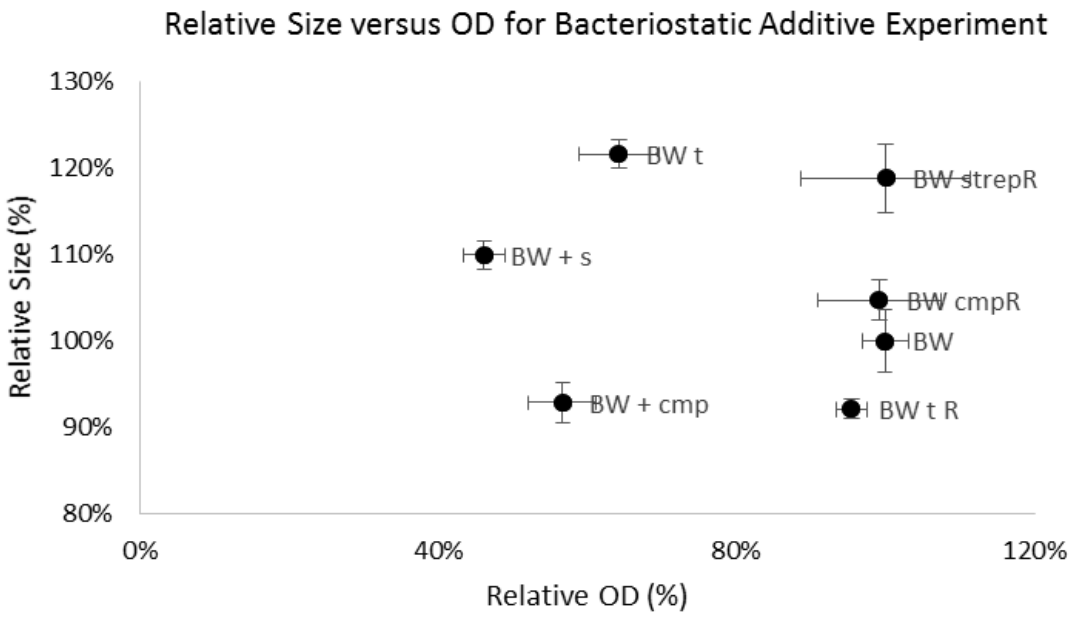

Figure 24: A Scatter Plot Illustrating the Relative Size versus the Relative OD for the Bacteriostatic Well-Plate Experiment at the Final Time Point.

In this figure it may be seen that there is once again no clear-cut relationship between the degree of growth suppression and the degree of filamentation from the data taken into consideration. While this does not suggest the filamentation does not influence the optical density measurements, because for the same quantity of cells, longer cells in theory may block more light, but this does suggest that the influence may not be straight-forward, or may be insignificant. The scatterplot is also useful as it shows the bacteriostatic resistant strains all have a similar final optical density relative to the control strain; furthermore, it shows that the bacteriostatics all had a very similar effect in growth suppression.

3.4 Viability and Metabolic Activity Screening Results in BW25113 Strain

After selecting the most viable candidates from the first phase of the study based on optical density and relative cell size data, scale-up to a working volume of 50 mL for culturing the cells was achieved to analyze the cell viability and metabolic activity. Scaling up the working volume from microplates to flasks also sheds light on plasmid stability. As mentioned in Section 2.8, glucose concentration was analyzed via HPLC.

Investigating the dynamic glucose consumption for each pSRNA variant may shed light into the mechanism by which resources are diverted after inhibiting growth through various growth essential gene targets. It is possible glucose consumption may decrease as the growth is inhibited, but it is not certain that this will lead to an increase in titer or productivity associated with a desirable product with an appropriate pathway engineering; it is also possible that glucose consumption may not decrease significantly when growth is inhibited, but it is also not certain that this will lead to decreased titer or productivity associated with a desirable product under appropriate engineered conditions. Ideally the variants should continue to consume glucose at an uninhibited rate after induction, mimicking the effect of bacteriostatic additives where only the optical density is suppressed but other metabolic functionality remains the same, but these possibilities demonstrate the need to characterize the pSRNA variants. Seen below is the data for the OD_{600} and the glucose consumption for the candidates discussed above. Each panel contains the strain mentioned in the title, both induced and uninduced; the uninduced variants are represented by closed circles and solid lines while the induced are represented by the opposite. The left axis represents the OD_{600}, and the right axis represents the glucose concentration in grams per liter. The lines representing the OD_{600}

are the ones which increase in all cases while the lines representing the glucose concentration are the ones which decrease in all cases.

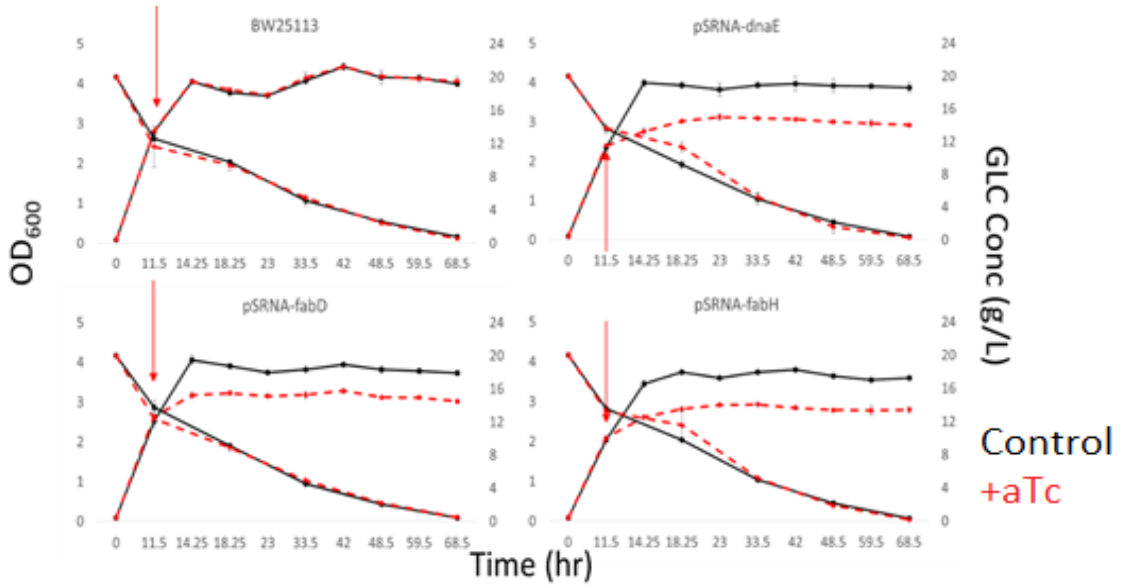

Figure 25: The Relationship between the OD_{600} (Left Axis), Glucose Concentration (Right Axis), and Time after the Addition of Anhydrous Tetracycline (Red) for the BW25113 Background Strain and Three pSRNA Variants Grown in M9 Media (Black). BW25113, Top Left; BW-dnaE, Top Right; BW-fabD, Bottom Left, BW-fabH, Bottom Right.

As mentioned, the four panels above and the three panels below show the results from the 50 mL flask cultures; in all cases the glucose concentration decreased with time, and the OD_{600} increased with time as would be expected. It may be seen in the case of the background strain that the anhydrous tetracycline had no effect on cells without the plasmid in regards to cell growth or metabolic activity; both the optical density and glucose consumption is unaffected. In the case of the other six BW25113 mutants, all were fairly effective at inhibiting growth in a reasonable amount of time – roughly five hours. The growth remained suppressed for the duration of the experiment as well, indicating a stable plasmid. Furthermore, all induced pSRNA variants consumed all the

glucose in the time of the experiment, at the same rate as the uninduced background strain, resulting in an inherently increased metabolic activity on a cellular level; the uninduced pSRNA variants showed a similar metabolic activity to that of the background strains considering the similar final cell density and glucose concentration, and as a result had a very similar metabolic activity to the background strain.

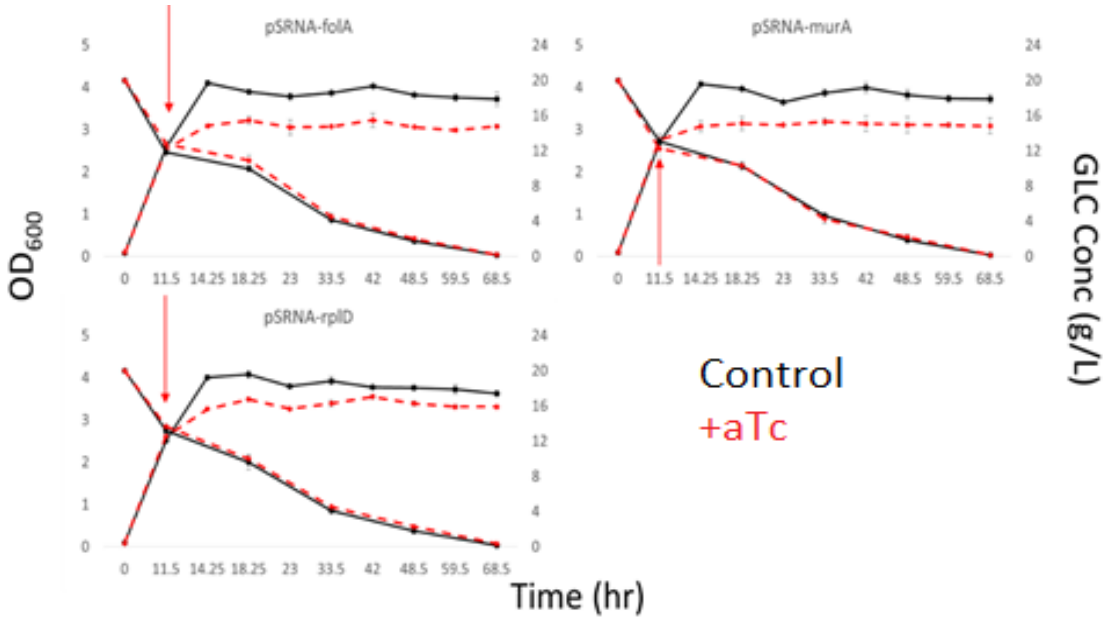

Figure 26: The Relationship between the OD_{600} (Left Axis), Glucose Concentration (Right Axis), and Time after the Addition of Anhydrous Tetracycline (Red) for Three pSRNA Variants (Black) Grown in M9 Media. BW-folA, Top Left; BW-murA, Top Right; BW-rplD, Bottom Left.

To better put the data from the graphs into perspective, quantified below is the specific glucose consumption rate, typically in units of $\frac{g_{glc}}{hr*CDW_{E.coli}}$, for the each of the pSRNA variants normalized as a percentage relative to the specific glucose consumption of the uninduced background strain, wild-type BW25113. This metric gives insight into how much glucose each cell relatively consumes when uninduced and induced,

Figure 27: Relative Specific Glucose Consumption Rates ($\frac{g_{Glc}}{hr*CDW_{E.coli}}$) for the BW25113 pSRNA Variants Strain at the Final Time Point in Shaker Flask.

As illustrated graphically, in all cases the induced variants have a higher specific glucose consumption than their uninduced counter-parts and the background strain; in the case of BW-rplD, the smaller change than the other strains is an inherent result of the higher OD at the time of induction, translating to an inherently higher cell density. Though only marginally larger than the specific glucose consumption rate of the background strain, it is also worth noting the consistently increased specific glucose consumption rate associated with the uninduced pSRNA variants. This may be a result of the plasmid putting a burden on the cells, but more likely it may be the result of the uninduced variants still consuming all the glucose, but at marginally lower optical densities, considering the uninduced variants do not appear to affect the cell size.

Supplementing the dynamic OD_{600} and glucose concentration data outlined above are microscopy pictures showing the morphology of the cells, overlaid with the fluorescent

image results from the viability assay, performed at a time of 42 hours. The viability stain tags metabolically viable cells as green, and tags non-viable cells as red; fluorescent emission may be detected using a blue light to excite the cells stained green, and a green light to detect those stained red. It is worth noting that in a similar fashion to the microscopy pictures displayed in Figures 10 through 13, these microscopy images are the same resolution as the original images taken by the microscope so the morphology of the cells may be seen; as a result, the panels above are small segments cropped from the much larger images taken by the microscope.

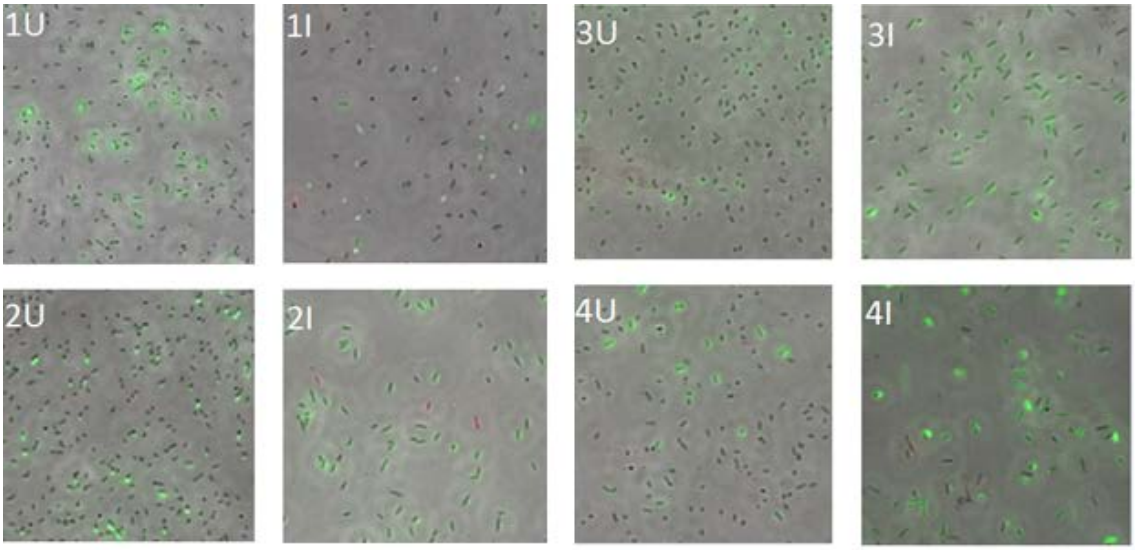

Figure 28: Microscopy Pictures of the Cells Overlaid with Fluorescent Staining Images from the Viability Assay Kit Taken at the 42 Hr Mark. Green Staining Indicates Viable Cells, and Red Staining Indicates Non-Viable Cells. *U* Refers to Uninduced, and *I* Refers to Induced Variants of Each Strain. Top Left, BW25113; Bottom Left, BW-dnaE; Top Right, BW-fabD; Bottom Right, BW-fabH.

In almost all cases seen in Figure Figure *25*2 and Figure 273, nearly every detectable cell was viable, and there were almost no detectable non-viable cells; any non-viable cells that were detected were included in the images to showcase their characteristics – non-viable cells may be seen in panels 2I and 5I.

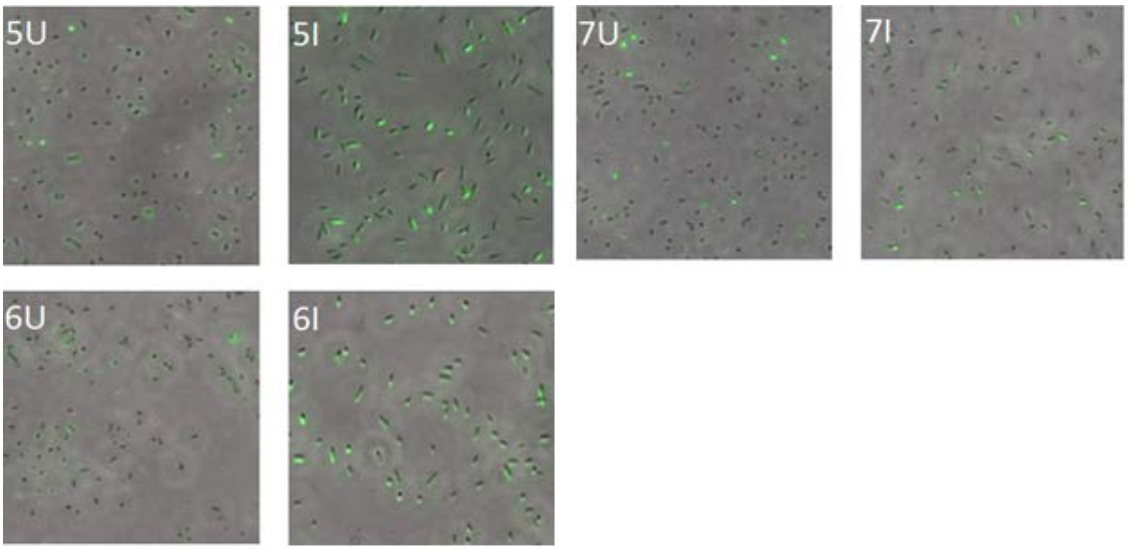

Figure 29: Microscopy Pictures of the Cells Overlaid with Fluorescent Staining Images from the Viability Assay Kit Taken at the 42 Hr Mark. Green Staining Indicates Viable Cells, and Red Staining Indicates Non-Viable Cells. *U* Refers to Uninduced, and *I* Refers to Induced Variants of Each Strain. Top Left, BW-folA; Bottom Left, BW-murA; Top Right, BW-rplD.

It is also worth noting the morphology of the background strain and the pSRNA variants appears representative of the results on the plate reader scale, shown in Figure 14. To get a feel for how the metabolic activity in the pSRNA variants compares with common bacteriostatic additives that are known to suppress growth while otherwise having a minimal effect on metabolic activity, tetracycline, streptomycin, and chloramphenicol in concentrations of 10 milligrams per liter, 100 milligrams per liter and 34 milligrams per liter were added to the background strain BW25113 in a shaker flask environment. It is worth reiterating that BW25113 is a wild type strain and does not have any antibiotic resistance; the resulting optical density and dynamic glucose concentrations may be seen below in Figure 29,

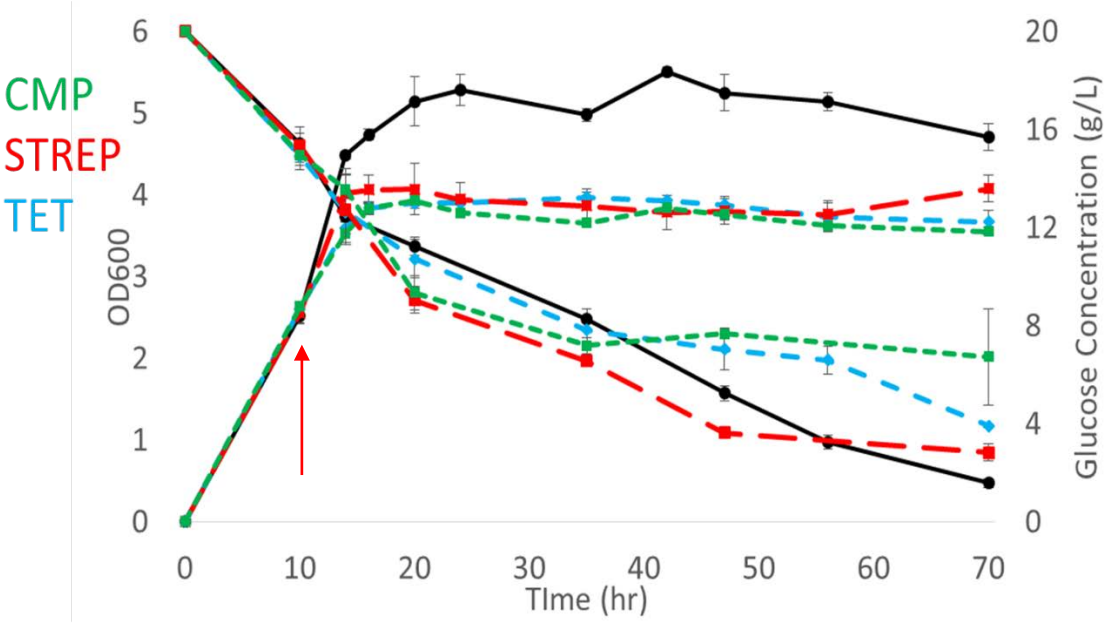

Figure 30: The Relationship between the OD_{600} (Left Axis), Glucose Concentration (Right Axis), and Time after the Addition of Three Different Bacteriostatics – Tetracycline (Blue), Streptomycin (Red), and Chloramphenicol (Green).

As noted, seen above is the dynamic response of the optical density and glucose concentration in a shaker flask environment for background strain BW25113 induced with three different bacteriostatic additives. While the data above shows the bacteriostatic additives seem to have a fast response in regards to growth suppression relative to the response of the sRNA-mediated approach, it appears that the metabolic activity was also affected relative to the induced pSRNA variants. Seen below is the specific glucose consumption rate for BW25113 with the addition of the three bacteriostatic additives, relative to the specific glucose consumption rate for wild-type BW25113.

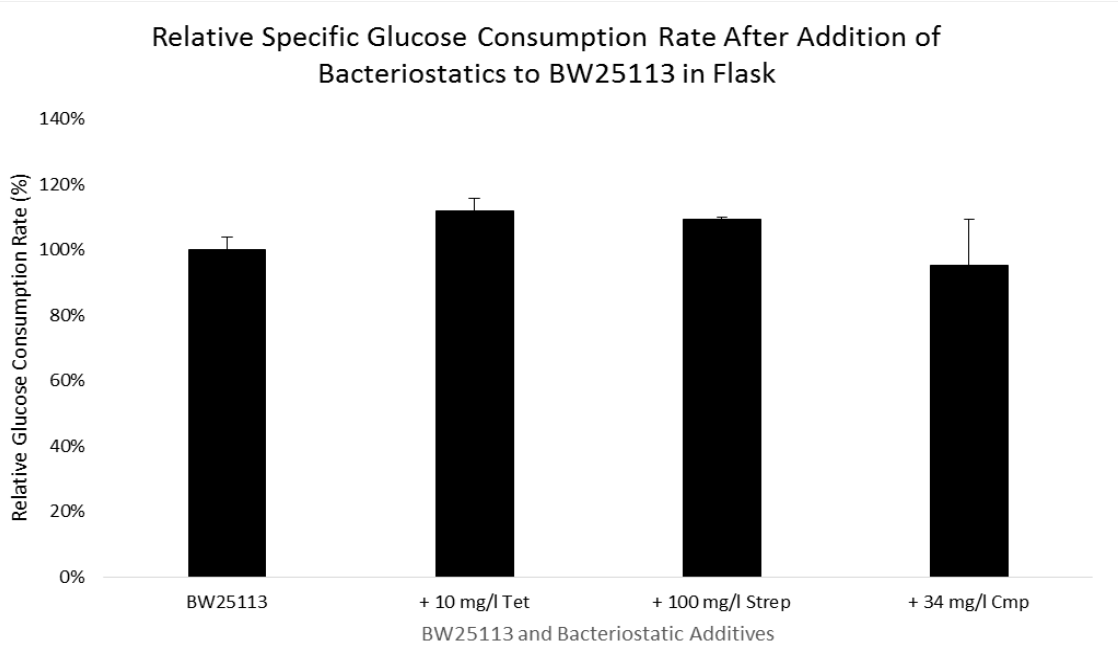

Figure 31: Relative Specific glucose Consumption Rates ($\frac{g_{Glc}}{hr*CDW_{E.coli}}$) for Background Strain BW25113 with Bacteriostatic Additives at the Final Time Point in Shaker Flask.

As mentioned, while the bacteriostatic additives were efficient at suppressing growth in a similar amount of time that it took with the sRNA-mediated approach, the specific glucose consumption rate did not appear to increase as significantly relative to the sRNA-mediated approach. Referring back to Figure 29 above, this is likely a result of the fact that not all the glucose was consumed in the case of the strains with bacteriostatic additives. Especially in the case of chloramphenicol addition it appears that a significant amount of glucose was left over, indicating that metabolic activity was diminished; a result not observed with the sRNA approach.

To further gauge the metabolic activity of the cells, a fed-batch culture was grown using the BW25113 pSRNA-murA variant to determine if the induced cells remained metabolically active over a longer period; this may shed insight into the potential for the

variants to convert resources into desirable products. The pSRNA-murA variant was chosen for its effective OD repression, good specific glucose consumption rate and vivid viability stain results. In the fed batch experiment, BW25113 and the pSRNA-murA variant were both grown in M9 minimal media; once more induction occurred in the mid-exponential phase. This time however, a charge of the dextrose, ammonium chloride, magnesium sulfate and calcium chloride were added. The amount of dextrose fed, 0.5 grams added to the 50 mL culture, is half of what was initially present in the fresh M9 media; the amounts of ammonium chloride, 0.05 grams, magnesium sulfate, 0.1 mol, and calcium chloride, 0.005 mol, fed are equivalent to the amount originally in a fresh 50 mL flask of M9 media. The charge of nutrients was added to prolong the exponential phase, increasing the total cell density of the culture – this inherently means the feed must be added during exponential phase. Seen below are the resulting optical density and metabolite analyses for the fed batch experiment,

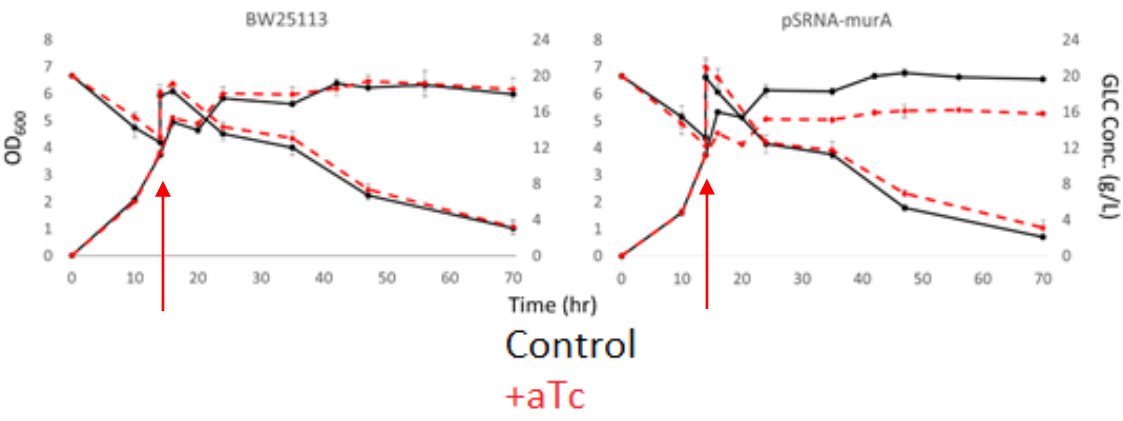

Figure 32: The Relationship between the OD_{600} (Left Axis), Glucose Concentration (Right Axis), and Time after the Addition of Anhydrous Tetracycline (Red) to BW25113 and BW-murA (Black) in the Fed-Batch Experiment.

As shown in the figure above, the feed was added at the 15 hour mark, during the later end of the exponential growth phase; this was added to bring the total concentration of glucose back to roughly 20 grams per liter. Seen in the graph on the left, it appears that the aTc-induced wild type BW25113 did not experience any significant change in either glucose consumption rate or in final optical density, but looking at the optical density and glucose consumption rate versus time in the graph on the right, it appears that the aTc-induced pSRNA-murA variant never achieved the same final optical density as the uninduced variant, while still consuming glucose. These results parallel the results from the shaker-flask experiment seen above, while indicating that the induced sRNA variant is able to continue consuming glucose. Seen below is the specific glucose consumption rate of the wild-type BW25113 strain with the addition of aTc, and the pSRNA-murA variant, both induced and uninduced, relative to the uninduced wild-type BW25113 strain,

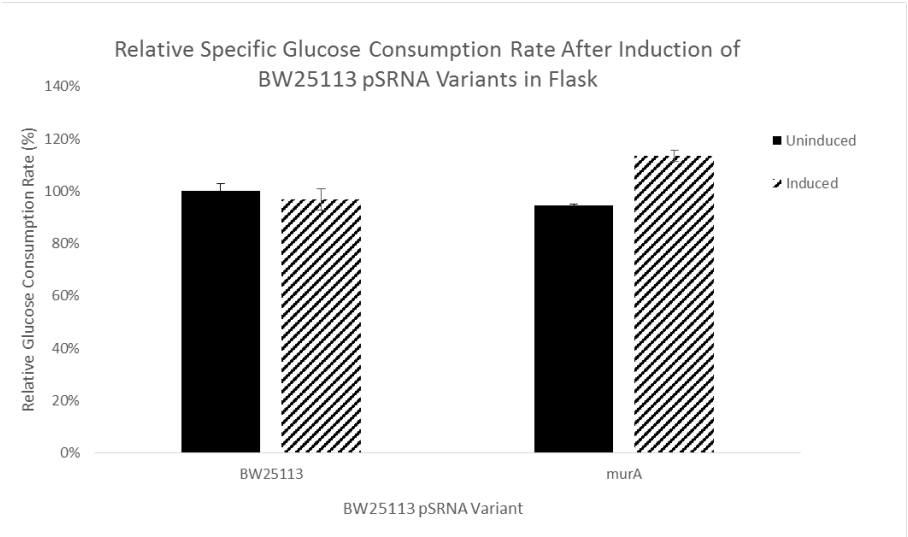

Figure 33: Relative Specific Glucose Consumption Rates ($\frac{g_{Glc}}{hr*CDW_{E.coli}}$) for the BW-murA Variant in a Fed Batch Environment.

As mentioned, the figure above shows the relative glucose consumption rate for the pSRNA-murA variant. While the addition of aTc did not seem to have any effect on the optical density or dynamic glucose concentration in the background BW25113 strain in the fed-batch environment, the induced pSRNA-murA variant did have an increased relative specific glucose consumption rate while its uninduced counterpart did not. In correspondence with the figure showing optical density and glucose concentration as a function of time, this is due to the fact that the induced sRNA variant continues to consume glucose even when growth is suppressed. Nonetheless, the increase in the specific glucose consumption rate in the fed-batch environment appears to be lower than the increase seen in the pSRNA-murA variant that was not fed, as shown in Figure 26; these results appear to be closer to the effect seen by the bacteriostatic additive suggesting in a long-term culture that the plasmid-based system may not be able to generate a consistent biosynthesis product. Though further discussed in the results section, this could be a result of the increased optical density seen in the fed-batch experiment. Nonetheless, these results indicate that the sRNA is effective at suppressing growth without having a significant effect on cell viability or metabolic activity, unlike the bacteriostatic additives.

3.5 Phenylalanine Production Optimization in BW25113 pINT-GA and pSRNA Variants

To supplement the results above which appear to show that the sRNA plasmid is effective at suppressing growth without affecting either the viability or metabolic activity of the cells, the sRNA plasmids corresponding to the same 6 gene candidates, *dnaE, fabD, fabH, folA, murA,* and *rplD,* were transformed into the phenylalanine overproducer BW25113 pINT-GA, which has a feedback resistant copy of the genes *aroG* and *pheA*

overexpressed as discussed further in the strain construction section of Materials And Methods. The capability of the pINT-GA strain coupled with the pSRNA plasmid to solely suppress growth was first screened in a plate reader experiment – the results of which may be seen below,

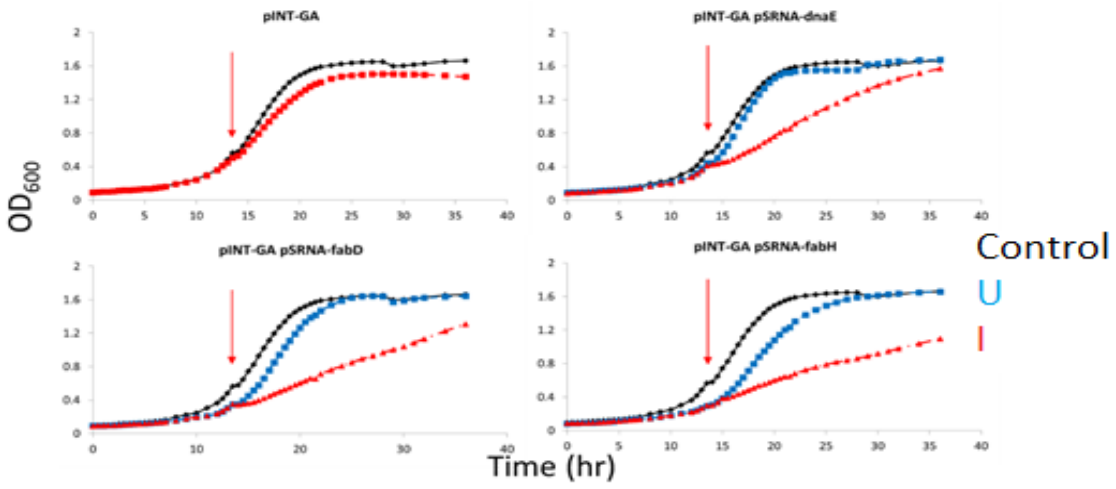

Figure 34: The Relationship between OD_{600} and Time after the Addition of Anhydrous Tetracycline (Red) at an OD_{600} of 0.4 for pINT-GA pSRNA Variants (Blue) Grown in M9M. pINT-GA, top left; pINT-GA dnaE, top right; pINT-GA fabD, bottom left; pINT-GA fabH, bottom right.

As noted, seen in the figures above and below, the pINT-GA strain and the pSRNA variants were run in a plate reader assay to screen the efficacy of growth suppression in the induced strains; the first panel in the figure above shows that the concentration of anhydrous tetracycline slightly slows the growth in the exponential phase of the pINT-GA strain which has no sRNA plasmid, and results in a marginally lowered optical density in the plate reader assay. While the effects of growth suppression are more robust in the strains with the sRNA plasmids, as expected, some of these strains ultimately reached an optical density close to the uninduced counterpart and the control strain, though it took much longer. Nonetheless, this indicates there may be interference

between using these two plasmids in conjunction with one another. While the *dnaE* variant very nearly reaches the uninduced optical density, *fabD, folA* and *rplD* seem to be rowing at a rate which could also reach the same optical density; nonetheless, in all four of these cases the exponential growth phase is significantly slowed down indicating the pSRNA plasmid is having some type of significant effect on targeting growth associated genes. These results differ from the observed behavior of the pSRNA variants in wild-type BW25113, which did not contain the pINT-GA plasmid. Nonetheless, the *fabH* variant and the *murA* variant exhibit the best growth suppression of the pINT-GA pSRNA strains, though it is worth noting in both cases there seems to be a shift in the overall growth, with *fabH* being more drastic than *murA.*

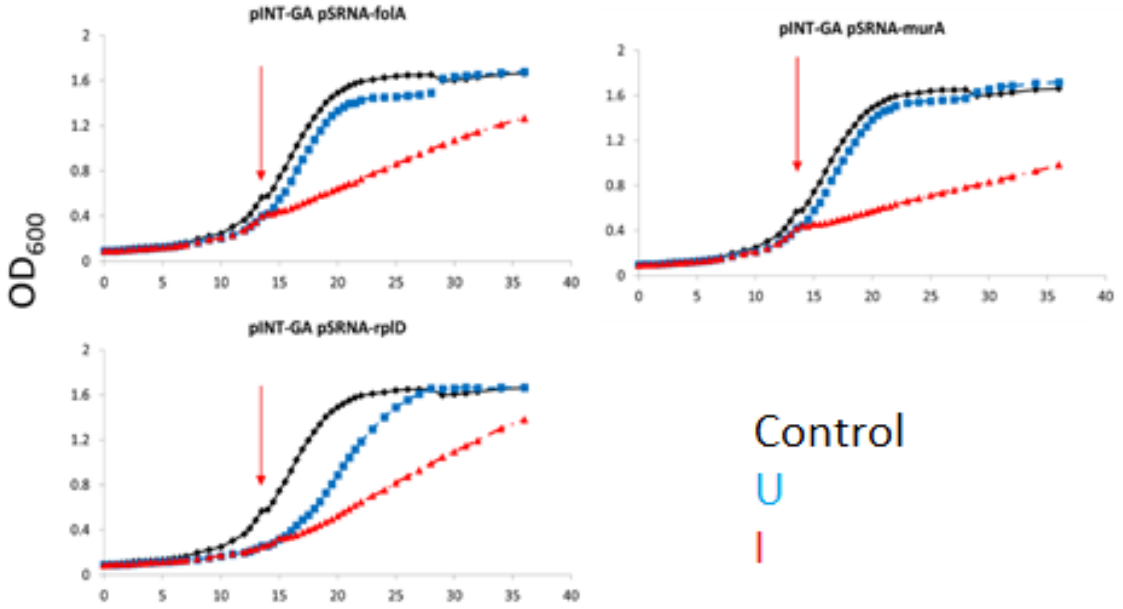

Figure 35: The Relationship between OD_{600} and Time after the Addition of Anhydrous Tetracycline (Red) at an OD_{600} of 0.4 for pINT-GA pSRNA Variants (Blue) Grown in M9M. pINT-GA folA, top left; pINT-GA murA, top right; pINT-GA rplD, bottom left.

Ultimately it appears as if the sRNA was more stable in the wild-type BW25113 strain than in the pINT-GA variant, as none of the growth suppression appeared to be as effective as it did in the background BW25113 strain. To gain further insight in regards to the morphology of the pINT-GA pSRNA strains which were screened in the plate reader experiment above, the cells at the final time point were imaged; these images may be seen below,

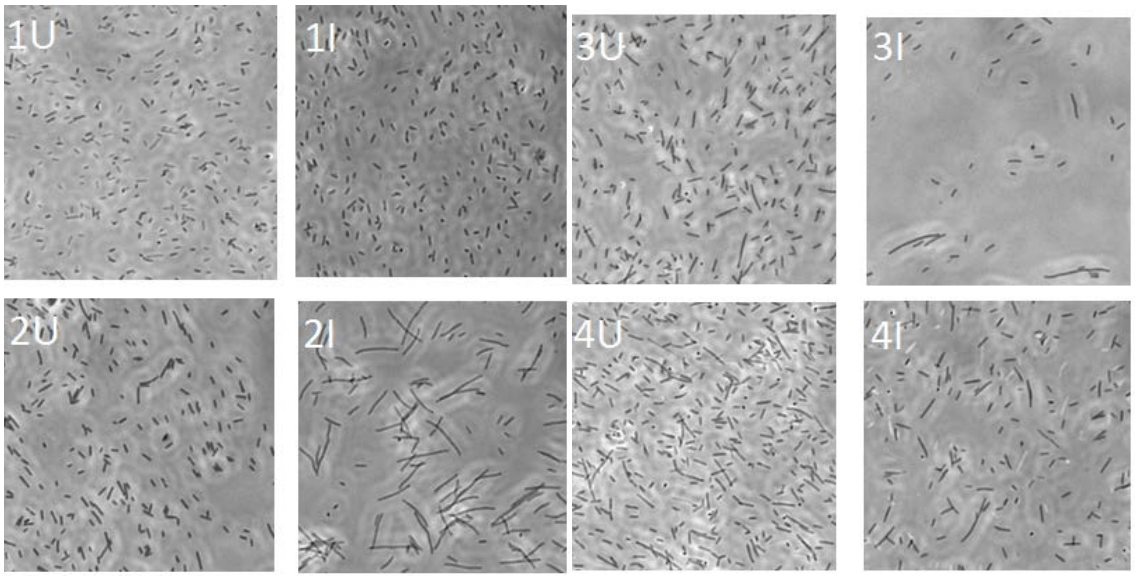

Figure 36: Microscopy Images Showing morphology of Uninduced (Left) and Induced (Right) Cells for pINT-GA pSRNA Variants Grown in M9M at the Final Time Point from the Plate Reader Assay; Panel 1: pINT-GA, Panel 2: pINT-GA dnaE, Panel 3: pINT-GA fabD, Panel 4: pINT-GA fabH.

As mentioned, the images above and below show the morphology of the pINT-GA background strain (Panel 1), and the pSRNA variants (Panels 2-7), both uninduced and induced at the final time point of 37 hours. The first thing to notice in these images is that once more the induced pSRNA variants take on a much longer, rod-shaped morphology, which again may be a result of trying to increase nutrient flux into the cell. In the case of the pINT-GA pSRNA induced variants, the filamentation that occurred was much more robust than observed in the pSRNA variants in the wild-type BW25113 strain. Furthermore, there appears to be a less consistent cell size amongst the induced pINT-GA pSRNA variants, especially in the case of the *fabD* gene target which blocks fatty acid biosynthesis. In the wild-type BW25113 strain, all the induced cells appeared to be elongated, but in the pINT-GA variant, there was a mixture of some elongated cells and some cells close to the size of the background pINT-GA strain. While it may seem plausible that the similar final optical density of the background strain and the induced

and uninduced pSRNA variants in cases like *fabD* could be due to the different morphologies observed, suggesting not all of the cells were affected equally by the sRNA plasmid, the case of *dnaE* as seen in Figure 2 seems to refute this observation. In the case of *dnaE* in particular, the most elongated cell morphology was observed with the average cell roughly 300% bigger than the uninduced background strain, however even in this case the cells reach nearly the same final optical density as the uninduced counter-part and the background strain. Furthermore, in one of the cases with the best growth suppression, *fabH*, the morphology was only 200% of the background strain; furthermore, in this particular case, it appears that the uninduced *fabH* pSRNA variant had nearly the same morphology as the induced variant, even to the naked eye as seen in Panel 4. Nonetheless, it is also apparent in this image that the cell density of the induced variant is much less than the uninduced variant.

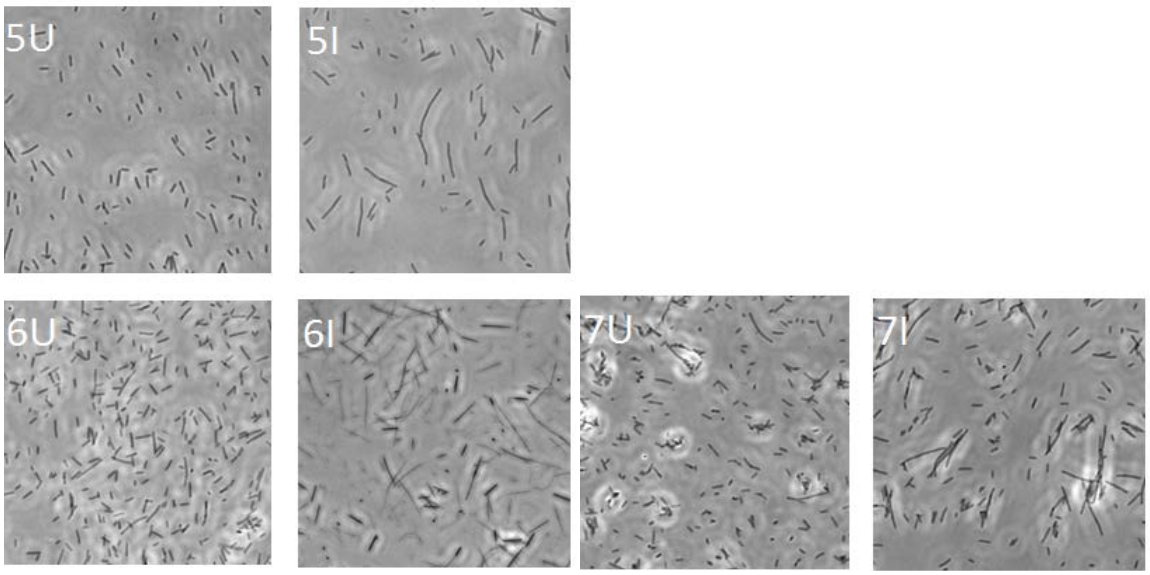

Figure 37: Microscopy Images Showing morphology of Uninduced (Left) and Induced (Right) Cells for pINT-GA pSRNA Variants Grown in M9M at the Final Time Point

from the Plate Reader Assay; Panel 1: pINT-GA folA, Panel 2: pINT-GA murA, Panel 3: pINT-GA rplD.

It is also interesting to examine in more detail the case of the gene target *murA*, which had effective optical density suppression as well as an increased cell size. This ultimately means there is no direct correlation to the enhanced cell size and effective optical density suppression; to summarize, *dnaE* had the largest morphology with ineffective growth suppression, while *fabH* and *murA* had effective growth suppression, but drastically different morphologies. This may indicate the morphology in the case of the pINT-GA strain is more sensitive to the selected gene target than in the case of wild-type BW25113. One final thing to note, and perhaps best visualized by the figure below which summarizes the cell size relative to the uninduced background strain, BW25113 pINT-GA, is the increased cell size of all the uninduced pSRNA variants, even though the induced pINT-GA variant does not have a significantly increased cell size.

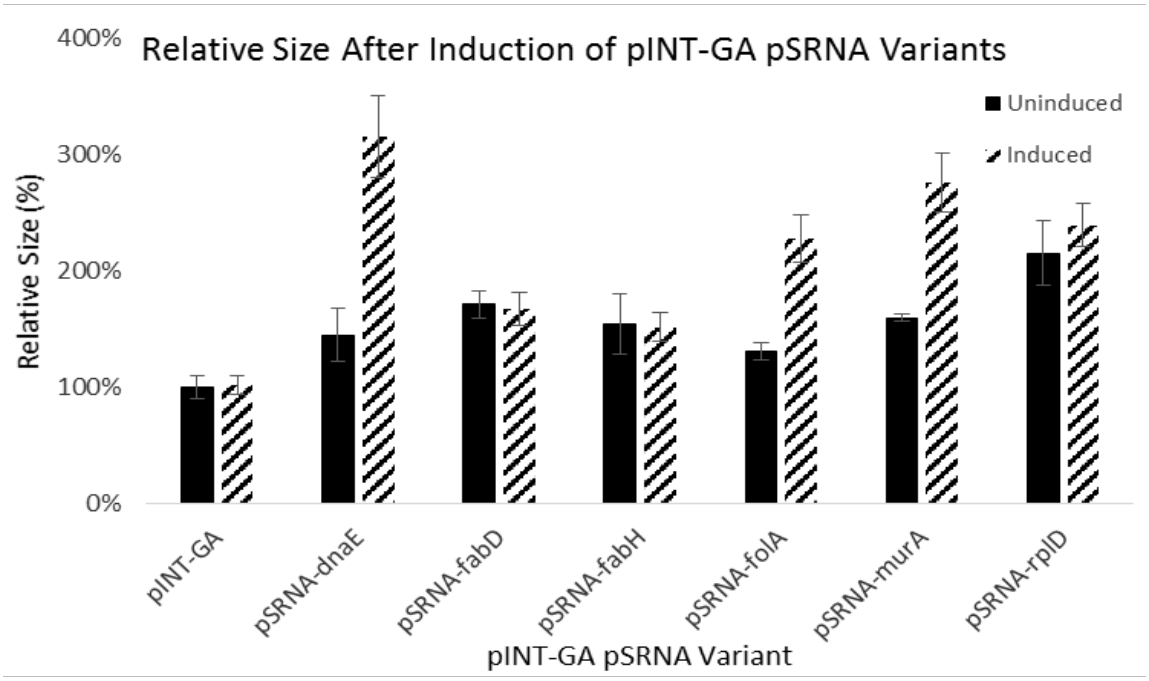

Figure 38: Relative Cell Size for the pINT-GA pSRNA Variants With and Without Anhydrous Tetracycline Induction; Cells Cultured in M9M Media.

As expressed above, the morphology changes in the BW25113 pINT-GA pSRNA variants suggests this may be a result of the gene targeted, and may be unrelated to the growth suppression; this is supported by considering the two genes responsible for fatty acid biosynthesis, *fabD* and *fabH*, were also the two genes that resulted in the smallest morphology changes. While the results of the growth suppression in the pINT-GA strain do not look as effective as they did in the background BW25113 strain, and the morphology changes do not see to be consistent with the wild-type BW25113 strain, this could be a result of the plasmid-based approach rather than integrating everything onto the chromosome of BW25113. To once more investigate the relationship regarding the degree of filamentation, which may be represented by the relative size change, with respect to the degree of growth suppression, represented by the relative final optical density, a scatter plot was constructed which may be seen in the figure below,

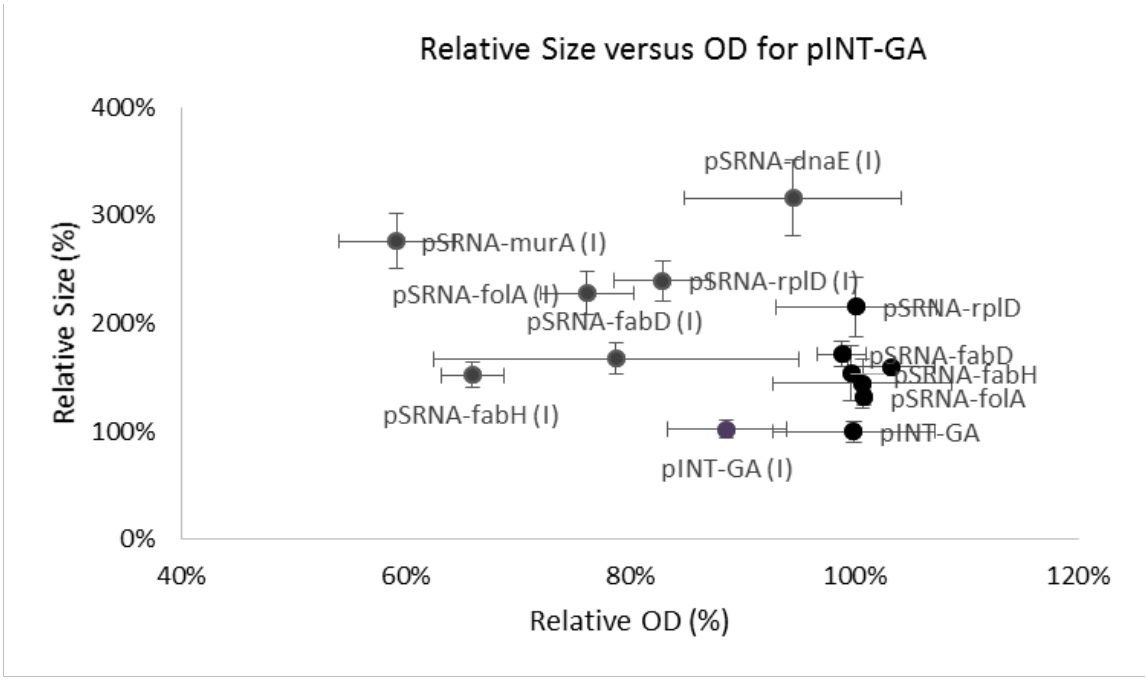

Figure 39: A Scatter Plot Illustrating the Relative Size versus the Relative OD for the pINT-GA Well-Plate Experiment at the Final Time Point

It appears in the figure above that there is not a clear relationship between any degree of filamentation resulting in any degree of growth suppression in either the induced variants or the uninduced variants. In the case of the uninduced variants this scatterplot makes it a bit easier to visualize that while the growth did not seem to be suppressed in any of the cases, they did seem to experience different degrees of filamentation. In the induced variants, growth was suppressed to different degrees, and while this has been shown to be a result of the gene targeted by the pSRNA system, once more it does not seem that there is any discernable background contribution in optical density due to filamentation. While this is not to say the filamentation is not having an influence on the optical density, more rigorous experiments are needed to further investigate this relationship to determine if it exists and to what degree.

Nonetheless, to examine the metabolic activity of the pINT-GA strain, the *murA* variant was once more selected based on its effective growth suppression and moderate morphology results. Using the pINT-GA pSRNA-murA strain, the dynamic optical density, glucose consumption rate, acetate production, and phenylalanine production was measured in the span of 70 hours, as summarized in the figures below,

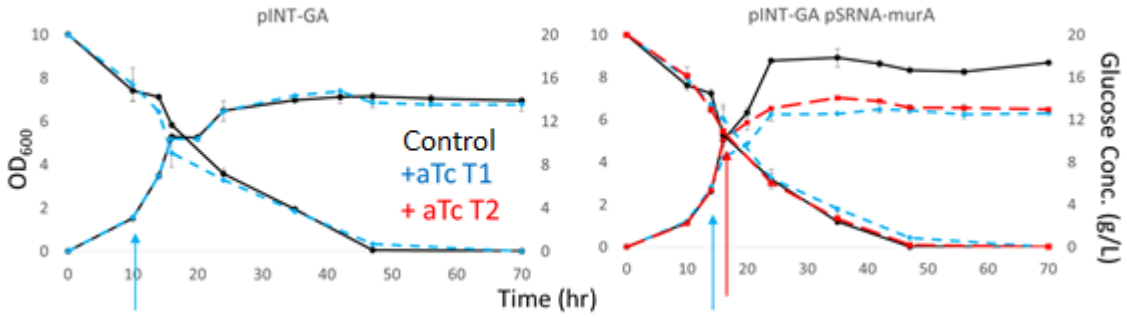

Figure 40: The Relationship between the OD_{600} (Left Axis), Glucose Concentration (Right Axis), and Time after the Addition of Anhydrous Tetracycline to pINT-GA (Left Graph) and the pINT-GA murA Variant (Right Graph) at Two Time Points (T1, Blue and T2, Red).

The figure above illustrates the dynamic optical density and glucose concentration as a function of time; there are many things to note in the figure above, but perhaps the most obvious is first that the marginally slower growth seen in the induced background pINT-GA strain in plate reader was not observed in the scaled-up shaker flask, and second that in all the cases the glucose is fully consumed in relatively the same amount of time. By the 50 hour mark, there appears to be no glucose left and the rate at which it was consumed is consistent across all strains. Another obvious thing to note is the increased optical density of all the strains, relative to the background BW25113 strain; these strains all grow to a higher optical density indicating the presence of the pINT-GA plasmid increases nutrient flux towards biomass synthesis. Even more interesting is the fact that the uninduced strain with two plasmids, pINT-GA murA, achieves a higher optical

density than the strain with one plasmid, pINT-GA, though in the plate reader screening experiment the *murA* variant did not achieve a higher optical density; this suggests that the effects of the pINT-GA plasmid is compounded by the sRNA plasmid in regards to reallocating resources to synthesizing more biomass. This is, unfortunately, the opposite of the ultimate goal. Also seen in the figure above, inducing pSRNA-murA variant at the two different time points during the exponential phase, first at the 14 hour mark and second at the 17 hour mark, did not seem to ultimately affect the final optical density, though it did appear to affect the final concentration of phenylalanine. The dynamic phenylalanine data may be seen below,

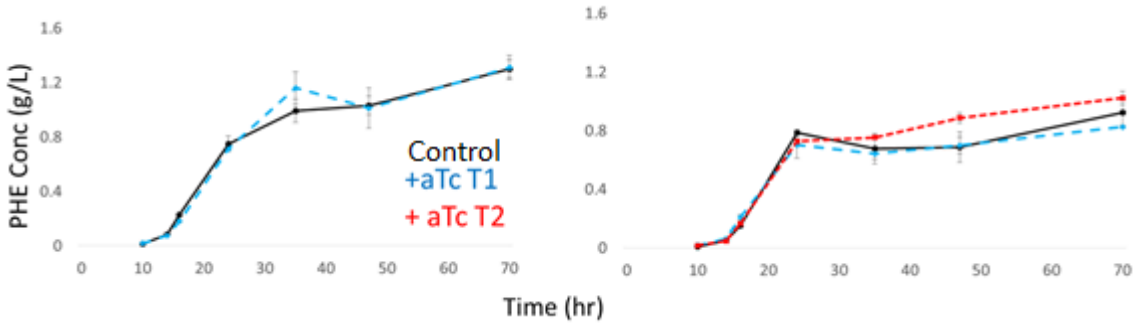

Figure 41: The Relationship between Phenylalanine Production and Time After the Addition of Anhydrous Tetracycline to BW25113-pINT-GA (Left Graph) and the pSRNA-murA Variant (Right Graph) At Two Different Time Points (T1 Blue, T2 Red).

The dynamic phenylalanine data is interesting because it shows that almost all of the phenylalanine produced was during the exponential phase, especially in the case of the pINT-GA murA variant. Examining the pINT-GA strain without the sRNA plasmid in more depth, it appears that both ultimately reach the same final concentration of phenylalanine. They appear to make it at the same rate as well, though paying notice to the insignificantly higher phenylalanine near the 35 hour mark, which appears to be consumed by the cells. This suggests that the aTc had no effect on the production of

phenylalanine in the background pINT-GA strain; in the case of the pSRNA-murA variant, the effect of the aTc is interesting. It appears in the uninduced strain that some of the phenylalanine was reuptaken by the cells, before ultimately being regenerated, and the same may be said but less pronounced with regards to the set induced at the first time point. However, the pSRNA-murA variant induced at the second time point did not appear to reuptake any phenylalanine, though it did appear to make most of the phenylalanine during the exponential phase, as was the case observed across the board. While the dynamic phenylalanine production data suggests phenylalanine production is tied closely to growth. While it is possible to generate a higher titer of phenylalanine by picking the right time point, as observed in case 2 where the final concentration is higher than the uninduced strain, it also suggests that the timing is very sensitive, as the first case generated less phenylalanine. Furthermore, the fact that all of the pSRNA variants did not generate as much phenylalanine as the background pINT-GA strain, the results suggest using there are conflicts with using this plasmid-based system, as it was also observed that the pSRNA variants had a higher optical density.

In environmental conditions with excess glucose, glucose may be directly converted to acetate; monitoring the production of acetate serves as a good indication for the ability of the cell to convert glucose into the desired product but also a good indication of stress on the cell. Seen in the figure below is the dynamic acetate production,

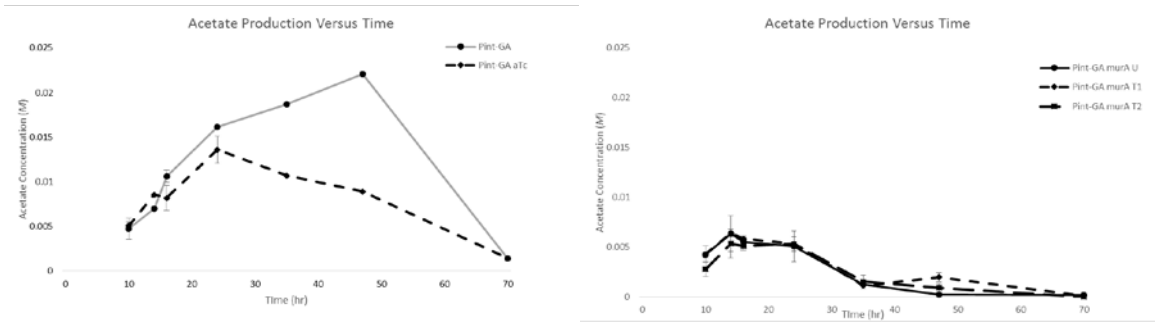

Figure 42: The Relationship between Acetate Production and Time After the Addition of Anhydrous Tetracycline to BW25113-pINT-GA (Left Graph) and the pSRNA-murA Variant (Right Graph).

Looking at the dynamic acetate production above, it is clear that the pSRNA variants do not make nearly as much acetate as the background pINT-GA strain; this has potential to be beneficial as it may reroute the excess glucose into phenylalanine, but unfortunately as summarized best in the figures below it would appear that the excess glucose, rather than being converted towards acetate or phenylalanine, is used towards biomass synthesis,

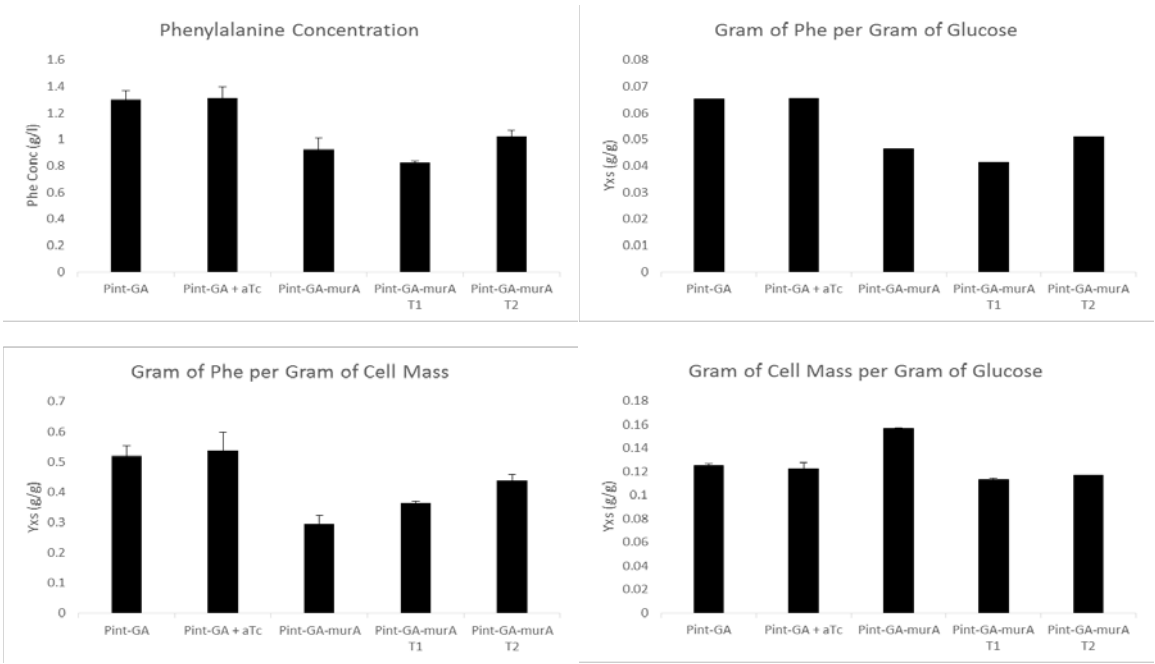

Figure 43: The Final Phenylalanine Concentration (Top Left), Gram of Phenylalanine per Gram of Glucose (Top Right), Gram of Phenylalanine per Gram of Cell Mass (Bottom Left), and Gram of Cell Mass per Gram of Glucose (Bottom Right) for the BW25113 pINT-GA and pSRNA-murA Variant.

The figures seen above indicate that, in general, the plasmid-based pSRNA approach was ineffective, and actually counterproductive, when coupled with the plasmid-based approach to overexpress the genes responsible for phenylalanine synthesis. In terms of final titer, the pINT-GA strain lacking the plasmid based pSRNA system performed best, and it was found that the pINT-GA murA variant induced at the second time point was the second best. The first time point of induction actually made less than the uninduced pSRNA variant. These results indicate the timing is very sensitive in regards to decoupling the production from growth, but it is possible – though plasmid compatibility or a plasmid based approach may be problematic. Looking next at the grams of phenylalanine per grams of glucose, it is also seen that the pINT-GA strain lacking the pSRNA system performed best; this indicates that the either more of the glucose was

used to make phenylalanine, or the phenylalanine was more efficiently made. Nonetheless, the same trend in regards to the pSRNA system that was seen in the case of titer is also seen in the case of phenylalanine yield with respect to glucose, wherein the second time point of induction performed best and the first time point of induction performed worst. Further In terms of yield of phenylalanine with respect to cell mass however, the first time point of induction was shown to be a bit better than the uninduced variant, indicating there is some sort of increased metabolic activity at this induction time for less cells to be able to make the same total concentration of phenylalanine. The grams of cell mass per grams of glucose provide more insight into how the glucose is being used; it is seen that the pINT-GA lacking the plasmid based system seems to exhaust significantly less glucose making cell mass then the uninduced pSRNA variant, indicating there is an increased flux towards biosynthesis in the double-plasmid system. Unfortunately, even though a relatively similar amount of glucose made a relatively similar amount of cell mass between the pINT-GA strain lacking the pSRNA system and the induced pSRNA variants, this did not scale to equal amounts of phenylalanine being produced. This indicates that in this plasmid based approach, while the sRNA does seem to increase relative efficiency, this system in particular puts a burden on the cell which makes it generate less phenylalanine than it would have if the plasmid were not present in the first place, and it is clear that it is losing glucose to some other mechanism aside from biomass synthesis that is not present in the strain that does not contain both the pINT-GA plasmid and the pSRNA plasmid.

In conclusion, while there is an interference between the two plasmids used in this particular case it still appears as if the pSRNA approach is effective at increasing the flux

of nutrients towards the production of phenylalanine, even considering how closely to growth phenylalanine production is tied. This proof-of-concept opens the door to further insight regarding more efficient ways to implement the afsRNA system generated with the purpose of metabolic engineering in mind.

4. DISCUSSION

4.1 Optical Density and Morphology Screening Discussion in BW25113 Strain

In the first phase of the experiment, the coding sequence corresponding to the target binding site for each of the potential gene targets was placed in the seed region of the modular synthetic afsRNA scaffold, which was then placed on a plasmid with the anhydrous tetracycline promoter and the T1/TE terminator as well as streptomycin resistance; this was effectively transformed into the background strain BW25113 and the OD_{600} and morphology of the cells were screened in nutrient rich LB media and M9 minimal media. Screening in LB before moving to M9 media warrants insight into nutrient deficiencies; a strain which grows in LB but not M9 may lack essential nutrients, whereas a strain that does not grow even in LB may be experiencing other problems. Nonetheless, a concentration of 0.5 μg of aTc per mL of culture was used in this study as it showed effective expression of the sRNA plasmid without affecting any metabolic functionality of the background strains that did not have the aTc inducible promoter; in another study using an aTc inducible promoter, aTc concentrations ranging from 1 to 10 ng per mL of culture were shown effective, a concentration orders of magnitude less than what is used in this study.[50] This implies that it may be possible to improve the affinity of aTc to bind with the promoter resulting in less aTc necessary; on an industrial scale this may result in significant cost reduction.

Aside from the growth essential genes which were targeted, an additional sRNA plasmid which targets the *lacZ* gene found on the chromosome of MG1655 to further characterize the underlying mechanism regarding how the sRNA suppresses growth. This was a useful experiment because cells which express the *lacZ* gene may consume x-galactose and as a

result may turn blue, but also because *lacZ* is a gene known to be unassociated with growth.[51] This experiment ultimately shows that the suppression of growth observed in other strains is likely a result of inhibited gene translation, as the MG1655 variant which expressed the *lacZ* gene without the *lacZ* sRNA plasmid did turn blue after being fed x-galactose, as expected. Furthermore, the MG1655 variant expressing the *lacZ* gene and containing the *lacZ* sRNA plasmid without the addition of aTc also turned blue in the presence of x-galactose, also expected because the psRNA was not induced and therefore should not disrupt translation. However, adding anhydrous tetracycline (aTc) to this variant, resulting in the expression of the *lacZ* sRNA plasmid, resulted in less blue cells with a relatively unscathed growth profile indicating it was successful at targeting the gene *lacZ* which is essential for the blue phenotype while not otherwise affecting metabolic activity of the cells. .

These results suggest that the addition of the aTc warrants expression of the *lacZ* sRNA plasmid, resulting in inhibition of only the *lacZ* gene expression with no observable effect on growth. This result concludes that the seed region in the sRNA plasmid must be responsible for the effects observed, considering the only factor changed amongst the various strains is the coding sequence in this region. This then suggests that the relatively different optical density differences may be a direct reflection of the efficacy in which the sRNA was able to suppress growth by inhibiting the transcription of potentially growth essential genes; this was assumed to be the case and the response of each gene in regards to growth suppression was used to make the decision regarding which targets to transform into the phenylalanine overproducer, pINT-GA. Making sense of the

responses, the pathways corresponding to the genes of interest and how this might relate to the results observed is discussed below.

To supplement this discussion, it is interesting to note the coupled changes in morphology that simultaneously occurred with the activation of the sRNA plasmid; while the induced background strain and all of the uninduced pSRNA variants did not show much of a size difference relative to the uninduced background strain, all of the induced variants with the exception of *fabI* showed relatively large increases in cell size. It is also worth noting *fabI* did not show good growth suppression either indicating it may have been ineffective at targeting growth, but also indicating the mechanism of action does not result in filamentation. The data from this experiment, summarized in Figure 15, suggests there is no significant, straight-forward correlation between background increases in optical density as a result of filamentation, though not to say this is not present. Considering the differences in the relative cell size, and once more considering the only thing changing is the seed region of the sRNA scaffold, the target gene once more must be directly responsible for the observed effect on cell size. One interesting trend to note is the observation that suppression of growth lead to an increase in cell size relative to the uninduced variants when the pSRNA targeted growth essential genes; perhaps targeting essential genes at a mid-exponential time point can cause an increase in cell size to possibly increase nutrient flux, as the change in cell size was only seen in the induction of essential genes and not so much in the *lacZ* experiment. This suggests that the pSRNA does not affect the background optical density, when induced and not targeting growth essential genes.

For example, in the case of the genes *fabB* and *fabH*, it was found that inhibiting *fabB* did not have much of an effect on OD suppression while blocking *fabH* significantly suppressed the optical density, as summarized in Figure 9. This is particularly interesting because *fabB* has been shown to be growth essential and blocks a critical step in the overall fatty acid biosynthesis I pathway, while *fabH* has been shown to be non-essential for growth, but this was only shown in knock-out strains and not in a strain that dynamically suppresses gene expression.[52] Nonetheless, consider the interaction between *fabB* and *fabH* in the synthesis of an acetoacetyl-(acp) from acetyl-CoA, as summarized in the figure below,[53]

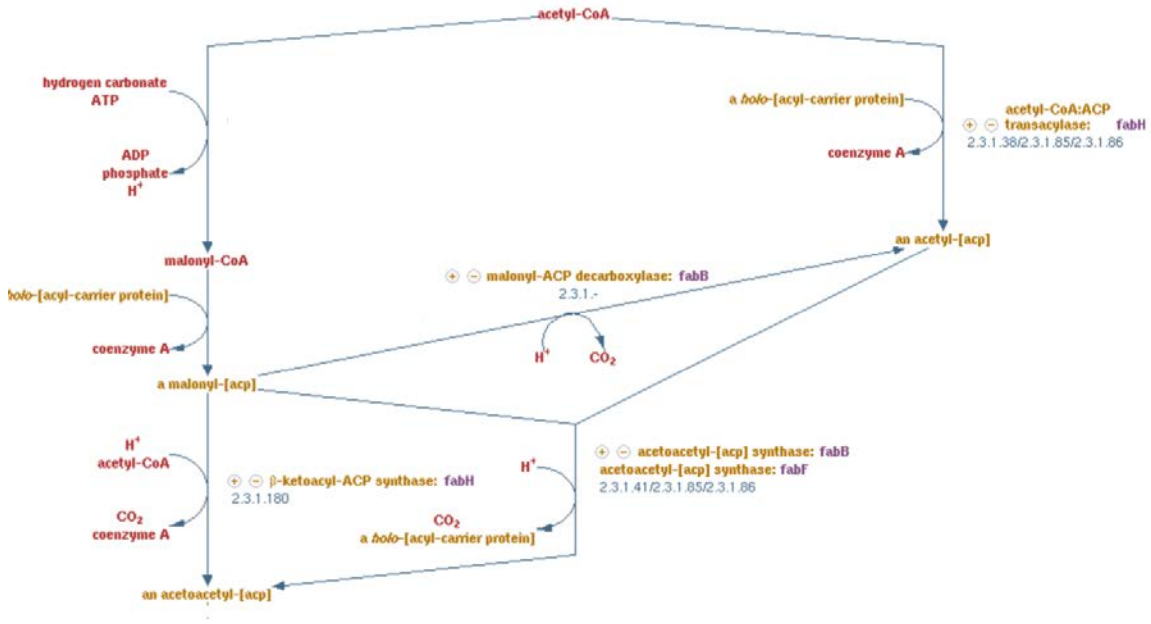

Figure 44: The Synthesis of an acetoacetyl-(acp) from acetyl-CoA in the Fatty Acid Biosynthesis Pathway Manifesting the Redundancy of the Presence of *fabB* and *fabH*.[53]

In the figure above, blocking *fabB* still warrants the formation of an acetoacetyl-(acp) from acetyl CoA as a route involving the *fabH* gene exist, and the same may be said in regards to inhibiting *fabH* (though in the case of *fabB*, it blocks a step later down the line

which there are no alternate pathways in which to circumnavigate).[52] However, one possible explanation for the data observed, where *fabH* was shown a more effective gene target than *fabB* in regards to growth suppression, may be due to the fact that blocking *fabH* makes the process much more energetically intensive to overcome than blocking *fabB*, relating back to the concept of kinetics versus thermodynamics that was discussed in the introduction.

The synthesis of an acetoaetyl-(acp) from acetyl-CoA without the *fabB* gene, but with the *fabH* gene, results in the formation of two intermediates – malonyl-CoA and a malonyl-(acp). The same synthesis, but now blocking the *fabH* gene and keeping the *fabB* gene requires the synthesis of four intermediates – malonyl-CoA, a malonyl-(acp), an acetyl-(acp), and acetoacetyl-(acp) synthase – and in the case of *fabB* inhibition, a malonyl-(acp) may be directly converted to an acetoacetyl-(acp), ending the process a step early.[52] Therefore it is possible that the burden put on the cell by blocking the *fabH* gene renders fatty acid biosynthesis not possible, likely because not enough acetoacetyl-acp is ever formed to carry the process forward. Considering this behavior was not seen in the knock-out strains generated in literature, the presence of growth of the pSRNA-fabB variant coupled with the effective suppression of growth in the pSRNA-fabH variant may be a result of the fact that this is different from a knock-out in the sense that it occurred at an optical density of ~0.4 and gave the cells time to grow and form intermediates. The increased optical density, resulting in an increase cell concentration, may have enabled build-up of intermediates which enabled the *fabB* variant to sustain while the *fabH* variant was not.

In any case, while the pathway governing the synthesis of an acetoacetyl-(acp) from acetyl-CoA warrants possible insight into the dynamic functionality of *fabB* and *fabH* and the general behavior of growth essential genes with dynamically suppressed expression, the corresponding morphology changes also offer an interesting take on things.[52] It may be observed that in both the case of pSRNA-fabB and pSRNA-fabH induction resulted in filamentation. Although growth was not suppressed with respect to *fabB,* it was suppressed to *fabH*; one possible reason for filamentation is that the cell increases its surface area to increase the nutrient flux to mitigate for the diminished gene activity. In the case of targeting *fabB,* it is possible that by increasing its size the cell was able to uptake enough nutrients to maintain viability; this is not to rule out the possibility that inherent activation of the pSRNA plasmid, when acting on a valid gene, results in a general background increase in size, though this was not the case in the pSRNA-lacZ analysis.

To further investigate the relationship between *fabB* and *fabH* and the stability of the pSRNA system at targeting more than one gene, a combination double-sRNA-scaffold plasmid strain was constructed, targeting both *fabB* and *fabH,* and referred to as *fabBH*; the results of this strain were nearly identical to the results observed in *fabH* in regards to both optical density and morphology, indicating effective suppression of growth. Construction of this strain would ensure that the literature-proven growth essential *fabB* gene would be targeted in addition to the *fabH* gene which was shown to suppress growth. However, when constructing the phenylalanine overproducer only the plasmid containing the *fabH* gene target was transformed into the cell as three plasmids puts significantly more of a burden on the cell than two plasmids. This is a trade-off as it has

been verified in literature that *fabB* is essential for viability and *fabH* is not, but the results observed in this investigation are opposite.

Further examining the behavior of growth suppression observed for each of the pSRNA variants grown in M9 minimal media, *dnaE* was seen to suppress growth effectively, reaching stationary phase at the same time as the uninduced background strain, with the uninduced *dnaE* showing a relatively similar size and optical density as the background strain. Compared to the bacteriostatic additives, the pSRNA-dnaE variant took much longer to take effect, and it also had a much higher degree of filamentation. This may be indicative that the plasmid put a stress on the cell, and perhaps the cell attempted to mitigate for the lack of essentiality by increasing nutrient flux; if this were the case it may be plausible the filamentation occurred during the lag between induction and stationary phase – the "pseudo-exponential" phase seen after induction – wherein the cell increases in size to "fight the plasmid" and remain viable, but ultimately fails. If this is the case it would suggest that a faster-acting system, one with a comparable speed to the bacteriostatic additives, may leave cell morphology unchanged. Nonetheless, the viability results make sense as *dnaE* has been shown to be a growth essential gene and appears to have been successfully targeted with the plasmid-based sRNA system.[52] The same conclusions can be said in regards to *fabD, fabI, folA, murA, rplD, rplP,* and *rpsE* – these are all growth essential gene that were shown to suppress growth when induced in the mid-exponential phase and these all resulted in an increased size. It may be assumed that the mechanism of action by which growth was suppressed for the aforementioned candidates is a result of a lack of functionality due to the inhibited translation of the target gene, as all of their uninduced variants did not show a suppressed optical density.

In the case of the pSRNA-fabD variant, since growth was not observed it is likely that the sRNA blocked the translation of the *fabD* gene which ultimately blocked the formation of a malonyl-(acp) from a malonyl-CoA; this step, as seen in Figure 43 above is essential for the formation of an aetoacetyl-(acp) and cannot be circumnavigated.[52] Nonetheless, further examining the results of the *fabD* optical density data shown in Figure 5 there is still a delay for the suppression to fully take effect, and filamentation seems to be just as drastic as gene targets which are not associated with fatty acid biosynthesis. Once more this indicates that improving the response of the system to make it suppress growth more rapidly after induction may mitigate these morphology changes. This is a hard judgement to make though, as the other fatty-acid biosynthesis gene explored, *fabI*, seemed to be relatively ineffective at inhibiting growth, but also experienced the least filamentation out of everything. The lack of filamentation suggests the cell may not have been under as much stress as in the case where other genes were inhibited, but the lack of rapid growth suppression indicates the sRNA approach was also not as effective in regards to this gene target. Considering *fabI* has been shown to be a growth-essential gene, more work should be done in regards to this gene target to further explore its efficacy in an sRNA-mediated approach if it is found that this would be an optimal gene to inhibit for reasons of conflicting pathways with other genes explored in this study.[52] Whereas *fabD* is only involved in one reaction, *fabI* is involved in 15 known reactions within *E. coli*, so in both cases it is possible that the build-up of intermediates in the time before induction occurred resulted in a while for the growth to be suppressed as first these intermediates had to be exhausted.[52]

However, it is interesting to note that, in general, the genes associated with fatty acid biosynthesis still resulted in an increased cell size; while it is possible that targeting the genes associated with fatty acid biosynthesis may not result in an increase in cell size as there are critical components missing to form a cell wall, this behavior was not observed. This is another indication that the pSRNA system could use some improvements in regard to its efficacy; finding a way to make the sRNA suppress growth with less of a delay would be a great starting point. This being said, the plasmid-based sRNA system does not appear to be leaky, considering the uninduced strains still had a relatively unaffected cell size and optical density.

The gene *folA*, which was shown to suppress growth when targeted with the afsRNA, is also only involved in one reaction – catalyzing the final step of the dihydrofolate reduction reaction wherein tetrahydrofolate is formed. Although *folA* has been shown to be a gene essential for viability, the gene *folM* has been shown to contain the same enzymatic activity as *folA* and may be one reason there was a delay in the time of induction to the time growth was suppressed.[52] Nonetheless, all variants considered, *folA* was shown to be a relatively successful gene target as the uninduced variant had no practical lag and reached a stationary phase with the same OD as the background wild-type BW25113 strain. *murA* was an interesting gene target as it was shown not to be essential for viability in a knock-out strain grown in LB media, but grown in a modified, minimal version of LB media it was shown essential for growth; this suggests that it may be a good target for practical applications wherein a seed may be grown in an enriched media without fear of unintended growth suppression before transferring to a more minimal media where growth suppression has been shown to occur.[52] The results of the

optical density data show that, like many of the other sRNA-mediated gene targets, there is a delay in the time of induction relative to when growth is actually suppressed. The growth does appear to be suppressed though it is worth noting that relative to the bacteriostatic additives there is quite a delay after induction time for this to occur. The delay in the uninduced pSRNA-murA variant may be due to the streptomycin resistance, as a similar delay was observed in the bacteriostatic additive experiment where a plasmid only containing streptomycin resistance was screened. Nonetheless, there was a notable size increase in the pSRNA-murA variant which is interesting as the *murA* gene is essential in the formation of the peptidoglycan layer in cells; this suggests there might not be totally efficient repression of the gene in cells, allowing it to still be expressed to some degree, resulting in filamentation.[52,53] Ultimately *murA* was a relatively effective gene target for growth suppression.

The genes *rplD*, *rplP*, and *rpsE* also showed relatively good growth suppression, as mentioned above, and they all target protein synthesis in the cell. The gene *rplD* codes for a ribosomal subunit protein on the 50S ribosome, the L4 site; the gene *rplP* is also on the 50S ribosome, but the L16 site.[53] On the other hand, the gene *rpsE* is on the 30S ribosomal site, and codes for the S5 subunit protein; these three genes all had relatively good growth suppression, but with notably high delays. Their morphology was quite interesting, as they experienced significant filamentation but no more than the genes which targeted fatty acid biosynthesis, which was left unrestricted in this approach, though targeting protein synthesis inherent affect fatty acid biosynthesis. The uninduced variants for these gene targets did not experience any significant filamentation relative to

the background strain indicating good control of plasmid expression for these gene targets as they also had a similar final OD.

In addition to *fabB*, the genes *fabG*, *folP*, and *rpsD* did not show significant growth suppression though they are listed as essential for viability in minimal media; this could be due to a multitude of reasons such as the target binding sequence being less than optimal, the plasmid being unstable, the build-up of intermediates, or even an increase in size skewing the optical density data, which assumes spherical cells.[53] The binding energy and nucleotide length of each sequence were designed according to experimental evidence that showed the most effective blocking of translation for the target gene, so it is unlikely changing this would have any effect, but ways to increase plasmid stability and activity as well as increase the response of induction could shed much more insight into the efficacy of the plasmid based system.[41]

In summary, the plate reader experiment showed that some growth-essential genes were not effective targets for the pSRNA system, such as *fabB*; the results also showed an increase in the size across the board for all of the induced pSRNA variants, which may have further implications in the efficacy of the system. The uninduced pSRNA variants showed the same phenotypes as the background strain in regards to optical density and morphology, and induction of the background strain did not show any significant differences which makes sense because it does not contain the pSRNA system. In the case of the *fabB* gene in particular, associated pathways were considered and a *fabH* construct was generated which did result in growth suppression; the *fabBH* construct was generated as an attempt to make the approach work better. Potential reasons for the lack

of growth suppression for relevant, essential gene targets could be plasmid instability wherein the plasmid may not have a strong binding affinity or may not work consistently, intermediate build-up rendering the cells to continue functioning for a period of time after induction, or filamentation which may increase nutrient flux, enabling cells to remain viable. Though the scatterplot in Figure 15 suggests there was no significant contribution in the optical density as a result of the filamentation, integrating the pSRNA plasmid containing each gene target onto the chromosome or also targeting genes responsible for filamentation may shed more insight into why these were ineffective at suppressing growth relative to the other gene targets. Nonetheless the screening results indicate a functional system for the suppression of growth using the afsRNA on a plasmid based system in a minimal media, capable of targeting multiple genes as observed in the *fabBH* construct, and also having minimal effect when left uninduced.

4.2 Bacteriostatic Additive Optical Density Screening Discussion in BW25113 Strains

As noted, bacteriostatic additives were also explored in this investigation for their ability to suppress growth, as well as their effect on morphology, cell viability and metabolic activity. The bacteriostatics chloramphenicol (cmp), streptomycin (strep) and tetracycline (tet) were added to the background strain BW25113 in a well-plate experiment to first assess the effect on growth suppression and morphology. In addition to this, strains resistant to each of these bacteriostatic additives were also generated and tested in the well-plate experiment to gauge the effect of the plasmid on cell growth and morphology.

The bacteriostatic chloramphenicol works by binding to the 23S RNA on the 50S subunit of the ribosome; the genes *rplD* and *rplP* also bind to the 50S subunit of the ribosome

though at different sites. In a sense, this bacteriostatic parallels the functionality of suppressing these genes. Tetracycline on the other hand binds to the 30S ribosomal site, paralleling the functionality of the genes *rpsE* and *rpsD*. Tetracycline also binds to the 30S ribosomal site but targets a different subunit protein.

In the case of the bacteriostatic additives, it was interesting to note that the streptomycin and chloramphenicol did not result in as much filamentation as the tetracycline. While the streptomycin appeared to have more filamentation than the chloramphenicol, the filamentation did not appear to be as homogenous throughout the sample as it did in the tetracycline and it did not appear to be as robust as in the pSRNA variants. Nonetheless, all three were effective at stopping growth in the cells and took action much faster than the pSRNA system. This sheds light that the delay in growth suppression in the pSRNA system is similar to the bacteriostatic system though, in the sense that perhaps both may be attributed to the filamentation wherein the cells may be trying to increase nutrient flux to counter the lack of essential gene function. Perhaps a higher degree of filamentation may be correlated with a longer pseudo-lag phase, though again looking at the scatterplot generated in Figure 23 it does not appear the filamentation has any effect on the background optical density data in either the strains with and without resistance to bacteriostatic additives. The filamentation still suggests that while the cells may be dividing, they may still be growing, which still results in nutrient flux being driven away from product synthesis. Nonetheless, the bacteriostatic resistant strains did not seem to show as much filamentation as the strains with the additives though the streptomycin resistant strain had a significant delay in growth which may be a contributing factor to the delay in growth observed in the pSRNA variants as they contain streptomycin resistance.

Investigating the bacteriostatic variants for further metabolic activity may shed light to their relative efficacy at decoupling growth from production.

4.3 Viability and Metabolic Activity Screening Discussion in BW25113 Strains

After the first phase of the study was completed, the optical density and morphology data was taken into consideration to select six gene candidates for further investigation in a scaled up, shaker flask environment to gauge the cell viability and metabolic activity again in BW25113. The six gene candidates, *dnaE, fabD, fabH, folA*, *murA*, and *rplD*, represent a diverse array of cellular functionalities associated with the growth process as discussed earlier, while also exhibiting efficient suppression of growth in the well plate environment. The gene *dnaE* is responsible in the catalysis of DNA polymerase activity; *fabD* and *fabH* are involved in cell wall synthesis, with *fabD* playing a similar role as *fabB* and *fabH*, as it is involved in the initiation step of fatty acid biosynthesis I as discussed above.[53] The gene *folA* is responsible for DNA synthesis, particularly in catalyzing the reaction in the final step of the tetrahydrofolate synthesis pathway, and has been shown growth essential in knock-out strains; although not explored in this, the gene *folM* has been shown to catalyze the same reaction as *folA* but *folM* knockout studies have shown this gene is not growth essential.[53] Similar to the *fab*-genes, *murA* also catalyzes cell wall biosynthesis, particularly the first step in the synthesis of the peptidoglycan layer in bacteria instead of fatty acid biosynthesis however.[53] Finally, *rplD* is a ribosomal subunit protein, L4, and is involved with the synthesis of proteins.[53]

Culturing the pSRNA variants containing the aforementioned gene targets in a flask environment and monitoring the succeeding viability and metabolic activity gave insight

into the redistribution of resources after cell growth was arrested; Figure 25 illustrates the dynamic optical density data after induction with aTc. In this figure it may be seen that the cells almost immediately suppress growth, with a faster response than observed in the well-plate experiment. Not only did the rise in optical density after induction seem smaller than it did in the well-plate experiment, the delay was also shorter indicating enhanced performance in the flask environment. Adding to this, the glucose was consumed in relatively the same amount of time for all of the variants, both induced and uninduced, indicating increased metabolic activity; the growth was suppressed for the full duration of the experiment – 70 hours. Figure 26 summarizes the specific glucose consumption rate relative to the uninduced background strain, a measure of the metabolic activity. Figure 26 contains a lot of information; the first thing to note is the unaffected specific glucose consumption rate associated with the induced background strain. In the first phase of the experiment it was shown that the concentration of anhydrous tetracycline used did not have any apparent effect on growth or morphology in the background strain, and the findings from this experiment indicate that the anhydrous tetracycline did not affect the metabolism of glucose in the background strain either; the cells also remained metabolically active as the induced pSRNA variants consumed more glucose per cell than the background strain and the uninduced variants; the increased metabolic activity seen with the induced pSRNA variants in the minimal media environment suggests that they would still be capable of generating phenylalanine after suppressing growth. While both the uninduced and induced variants consumed all the glucose, because there were less induced cells they had a higher metabolic activity.

These results suggest the plasmid based sRNA system is effective at decoupling growth from other metabolic processes in the cell, but to confirm the cells remained viable and still capable of generating phenylalanine, a viability assay was performed. Shown in Figure 27 and Figure 28, viable cells fluoresce green and non-viable cells fluoresce red; approximately 100% of the cells appeared to be viable. The few viable cells that were spotted amongst the samples were included and may be seen best in Panel 2I and 5I. The morphology did not appear to have an effect on the viability of the cells.

To compare the metabolic activity of the bacteriostatic additives relative to the pSRNA system, in the same flask-environment chloramphenicol, streptomycin and tetracycline were added at an optical density of ~3.0, as seen in Figure 29. This figure illustrates that the bacteriostatic additives were effective at suppressing growth and acted just as fast as they did in the well-plate experiment, and just as fast as the pSRNA system did in the flask experiment. The growth suppression lasted the duration of the experiment, 80 hours, but it is interesting to note the amount of glucose consumed in either of the three cases was not as high as the background strain. This suggests that these bacteriostatics have an effect on the metabolic activity; considering these bacteriostatics all target 50S or 30S subunit of the ribosome, their metabolic activity may best be reflected by the pSRNA-rplD variant which targets the L4 site of the 50S ribosome. In this variant, the specific glucose consumption rate as seen in Figure 26 was the lowest of all the induced pSRNA strains, though still higher than the background strain. Even taking this into consideration, the strains which received bacteriostatic additives still did not reach a specific glucose consumption rate that was as high. While this shows the bacteriostatics may be effective at suppressing growth, it shows there may be complications in

warranting the continuation of a bioproduct like phenylalanine which is closely tied to growth.

To further investigate the influence of the pSRNA system on the metabolic activity of the cell, a fed-batch experiment was conducted wherein the pSRNA-murA variant was once more grown in a shaker flask environment, and a charge of nutrients, containing more glucose in particular, was added during the exponential phase. The nutrient charge was added during the exponential phase because there is an exogenous and endogenous accumulation of nucleobases when *E. coli* cells reach stationary phase that makes it unlikely for them to continue to consume nutrients and generate a substantial amount of product afterwards, so by targeting the exponential phase and then inducing the variants they may continue to consume nutrients while growth is stopped.[54]

The dynamic optical density results of this experiment, seen in Figure 31, suggest that the cells are able to continue consuming the excess glucose in the fed batch environment. As shown before, this data also suggests the aTc has no effect on the metabolic activity of the background strain which does not contain the pSRNA system, and it also suggests that the pSRNA system has no effect on the metabolic activity of the cell when left uninduced. The resulting specific glucose consumption rates from this experiment are then summarized in Figure 32; the results suggest that the pSRNA-murA variant has a significantly higher glucose consumption rate, around 20% greater than the other strains. In the well plate experiment, the uninduced pSRNA-murA variant had a specific glucose consumption rate 10% greater than the background strain and the induced, 30%. These results are similar to the fed-batch experiment and support the observation that the

metabolic activity was not suppressed during the suppression of growth. A mor significant observation to note form this experiment, however, is the fact that the induced pSRNA-murA variant continued to consume all the glucose from the fed-batch experiment.

4.4 Phenylalanine Production in BW25113 pINT-GA and pSRNA Variants Discussion

In this final phase of the investigation, the efficacy of the pSRNA system towards decoupling growth from the production of phenylalanine, a product known to be tied closely to growth, is assessed.[55] First the 6 gene targets which were further analyzed after the plate reader run, *dnaE, fabD, fabH, folA, murA,* and *rplD* were transformed into a BW25113 pINT-GA variant. As discussed in the Materials and Methods section, the pINT-GA variant produces phenylalanine because it has feedback resistant copies of the genes *aroG* and *pheA* overexpressed.

In the plate reader experiment, well-plates were induced at an optical density of ~0.4 as before and the resulting dynamic optical density was measured. The results of the plate reader experiment were quite interesting and suggest there may be some plasmid interference occurring, as the combination of the two plasmids seems to result in worse efficiency than either single plasmid individually. Starting with the pINT-GA variant which lacks the pSRNA system, it appears as if the addition of aTc still had some effect on growth, resulting in a slightly depressed growth cycle after induction. While this effect was interesting on the optical density it appeared there was no significant effect in regards to cell morphology, suggesting this may not be a significant change in cell activity.

The pSRNA-dnaE variant appeared to have the worst growth suppression out of all those tested in the pINT-GA strain; in this strain it appears that induction resulted in a significant degree of activity related to growth suppression but it appears the cell was able to overcome these limitations and ultimately replicate, soon reaching a final density similar to the control strains. It is also worth noting that the induced *dnaE* variant contained highly elongated morphology that was consistent throughout, and this may be a contributing factor as to why there might be an increase in optical density, though the data from the *murA* variant, which also had surprisingly long morphology, suggests otherwise. Nonetheless, filamentation might suggest the cells are still directing this nutrient flux towards growth in the sense of increasing cell mass without cell division taking place. This is definitely an area of research which could shed more light regarding the underlying mechanisms of the system. The other gene targets all show relatively similar efficiency with regards to growth suppression with the exception of *murA* which appears to suppress growth the best. In the *murA* variant, the optical density appears to keep increasing steadily as it did with the other targets but the rate at which it increases is slower than all others suggesting it would not be able to reach the same cell density as the control strains, as nutrients may eventually limit this process and the cell may reach a point where it no longer may replicate. The morphology of the *murA* was interesting too; it appeared to have the second degree of filamentation, just behind the *dnaE* variant, but the optical density did not appear to increase as significantly suggesting filamentation may not have such a significant effect on optical density relative to the sheer number of cells, though it is likely a contributing factor to some degree.

Ultimately there were mixed morphology results that did not seem to have much of a correlation to the final optical density results though it is likely they did contribute to any background increases in optical density as summarized in the scatterplot generated in Figure 38. The significance of this interaction should be further investigated to more accurately gauge the cell mass in the culture, but taking this into consideration the results suggest it is possible that there is some interference between these two plasmids, with strains like *dnaE* showing worse growth suppression than it did in the BW25113 background strain (seen in Figure 8). Testing the pSRNA system in a strain which has the genes to make phenylalanine on the chromosome, such as NST74, might shed more light into the efficacy of the growth suppression.

For its efficient growth suppression and consistency from the first phase of the investigation, the BW25113 pINT-GA pSRNA-murA variant was chosen to run in a shaker-flask experiment wherein a metabolite analysis tracked the dynamic consumption of glucose as well as the production of acetate and phenylalanine. The results of the optical density from the shaker flak experiment may be seen in Figure 39 and suggest interesting phenomena.

In the shaker flask experiment the first thing to note is that the uninduced pSRNA variant has a larger optical density than the background pINT-GA strain; in the plate-reader experiment the two strains essentially grew at the same rate. This suggests there may be an inherent increase in nutrient flux towards growth, where growth could be summarized by cell division and filamentation. In the case of the uninduced pSRNA variant where cell division is left uninhibited, the cells filament and also divide. The second thing to

note is that, while the aTc did not have any effect on the metabolic activity or cell viability of the background pINT-GA strain in the shaker-flask experiment, though it did appear to have an insignificant but present effect in the well-plate experiment, the aTc did seem to have an effect on the pSRNA-murA variant suggesting growth may have been decoupled from biomass synthesis. More interesting to note in the case of the pSRNA-murA variant is not necessarily that the aTc had an effect on the growth, but that the two induction times ultimately resulted in the same final optical density. This suggests that the time of induction might not have as significant of an effect on the final optical density as one would have expected, but the implications of this on the phenylalanine production do not appear to have the same lack of sensitivity.

Looking next at the pINT-GA and the pSRNA-murA variant in regards to glucose consumption in the uninduced and induced types, all of the strains appear to have consumed glucose in relatively the same amount of time suggesting that the pSRNA system does not appear to inhibit any metabolic activity even in the double-plasmid pINT-GA pSRNA system. This results in an inherently higher specific glucose consumption rate relative to the uninduced strains. While there is a lot of similarity amongst the strains, the phenylalanine production is a bit, most notably there is significantly less phenylalanine being produced in the pINT-GA pSRNA-murA variant than in the pINT-GA background variant. As shown in Figure 35, while there does appear to be a similarity in the sense that majority of the phenylalanine was made during the exponential growth phase with a bit of residual phenylalanine synthesized during stationary phase, further analysis reveals more interesting observations. In the pINT-GA background strain it seems as if not as much phenylalanine is generated during the

exponential phase as in the pSRNA-murA variants, capping out close to ~0.8 grams per liter versus ~1.0 grams per liter, but during stationary phase these cells seem much more active, effectively generating ~1.3 grams per liter versus the range of ~1.0 to ~0.8 grams per liter seen in the pSRNA-murA variant. In the pSRNA-murA variants, particularly the uninduced strain, there appears to be a depression in the phenylalanine concentration immediately after exponential phase where some of the phenylalanine appears to be reuptaken; while this appears to be regenerated near the end of the duration of the study it never reaches a level as high as the pSRNA-murA variant which was induced at the second time point, late in the exponential phase. The second time point of induction does not appear to experience any depression in phenylalanine concentration and continues to make a bit of phenylalanine for the duration of the study. Unfortunately the first time point of induction did not appear to be as good as either of the other two pSRNA-murA strains in regards to phenylalanine generation, not making any significant quantities of phenylalanine after the exponential phase.

These results indicate that, while the pSRNA system was relatively effective at decoupling growth from the production of phenylalanine, it was not as effective as one might hope. Whereas in the optical density data the system seemed insensitive to induction point versus relative final cell density, as the two induction time points leveled off at the same final cell density, the results suggest the phenylalanine production is a bit more sensitive. By manipulating the time of induction to be just right, it was shown that the induced pSRNA variant beat the uninduced pSRNA variant, though it was not enough to out-perform the strain which lacked the pSRNA plasmid. Once more tightening the

degree to which filamentation occurs and making the pSRNA act faster after induction may be contributing factors to the room for improvement.

Gauging the acetate production shed interesting observations as well; it was found that the presence of the pSRNA plasmid resulted in much less acetate production across the board relative to the pINT-GA strain without the pSRNA plasmid. As was the case with the phenylalanine production, much of the production of acetate was made during the exponential phase, but in both cases any acetate was reuptaken during the stationary phase. Coupling this with the results from the optical density and glucose consumption data suggests interesting possibilities. It may be possible that the acetate generated during the exponential phase in the pINT-GA strain, when reuptaken during the stationary phase, was responsible for the increase in phenylalanine which was observed; this increase during the stationary phase was not seen in the pSRNA variants, and the pSRNA variants also did not generate nearly as much acetate. As acetate is generated when glucose is being consumed too fast, this also supports the suggestion that the two-plasmid system may result in an interference which puts a burden on the cell which requires it to inherently consume more glucose to remain viable, leaving less for the production of both acetate and ultimately phenylalanine, though this is an interesting proposition because acetate is associated with suppressed cell growth.[55] While acetate is generally used as an indication that the cell is under stress, consuming glucose too fast, in this case it might be desirable to see a build-up of acetate in the pINT-GA pSRNA variants as it might indicate there is free glucose which may be converted to a useful product; the degree of acetate production and if there is any correlation to the final titer of phenylalanine should be explored in more depth.

Nonetheless, the final metrics to gauge the performance of the pINT-GA strain with the pSRNA system may be summarized in Figure 42; seen in this figure, four metrics are generated – the final phenylalanine concentration, the grams of phenylalanine produced per grams of glucose consumed, the grams of phenylalanine produced per mass of cells, and the grams of cell mass produced per gram of glucose consumed. Ideally, decoupling growth from production would result in increases in grams of phenylalanine per grams of glucose and per grams of cell mass as well as a decrease in the amount of cell mass per grams of glucose. While there is a trend that suggests this may be occurring to some degree, it is only seen with respect to the second time point of induction and the increases do not succeed those of the pINT-GA strain lacking the pSRNA system entirely.

In all metrics, the pINT-GA strain lacking the pSRNA system performs best – it makes the most phenylalanine, per gram of glucose and cell mass, and makes the lowest amount of cell mass per gram of glucose as well. It is worth noting that with respect to the grams of cell mass per grams of glucose, the two induced pSRNA variants are equivalent, and looking at the uninduced pSRNA strain it is apparent the pSRNA system is effective at decoupling growth, though it is also apparent it inherently directs more resources towards growth, which is likely a combination of filamentation and cell division. Nonetheless, there is not much of an observable difference in the grams of cell mass per grams of glucose with respect to the two induction times, a reflection of the optical density data showing they leveled out at the same cell density, which shows the sensitivity to induction may be a target for further investigation. With respect to the total amount of phenylalanine produced, it does not appear that the aTc has an effect on the strain which lacks the pSRNA system as one might expect. Though the strain lacking the pSRNA

system did generate more phenylalanine, again it appears that the pSRNA system was relatively efficient at directing nutrient flux away from growth and towards production of phenylalanine. Compared to the control, making ~10% more phenylalanine (1 gram per liter versus 0.9 gram per liter), even considering it had a suppressed OD_{600} (6.5 versus 8.7). Ultimately this suggests there is more work that needs to be done in regards to upping the total phenylalanine generated. The grams of phenylalanine produced per grams of glucose, and grams of phenylalanine per grams of cell mass are again highest in the second induction time amongst the pSRNA-murA variants, suggesting that the system was efficient to some degree at decoupling growth from production, but it was not enough to offset the apparent interaction between the two plasmids which resulted in inherently less phenylalanine being generated. While the first time point of induction produced more phenylalanine per cell mass, when normalized to the amount of glucose it did not outperform the uninduced strain. This suggests that the timing of induction has a large influence on decoupling the growth from production – likely a reflection of the observation that the first time point of induction did not result in a lower cell density than the second time point of induction.

Ultimately while the system was shown to be relatively effective at accomplishing the tricky feat of decoupling biomass synthesis from the production of phenylalanine, this investigation opens a lot of potential for improvements, such as focusing on increasing the performance and efficacy of the system, selecting other interesting biological systems to metabolically engineer using the pSRNA approach, and investigating other bioproducts which may benefit from this approach.

5. CONCLUSIONS

5.1 Summary of Observations

In conclusion, it was ultimately found that the plasmid-based afsRNA system was effective at inhibiting growth by blocking the translation of growth-essential genes, with different degrees of growth suppression and interesting morphology changes associated with each gene target; the system was also found to be relatively effective at redirecting nutrient flux towards the production of phenylalanine when targeting the gene *murA*. Cells remained more metabolically active than a comparison done with bacteriostatic additives, with a higher specific glucose consumption rate, but had a higher degree of fillamentation growth took longer to suppress in the well-plate experiment. While the resulting efficiencies may be an indication regarding the relative essentiality of each gene target, it may also be a reflection of the efficacy of the afsRNA approach. Nonetheless, the system was shown capable of targeting more than one gene at once, as it was demonstrated that two afsRNA scaffolds could be combined on the same plasmid without affecting efficiency of either (the *fabBH* construct performed as well as the *fabB* and *fabH* did, individually), and the system was shown to remain metabolically active in a fed-batch environment. It was also shown the pSRNA-murA plasmid was able to be co-transformed with the pINT-GA plasmid, though in this case it is worth noting a bit of interference was observed which resulted in a diminished background performance. Although filamentation associated with the pSRNA variants was consistently observed across the board with some gene targets resulting in higher degrees of morphology changes than others, the double-plasmid pINT-GA pSRNA variants had the highest degree of fillamentation, suggesting this is a suitable area for further investigation.

Furthermore, in the strain where the plasmid pINT-GA was co-transformed with the pSRNA plasmid, the results showed the system was working but there was much room for improvement. While significant increases in both final titer and specific yields of phenylalanine were observed in the variant that was induced at the second time point, relative to the uninduced double-plasmid variant and the one induced at the first time point, these increases in efficiency did not outweigh the single-plasmid pINT-GA strain where the pSRNA plasmid was not present. There appeared to be a general background increase in nutrient flux away from phenylalanine production and towards growth in the strain which the pSRNA was not induced, relative to the strain without the pSRNA.

Ultimately the system constructed was shown to work moderately well, addressing the tricky problem of decoupling biomass synthesis from growth; further improvements on this system may make it a formidable tool to use on an industrial scale as it is versatile and not limited to targeting one particular cell mechanism or one particular product pathway but rather may be used in a plethora of applications related to metabolic engineering considering there are still many improvements to be made.

5.2 Suggestions and Future Aims

Future research related to this project may extend in many directions with a lot of possible depth; in general, the most interesting candidates for future research may be the filamentation (particularly of the induced cells), the time it takes after induction for growth to stop, the effect of induction time, the relationship between acetate production and performance of the system, exploration of gene targets related to other aspects of

cellular processes that may be coupled with current candidates from this paper, and applications in different strains to name a few.

The relationship filamentation has with many factors in this investigation is quite interesting; first, accounting for the filamentation to achieve more accurate cell density measurements may shed more light into the efficacy of the system, though the results from the pINT-GA plate reader experiment indicate this probably did not play as significant of a role as expected. This may require a calibration curve relating optical density to dry cell mass, for various degrees of fillamentation. Second, targeting genes associated with filamentation and coupling this with the growth-essential genes may increase the efficacy of the system and would be especially interesting to observe in the pINT-GA pSRNA double-plasmid scenario. It would also be interesting to explore other strategies at suppressing filamentation of the cells, in addition to suppressing cell division – such strategies may involve a synthetic oscillator switch, which may cycle the expression of the pSRNA plasmid so as to block growth essential genes long enough to prevent increases in cell density, but short enough to prevent the cell from filamenting.[56]

Seeing if there is any relationship between the delay between induction time and growth suppression, and the final degree of filamentation might also be interesting, as well as acetate production and final degree of filamentation would be interesting a well – ultimately, characterizing the effect of filamentation on the overall performance of the system would shed a lot of light into the underlying mechanism of the plasmid-based afsRNA approach. Somewhat related to the degree of filamentation, it would also be interesting to further explore the effect of various induction times during the exponential

phase as the system did not have a sensitive response to this in regards to growth suppression but did appear to have a sensitive response to this in regards to phenylalanine production.

Branching off of this, integrating the sRNA plasmid on chromosome may show cleaner results across the board as well. Furthermore, because the strain used to make phenylalanine was also plasmid-based, testing the pSRNA system in a strain like NST74 in which the genes to make phenylalanine are on the chromosome would be an interesting comparison, as would the efficacy of bacteriostatics at making phenylalanine as it was found they are not as efficient at keeping metabolic activity unscathed. Other products would also be interesting to investigate in conjunction with the sRNA, even in other scenarios for example in which it may not be used to necessarily target growth essential genes but perhaps a step branching off to a competing pathway which could result in the build-up of a rate limiting intermediate product, in turn increasing the titer and yield of a desired pathway. Ultimately, the plasmid based sRNA approach was found to show a lot of potential, but like anything interesting the possibilities for further investigation are nearly endless; addressing some of the questions raised in this section may make this a formidable technique to be used on an industrial scale, as it may retrofit completely with existing technologies.

REFERENCES

1. Agency, I. E., Tracking Industrial Energy Efficiency and CO2 Emissions. OECD/IEA: 2007.

2. Leimkuhler, H.-J., *Managing CO_2 Emissions in the Chemical Industry*. Wiley-VCH Verlag GmbH & Co. KGaA: Weinheim, 2010.

3. Carothers, J. M.; Goler, J. A.; Keasling, J. D., Chemical synthesis using synthetic biology. *Current Opinion in Biotechnology* **2009,** *20* (4), 498-503.

4. Jones, D. T.; Woods, D. R., Acetone-butanol fermentation revisited. *Microbiological Reviews* **1986,** *50* (4), 484-524.

5. Acetone. In *Kirk-Othermer Encyclopedia of Chemical Technology*, 14 January 2011 ed.; Wiley & Sons: 2011.

6. Qureshi, N.; Saha, B. C.; Cotta, M. A.; Singh, V., An economic evaluation of biological conversion of wheat straw to butanol: A biofuel. *Energy Conversion and Management* **2013,** *65*, 456-462.

7. Huang, T. In *Phenol: Asia's Rising Capacity and Changing Trade Flow*, APIC Conference, Pattaya, Thailand, ICIS, Ed. APIC: Pattaya, Thailand, 2014.

8. Pandia, R. M. In *Global Phenol-Acetone Markets*, Global Petrochemicals Conference, Cologne, Germany, World Refining Association: Cologne, Germany, 2009.

9. Nielsen, D. R.; Moon, T. S., From promise to practice: The role of synthetic biology in green chemistry. *EMBO Reports* **2013,** *14* (12), 1034-1038.

10. Bird, B. R. S., W.E.; Lightfoot, E.N., *Transport Phenomena*. 2 ed.; John Wiley & Sons, Inc.: 2008.

11. Prausnitz, J. M. L., R.N.; Gomes de Azevedo, E., *Molecular Thermodynamics of Fluid-Phase Equilibria*. 3 ed.; Prentice Hall: 1998.

12. Martin, C. H.; Nielsen, D. R.; Solomon, K. V.; Prather, K. L. J., Synthetic Metabolism: Engineering Biology at the Protein and Pathway Scales. *Chemistry & Biology 16* (3), 277-286.

13. Lu, X.; Vora, H.; Khosla, C., Overproduction of free fatty acids in E. coli: implications for biodiesel production. *Metab Eng* **2008,** *10* (6), 333-9.

14. Miao, L.; Li, Q.; Diao, A.; Zhang, X.; Ma, Y., Construction of a novel phenol synthetic pathway in Escherichia coli through 4-hydroxybenzoate decarboxylation. *Appl Microbiol Biotechnol* **2015,** *99* (12), 5163-73.

15. Copeland, N. G.; Jenkins, N. A.; Court, D. L., Recombineering: a powerful new tool for mouse functional genomics. *Nat Rev Genet* **2001,** *2* (10), 769-779.

16. Russell, J. B.; Cook, G. M., Energetics of bacterial growth: balance of anabolic and catabolic reactions. *Microbiological Reviews* **1995,** *59* (1), 48-62.

17. Thompson, B., Phenol Pathways in E. coli. In *ChemDraw*, Arizona State University, 2015.

18. Cohen, S. C., A.; Boyer, H.; Helling, R., Construction of Biologically Functional Bacterial Plasmids *In Vitro*. *proceedings of the National Academy of Science* **1973,** *70* (11), 3240-3244.

19. Blattner, F. R.; Plunkett, G.; Bloch, C. A.; Perna, N. T.; Burland, V.; Riley, M.; Collado-Vides, J.; Glasner, J. D.; Rode, C. K.; Mayhew, G. F.; Gregor, J.; Davis, N. W.; Kirkpatrick, H. A.; Goeden, M. A.; Rose, D. J.; Mau, B.; Shao, Y., The Complete Genome Sequence of Escherichia coli K-12. *Science* **1997,** *277* (5331), 1453-1469.

20. Bentley, R., THE SHIKIMATE PATHWAY - A METABOLIC TREE WITH MANY BRANCHES. *Critical Reviews in Biochemistry and Molecular Biology* **1990,** *25* (5), 307-384.

21. Curran, K. A.; Alper, H. S., Expanding the chemical palate of cells by combining systems biology and metabolic engineering. *Metabolic Engineering* **2012,** *14* (4), 289-297.

22. Cortassa, S.; Aon, M. A.; Lloyd, D., *Introduction to Metabolic and Cellular Engineering*. World Scientific: River Edge, NJ, USA, 2002.

23. Callura, J. M.; Cantor, C. R.; Collins, J. J., Genetic switchboard for synthetic biology applications. *Proceedings of the National Academy of Sciences of the United States of America* **2012,** *109* (15), 5850-5855.

24. Na, D.; Yoo, S. M.; Chung, H.; Park, H.; Park, J. H.; Lee, S. Y., Metabolic engineering of Escherichia coli using synthetic small regulatory RNAs. *Nat Biotechnol* **2013,** *31* (2), 170-4.

25. McCloskey, D.; Gangoiti, J. A.; King, Z. A.; Naviaux, R. K.; Barshop, B. A.; Palsson, B. O.; Feist, A. M., A model-driven quantitative metabolomics analysis of aerobic and anaerobic metabolism in E. coli K-12 MG1655 that is biochemically and thermodynamically consistent. *Biotechnology and Bioengineering* **2014,** *111* (4), 803-815.

26. Munjal, N.; Mattam, A. J.; Pramanik, D.; Srivastava, P. S.; Yazdani, S. S., Modulation of endogenous pathways enhances bioethanol yield and productivity in Escherichia coli. *Microbial Cell Factories* **2012,** *11* (1), 1-12.

27. Zhao, Y.; Yang, J.; Qin, B.; Li, Y.; Sun, Y.; Su, S.; Xian, M., Biosynthesis of isoprene in Escherichia coli via methylerythritol phosphate (MEP) pathway. *Applied Microbiology and Biotechnology* **2011,** *90* (6), 1915-22.

28. Thakur, C. S.; Brown, M. E.; Sama, J. N.; Jackson, M. E.; Dayie, T. K., Growth of wildtype and mutant E. coli strains in minimal media for optimal production of nucleic acids for preparing labeled nucleotides. *Applied Microbiology and Biotechnology* **2010,** *88* (3), 771-9.

29. Clomburg, J. M.; Gonzalez, R., Biofuel production in Escherichia coli: the role of metabolic engineering and synthetic biology. *Applied Microbiology and Biotechnology* **2010,** *86* (2), 419-34.

30. Park, H.; Bak, G.; Kim, S. C.; Lee, Y., Exploring sRNA-mediated gene silencing mechanisms using artificial small RNAs derived from a natural RNA scaffold in Escherichia coli. *Nucleic Acids Res* **2013,** *41* (6), 3787-804.

31. Turcot, J.; Bisaillon, A.; Hallenbeck, P. C., Hydrogen production by continuous cultures of Escherchia coli under different nutrient regimes. *International Journal of Hydrogen Energy* **2008,** *33* (5), 1465-1470.

32. Sakamoto, M.; Kimura, Y.; Ishii, D.; Nakaoki, T., Biosynthesis of Poly(3-hydroxyalkanoate) from Amino Acids in Medium with Nitrogen, Phosphate, and Magnesium, or Some Combination of These Nutrients. *J Polym Environ* **2014,** *22* (4), 488-493.

33. Hardin, C. C.; Knopp, J. A., Biochemistry - Essential Concepts. Oxford University Press.

34. Duan, Y.; Zhi, Z.; Ke, C.; Xiaoming, T.; Xuefeng, L., De novo Biosynthesis of Biodiesel by Escherichia coli in Optimized Fed-Batch Cultivation. *PLoS ONE* **2011,** *6* (5), 1-7.

35. Lim, C. G.; Fowler, Z. L.; Hueller, T.; Schaffer, S.; Koffas, M. A. G., High-Yield Resveratrol Production in Engineered Escherichia coli. *Applied and Environmental Microbiology* **2011,** *77* (10), 3451-3460.

36. Yakandawala, N.; Romeo, T.; Friesen, A. D.; Madhyastha, S., Metabolic engineering of Escherichia coli to enhance phenylalanine production. *Applied Microbiology and Biotechnology* **2008,** *78* (2), 283-91.

37. Huang, Q.; Lin, Y.; Yan, Y., Caffeic acid production enhancement by engineering a phenylalanine over-producing Escherichia coli strain. *Biotechnology and Bioengineering* **2013,** *110* (12), 3188-3196.

38. Izard, J.; Gomez Balderas, C. D.; Ropers, D.; Lacour, S., A synthetic growth switch based on controlled expression of RNA polymerase. *Molecular systems biology* **2015,** *11* (11), 840.

39. Storz, G.; Vogel, J.; Wassarman, K. M., Regulation by small RNAs in bacteria: expanding frontiers. *Mol Cell* **2011,** *43* (6), 880-91.

40. Waters, L. S.; Storz, G., Regulatory RNAs in bacteria. *Cell* **2009,** *136* (4), 615-28.

41. Yoo, S. M.; Na, D.; Lee, S. Y., Design and use of synthetic regulatory small RNAs to control gene expression in Escherichia coli. *Nat Protoc* **2013,** *8* (9), 1694-707.

42. Vogel, J.; Luisi, B. F., Hfq and its constellation of RNA. *Nat Rev Microbiol* **2011,** *9* (8), 578-89.

43. Otaka, H.; Ishikawa, H.; Morita, T.; Aiba, H., PolyU tail of rho-independent terminator of bacterial small RNAs is essential for Hfq action. *Proceedings of the National Academy of Sciences of the United States of America* **2011,** *108* (32), 13059-13064.

44. Seo, J. S.; Chong, H.; Park, H. S.; Yoon, K. O.; Jung, C.; Kim, J. J.; Hong, J. H.; Kim, H.; Kim, J. H.; Kil, J. I.; Park, C. J.; Oh, H. M.; Lee, J. S.; Jin, S. J.; Um, H. W.; Lee, H. J.; Oh, S. J.; Kim, J. Y.; Kang, H. L.; Lee, S. Y.; Lee, K. J.; Kang, H. S., The genome sequence of the ethanologenic bacterium Zymomonas mobilis ZM4. *Nat Biotechnol* **2005,** *23* (1), 63-8.

45. Qi, L. S.; Larson, M. H.; Gilbert, L. A.; Doudna, J. A.; Weissman, J. S.; Arkin, A. P.; Lim, W. A., Repurposing CRISPR as an RNA-guided platform for sequence-specific control of gene expression. *Cell* **2013,** *152* (5), 1173-83.

46. McKenna, R.; Nielsen, D. R., Styrene biosynthesis from glucose by engineered E. coli. *Metabolic Engineering* **2011,** *13* (5), 544-554.

47. Jiayuan, Q.; Jingdong, T., Circular Polymerase Extension Cloning of Complex Gene Libraries and Pathways. *PLoS ONE* **2009,** *4* (7), 1-6.

48. Schindelin, J.; Rueden, C. T.; Hiner, M. C.; Eliceiri, K. W., The ImageJ ecosystem: An open platform for biomedical image analysis. *Molecular Reproduction and Development* **2015,** *82* (7-8), 518-529.

49. Wepf, R. "Automatic" Determination of Particle Size Distribution 2015.

50. Brockman, I. M.; Prather, K. L. J., Dynamic knockdown of E. coli central metabolism for redirecting fluxes of primary metabolites. *Metabolic Engineering* **2015,** *28*, 104-113.

51. Müller-Hill, B., *The lac Operon*. De Gruyter: Berlin/Boston, DE, 1996.

52. Baba, T.; Ara, T.; Hasegawa, M.; Takai, Y.; Okumura, Y.; Baba, M.; Datsenko, K. A.; Tomita, M.; Wanner, B. L.; Mori, H., Construction of Escherichia coli K-12 in-frame, single-gene knockout mutants: the Keio collection. *Molecular Systems Biology* **2006,** *2* (1).

53. Keseler, I. M.; Mackie, A.; Peralta-Gil, M.; Santos-Zavaleta, A.; Gama-Castro, S.; Bonavides-Martínez, C.; Fulcher, C.; Huerta, A. M.; Kothari, A.; Krummenacker, M.; Latendresse, M.; Muñiz-Rascado, L.; Ong, Q.; Paley, S.; Schröder, I.; Shearer, A. G.; Subhraveti, P.; Travers, M.; Weerasinghe, D.; Weiss, V.; Collado-Vides, J.; Gunsalus, R. P.; Paulsen, I.; Karp, P. D., EcoCyc: fusing model organism databases with systems biology. *Nucleic Acids Research* **2013,** *41* (D1), D605-D612.

54. Rinas, U.; Hellmuth, K.; Kang, R.; Seeger, A.; Schlieker, H., Entry of Escherichia coli into stationary phase is indicated by endogenous and exogenous accumulation of nucleobases. *Appl Environ Microbiol* **1995,** *61* (12), 4147-51.

55. Gerigk, M.; Bujnicki, R.; Ganpo-Nkwenkwa, E.; Bongaerts, J.; Sprenger, G.; Takors, R., Process control for enhanced L-phenylalanine production using different recombinant Escherichia coli strains. *Biotechnology and bioengineering* **2002,** *80* (7), 746.

56. McMillen, D.; Kopell, N.; Hasty, J.; Collins, J. J., Synchronizing genetic relaxation oscillators by intercell signaling. *Proceedings of the National Academy of Sciences of the United States of America* **2002,** *99* (2), 679-684.

APPENDIX A

sRNA NUCLEOTIDE SEQUENCE USED IN CONSTRUCTION OF PLASMID

TCCCTATCAGTGATAGAGATTGACATCCCTATCAGTGATAGAGATACTGAGCACCTA
*GG***ATGCTTAACCAGCTCGATAACCTG**<u>TTTCTGTTGGGCCATTGCATTGCCAC
TGATTTTCCAACATATAAAAAGACAAGCCCGAACAGTCGTCCGGGCTTTTTTT</u>
CTCGAGCTCGAGCCAGGCATCAAATAAAACGAAAGGCTCAGTCGAAAGACT
GGGCCTTTCGTTTTATCTGTTTTTGTCGGTGAACGCTCTCTACTAGAGTCACAC
TGGCTCACCTTCGGGTGGGCCTTTCTGCGTTTATA

Figure 45: The Nucleotide Sequence Used to Construct the Modular Synthetic sRNA showing the Anhydrous Tetracycline Promoter Sequence (Italics), the Target Binding Sequence (**Bold**), the MicC sRNA Scaffold Sequence (<u>Underlined</u>), and the T1/TE Terminator Sequence (Normal).

APPENDIX B

NUCLEOTIDE TARGET BINDING SEQUENCES OF THE SEED REGIONS USED IN afsRNA

Table 4: Coding and Target Binding Sequences as well as Binding Energies for the Different Candidate Gene Targets

nt	sRNA gene targets	Coding sequence (5' → 3')	Target-binding sequence (5' -> 3')	Binding energy (kcal/mol)
23	dnaE	ATG TCT GAA CCA CGT TTC GTA CA	TGT ACG AAA CGT GGT TCA GAC AT	-38.7
23	fabB	ATG AAA CGT GCA GTG ATT ACT GG	CCA GTA ATC ACT GCA CGT TTC AT	-38
24	fabD	ATG ACG CAA TTT GCA TTT GTG TTC	GAA CAC AAA TGC AAA TTG CGT CAT	-37.4
24	fabG	ATG AAT TTT GAA GGA AAA ATC GCA	TGC GAT TTT TCC TTC AAA ATT CAT	-34.1
26	fabH	ATG TAT ACG AAG ATT ATT GGT ACT GG	CC AGT ACC AAT AAT CTT CGT ATA CAT	-39.2
23	fabI	ATG GGT TTT CTT TCC GGT AAG CG	CGC TTA CCG GAA AGA AAA CCC AT	-39
20	folA	ATG CGG CGA GTC CAG GGA GA	TC TCC CTG GAC TCG CCG CAT	-41.9
23	folD	ATG GCA GCA AAG ATT ATT GAC GG	CCG TCA ATA ATC TTT GCT GCC AT	-38
23	folP	GTG CTC CGG GGT TTT TTC TTA TC	GAT AAG AAA AAA CCC CGG AGC AC	-39.4
26	lacZ	ATG ACC ATG ATT ACG GAT TCA CTG GC	GC CAG TGA ATC CGT AAT CAT GGT CAT	-34.8
24	murA	ATG GAT AAA TTT CGT GTT CAG GGG	CCC CTG AAC ACG AAA TTT ATC CAT	-38.9
24	rplD	ATG GAA TTA GTA TTG AAA GAC GCG	CGC GTC TTT CAA TAC TAA TTC CAT	-36.5
24	rplP	ATG TTA CAA CCA AAG CGT ACA AAA	TTT TGT ACG CTT TGG TTG TAA CAT	-35.8
24	rpsD	ATG GCA AGA TAT TTG GGT CCT AAG	CTT AGG ACC CAA ATA TCT TGC CAT	-39.5
23	rpsE	ATG GCT CAC ATC GAA AAA CAA GC	GCT TGT TTT TCG ATG TGA GCC AT	-38.4

APPENDIX C

LIST OF STRAINS AND VARIANTS USED IN THIS STUDY

Table 5: List of All Strain Names and a Description; [1]DH5-alpha was sourced from ThermoFisher, [2]BW25113 was sourced from CGSC, [3]NST74 and ZM4 were sourced from ATCC, and all else from This Study

Strains	Description
E. coli DH5-alpha[1]	*dlacZ Delta M15 Delta(lacZYA-argF) U169 recA1 endA1 hsdR17(rK-mK+) supE44 thi-1 gyrA96 relA1*
E. coli BW25113[2]	*F-, DE(araD-araB)567, lacZ4787(del)::rrnB-3, LAM-, rph-1, DE(rhaD-rhaB)568, hsdR514*
E. coli NST74[3]	*aroH367, tyrR366, tna-2, lacY5, aroF394(fbr), malT384, pheA101(fbr), pheO352, aroG397(fbr)*
Z. mobilis ZM4[3]	*See References*[44]
E. coli MG1655	*K-12 F⁻ λ⁻ ilvG⁻ rfb-50 rph-1*
MG1655-lacZ	*E. coli* MG1655 pSRNA-lacZ
BW-cmp	*E. coli* BW25113 pACYC-DUET
BW-strep	*E. coli* BW25113 pCDF-DUET
BW-tet	*E. coli* BW25113 pRK415
BW-dnaE	*E. coli* BW25113 pSRNA-dnaE
BW-fabB	*E. coli* BW25113 pSRNA-fabB
BW-fabBH	*E. coli* BW25113 pSRNA-fabBH
BW-fabD	*E. coli* BW25113 pSRNA-fabD
BW-fabG	*E. coli* BW25113 pSRNA-fabG
BW-fabH	*E. coli* BW25113 pSRNA-fabH
BW-fabI	*E. coli* BW25113 pSRNA-fabI
BW-folA	*E. coli* BW25113 pSRNA-folA
BW-folD	*E. coli* BW25113 pSRNA-folD
BW-folP	*E. coli* BW25113 pSRNA-folP
BW-murA	*E. coli* BW25113 pSRNA-murA
BW-rplD	*E. coli* BW25113 pSRNA-rplD
BW-rplP	*E. coli* BW25113 pSRNA-rplP
BW-rpsD	*E. coli* BW25113 pSRNA-rpsD
BW-rpsE	*E. coli* BW25113 pSRNA-rpsE
pINT-GA	*E. coli* BW25113 pINT-GA
pINT-GA dnaE	*E. coli* BW25113 pINT-GA pSRNA-dnaE
pINT-GA fabD	*E. coli* BW25113 pINT-GA pSRNA-fabD
pINT-GA fabH	*E. coli* BW25113 pINT-GA pSRNA-fabH
pINT-GA folA	*E. coli* BW25113 pINT-GA pSRNA-folA
pINT-GA murA	*E. coli* BW25113 pINT-GA pSRNA-murA
pINT-GA rplD	*E. coli* BW25113 pINT-GA pSRNA-rplD

APPENDIX D
ASSORTED MEDIA RECIPES

Miller's LB contains 10 grams of tryptone, 5 grams of yeast extract, and 10 grams of sodium chloride per liter of solution; the Miller's LB powder used in this study is pre-formulated (Growcells).

To generate a 50 milliliter shake flask of M9 minimal media, 100 microliters of *1M* $MgSO_4$ (Caroline Biological Supply Co.), 5 microliters of $CaCl_2$ (Sigma Aldrich), 10 milliliters of 5X M9 salts, 5 milliliters of 20% (w/v) glucose (Sigma Aldrich), and 35 milliliters of deionized water. The 5X M9 salts are comprised of 64 grams of Na_2HPO_4 (Santa Cruz), 15 grams of KH_2PO_4 (G Biosciences), 2.5 grams of *NaCl* (Sigma Aldrich), and 5 grams of NH_4Cl (MP Biochemicals).

M9M was comprised of 11.33 grams of Na_2HPO_4 heptahydrate, 3 grams of KH_2PO_4, 0.5 grams of *NaCl*, 2 grams of NH_2Cl for half a liter of a stock solution. To generate a 50 milliliter flask, 25 milliliters of this solution were mixed with 20 milliliters of water, 5 milliliters of 20% (w/v) glucose, 50 microliters of $MgSO_4$ and 5 microliters of $CaCl_2$.

APPENDIX E

POST-PROCESSING METHODOLOGY FOR AUTOMATIC CELL SIZE DISTRIBUTION

As a demonstration of the post processing method used to determine the relativistic cell sizes, consider starting with the images below, which display the morphology of BW25113 pSRNA-folA when uninduced and induced,

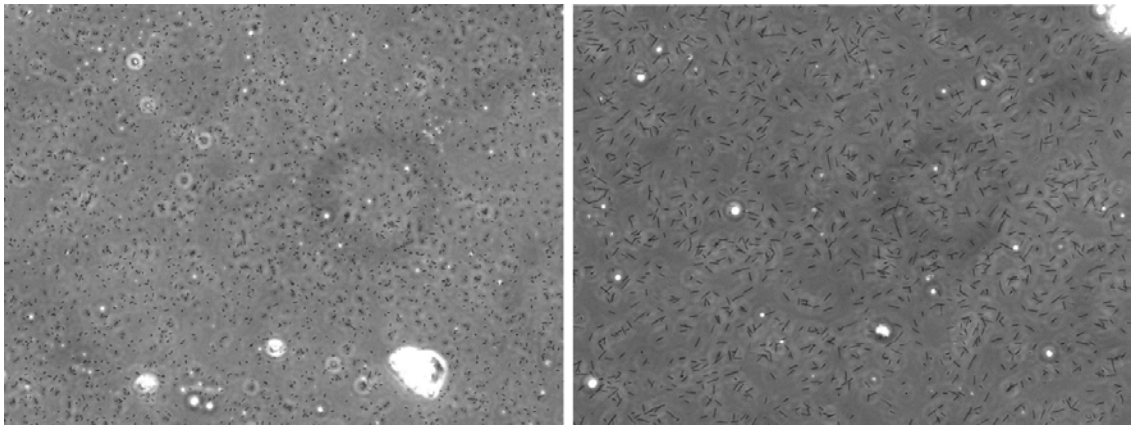

Figure 46: Microscopy Images of BW-folA Without the Addition of aTc (Left) and With the Addition of aTc (Right)

Opening these images in the ImageJ program, a threshold may be applied to effectively convert them to black and white. From this point it is a bit clearer that the induced cells have a larger morphology, but hard to quantify, especially with background noise,

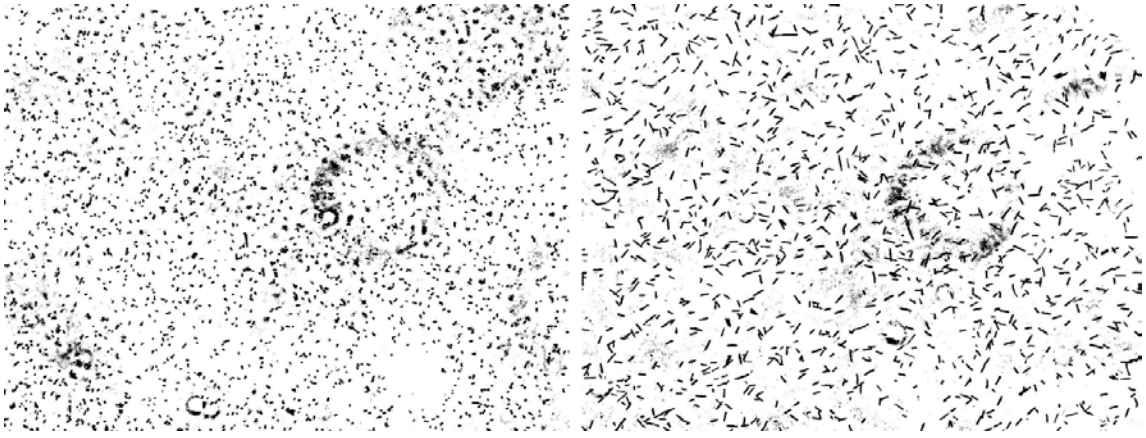

Figure 47: Microscopy Images of BW-folA Without the Addition of aTc (Left) and With the Addition of aTc (Right) after a Threshold is Applied

The images may then be duplicated, where a Gaussian blur filter may be applied to smooth out background noise and artifacts in the image. The original image with the

threshold applied may once more be subtracted from the Gaussian blurred image to reveal an image with less background noise. Applying a threshold on this image once more reduces the amount of noise present in the image.

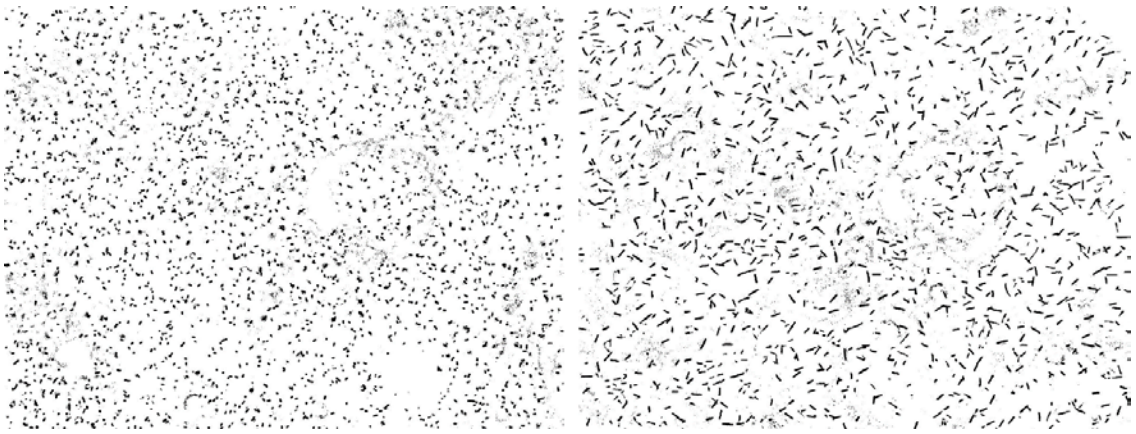

Figure 48: Microscopy Images of BW-folA Without the Addition of aTc (Left) and With the Addition of aTc (Right) after applying a Gaussian Blur, Subtracting this from the Original, and Once more applying a Threshold

Finally, using the particle analysis tool built into ImageJ, clean results may be obtained for average particle size distribution,

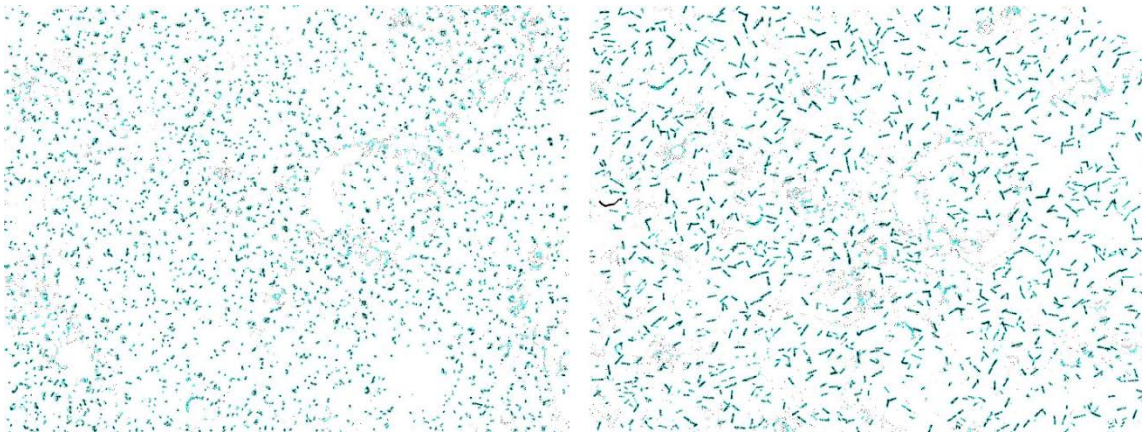

Figure 49: Results from the Particle Size Distribution Analysis Using ImageJ

Results from this analysis in particular showed the induced cells were 2.18 times larger than the uninduced cells.

APPENDIX F

SELECTED PLATE READER OD_{600} DATA FOR BW25113 AND STRAIN VARIANTS IN LB

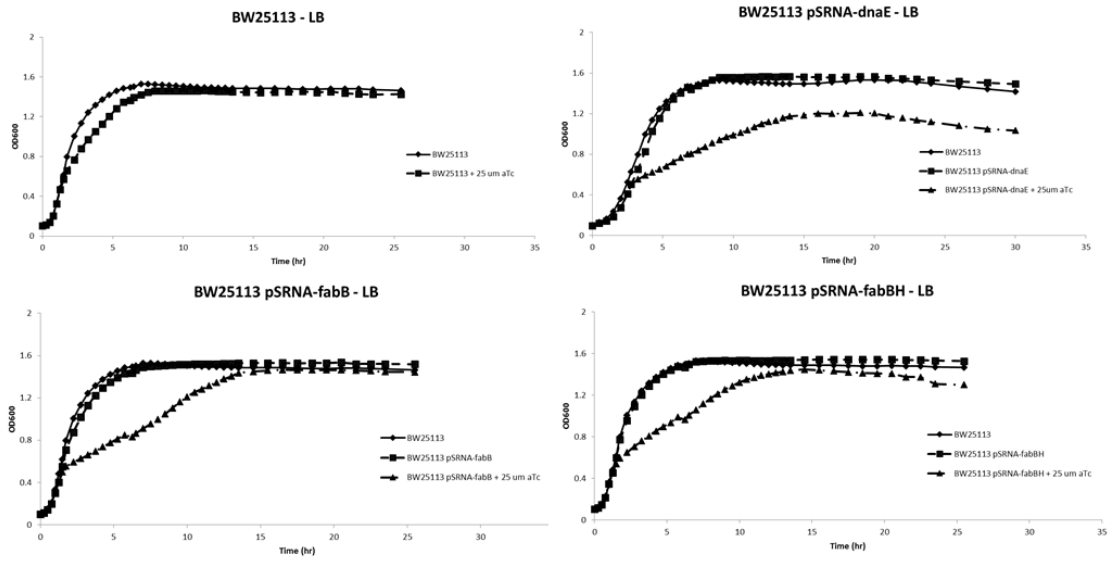

Figure 50: Data Showing the Relationship between Optical Density and Time for Various Strains in LB, Induced with 0.5 Microliters of Anhydrous Tetracycline (aTc) per Milliliter of Culture, Relative to the Background Strain BW25113 without aTc and the Respective Uninduced Strain Variant. (Top Left, BW25113, no sRNA plasmid, with aTc; Top Right, BW-dnaE; Bottom Left, BW-fabB; Bottom Right, BW-fabBH).

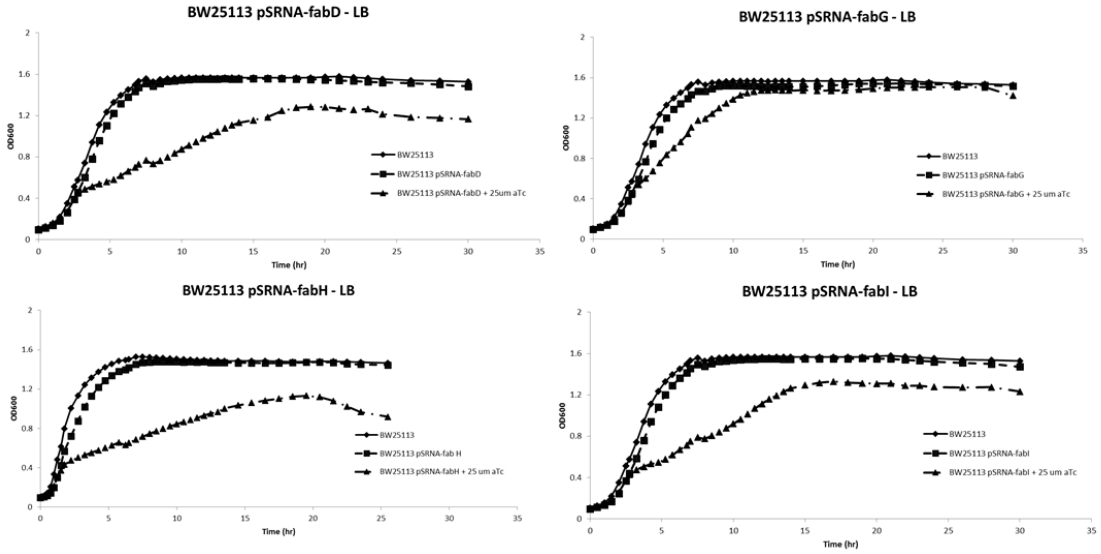

Figure 51: Data Showing the Relationship between Optical Density and Time for Various Strains in LB, Induced with 0.5 Microliters of Anhydrous Tetracycline (aTc) per Milliliter of Culture, Relative to the Background Strain BW25113 without aTc and the Respective Uninduced Strain Variant. (Top Left, BW-fabD; Top Right, BW-fabG; Bottom Left, BW-fabH; Bottom Right, BW-fabI).

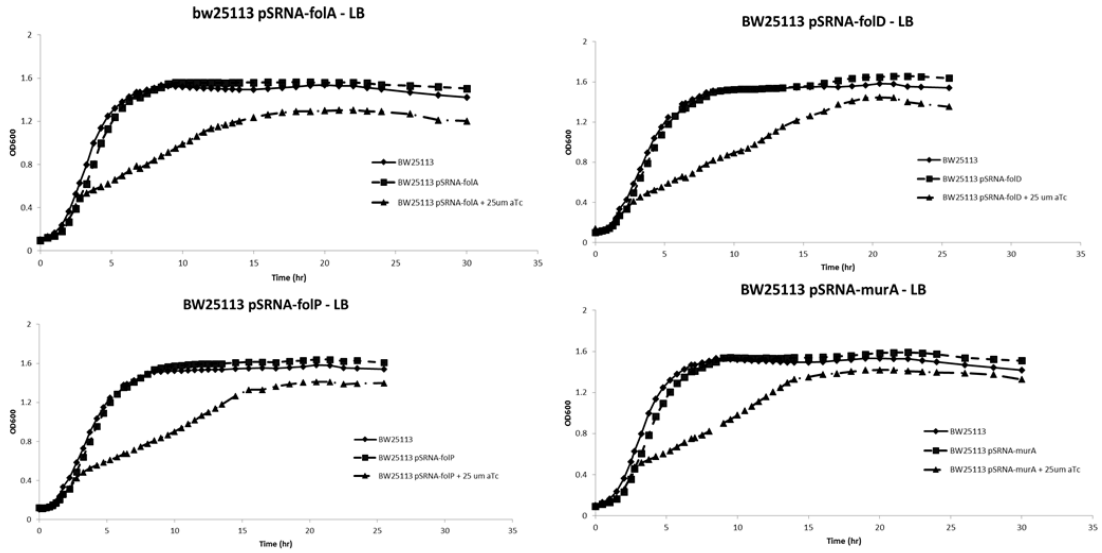

Figure 52: Data Showing the Relationship between Optical Density and Time for Various Strains in LB, Induced with 0.5 Microliters of Anhydrous Tetracycline (aTc) per Milliliter of Culture, Relative to the Background Strain BW25113 without aTc and the Respective Uninduced Strain Variant. (Top Left, BW-folA; Top Right, BW-folD; Bottom Left, BW-folP; Bottom Right, BW-murA).

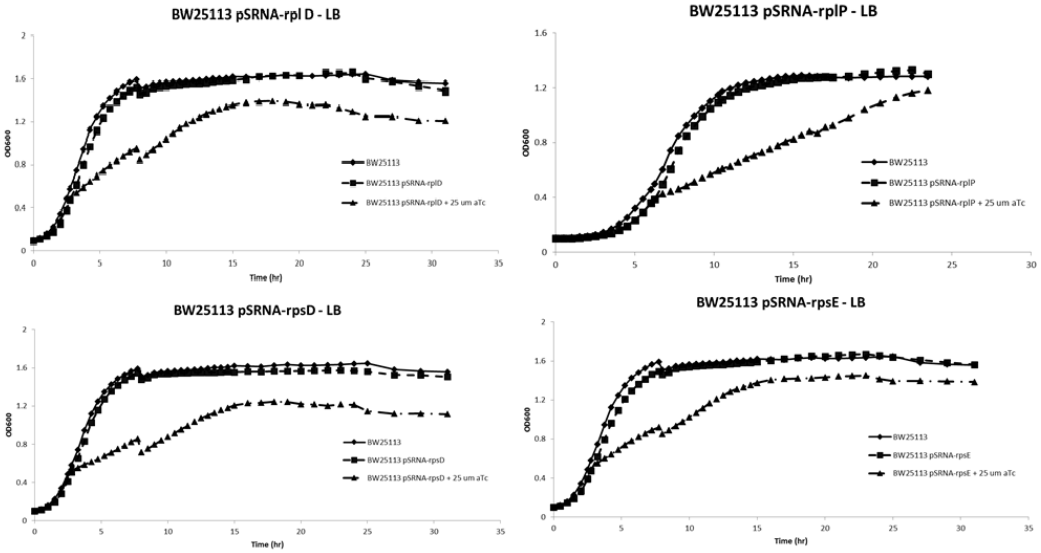

Figure 53: Data Showing the Relationship between Optical Density and Time for Various Strains in LB, Induced with 0.5 Microliters of Anhydrous Tetracycline (aTc) per Milliliter of Culture, Relative to the Background Strain BW25113 without aTc and the Respective Uninduced Strain Variant. (Top Left, BW-rplD; Top Right, BW-rplP; Bottom Left, BW-rpsD; Bottom Right, BW-rpsE.